Electrophysiological and Genetic Aspects of Age-Related Macular Degeneration (AMD): Treatment Implications

by

Ioannis Dimopoulos

A thesis submitted in partial fulfillment of the requirements for the degree of

Master of Science

in

Medical Sciences-Ophthalmology

University of Alberta

Abstract

Age-related macular degeneration (AMD) is considered a heterogeneous group of disorders. Although many genes influence susceptibility to disease, none has shown to be the primary contributor. To identify genetic contributors, distinct AMD phenotypes need to be established. We relied on electrophysiological testing (ERG) to detect homogeneous subgroups for future genotype-phenotype association studies. We also classified AMD patients based on refractoriness to anti-VEGF treatment to investigate genetic associations with known high-risk single nucleotide polymorphisms (SNPs). Our results suggest that generalized cone dysfunction and delayed rod phototransduction activation characterizes a subset of AMD patients, while impaired dark adaptation constitutes a universal feature of the disease. We were unable to unify all patients unresponsive to anti-VEGF monotherapy under a single SNP haplotype, highlighting the genetic complexity underlying the disorder and its treatment prediction. By applying a novel approach to investigate potential pharmacogenetic interactions, we provided evidence that variation in multiple susceptibility loci may better explain differential response to anti-VEGF therapy. Treatment with prolonged VEGF blockade was found to result in inner retina dysfunction in a subset of AMD patients. Therefore, pharmacogenetic research holds promise in developing individualized approaches for AMD treatment in the future, which will not only optimize final patient outcome, but also reduce the risk of adverse effects.

Preface

This thesis is an original work by Ioannis Dimopoulos. The research project, of which this thesis is a part, received research ethics approval from the University of Alberta Research Ethics Board, Project Name "Correlation of DHA/EPA blood levels with AMD progression among various genetically susceptible subgroups", No. 27538, 12/19/2012.

Chapter 2 of this thesis has been published as Dimopoulos IS, Tennant M, Johnson A, Fisher S, Freund PR, Sauvé Y. "Subjects with unilateral neovascular AMD have bilateral delays in rod-mediated phototransduction activation kinetics and in dark adaptation recovery", *Investigative Ophthalmology and Visual Sciences*, August 5, 2013 vol. 54 no. 8, 5186-5195.

Chapter 3 of this thesis has been submitted for publication as Dimopoulos IS, Freund PR, Redel T, Dornstauder B, Gilmour G, Sauvé Y. "Simultaneous precocious changes in rod and cone-driven inner retinal function in the aging human retina" in *Investigative Ophthalmology and Visual Sciences*, February 21, 2014.

I was responsible for the data collection and analysis as well as the manuscript composition. The rest of the authors assisted with subject recruitment, data collection and analysis and contributed to manuscript edit. Sauvé Y. was the supervisory author and was involved with concept formation and manuscript composition.

Acknowledgments

I would like to express my deepest appreciation to my supervisor, Dr. Yves Sauvé, for giving me the opportunity to work in his lab and for all the support and guidance throughout my graduate studies. His enthusiasm and dedication to research has been fundamental to my development as a clinician scientist. I would also like to express my warm gratitude to Dr. Ian MacDonald for his continuous support and for being a great mentor and teacher; and to Dr. Matthew Tennant and all retina specialists at the Alberta Retina Consultants (ARC) for allowing me to conduct research with their patients.

I owe many thanks to ARC staff members and technicians for assisting tremendously in recruitment of study participants. I am also thankful to: Ms. Jane Armstrong, former grader and distinguished researcher at the University of Wisconsin Fundus Photograph Reading Center, for teaching me how to grade AMD fundus photographs; Mr. Bernd Schwanke for providing extensive training in ophthalmic imaging and fundus photography; Dr. Marios Fokaefs for his computer science expertise and contribution and Ms. Sharee Kuny for all her help and support during my research.

I am truly grateful for the support and unconditional love of my family, which has been essential in every achievement of my life.

All work reported in this thesis was conducted with the financial support of the following funding agencies: *The Alexander S. Onassis Public Benefit Foundation* and *The Alberta Innovates Health Solutions*.

Table of Contents

List of Tables

List of Figures

Supplementary Figures

List of Abbreviations

AMD - age-related macular degeneration

ANOVA - analysis of variance

AREDS - Age-Related Eye Disease Study

ARMS2 – age-related maculopathy susceptibility protein 2

CATT – Comparison of AMD Treatment Trials

CCL2 – Chemokine (C-C motif) ligand 2

CCR2 – C-C chemokine receptor type 2

CF – counting fingers

CFH - complement factor H

cGMP - cyclic guanosine monophosphate

CI – confidence interval

CMT – central macular thickness

CNV – choroidal neovascularization

DA – disc area

DHA - docosahexaenoic acid

DTL – Dawson – Trick – Litzkow

ERG - electroretinogram

FFT – fast fourier transform

GA – geographic atrophy

GABA – gamma-Aminobutyric acid

GWAS – genome-wide association studies

HTRA1 – high-temperature requirement serine protease A1

IPL - inner plexiform layer

IRBP - interphotoreceptor retinoid-binding protein

ISCEV – international society for clinical electrophysiology of vision

IVAN – Inhibit VEGF in Age-related choroidal Neovascularisation

logMAR – logarithm of the minimum angle of resolution

MWT – morlet wavelet transform

OCT - optical coherence tomography

ONL - outer nuclear layer

OPs – oscillatory potentials

PED – pigment epithelial detachment

PIR - photopic intensity response

RPE - retinal pigmented epithelium

SD - standard deviation

SEM - standard error of mean

SIR - scotopic intensity response

SMOTE – synthetic minority oversampling technique

SNP – single nucleotide polymorphism

VEGF - vascular endothelial growth factor

Chapter 1. INTRODUCTION

1.1) Age-related Macular Degeneration (AMD)

Age-related macular degeneration (AMD) is a complex, late-onset, neurodegenerative disease affecting primarily the macular region of the retina. AMD is the leading cause of irreversible blindness in the elderly of the Western world, affecting 10% of individuals older than 65 years of age and nearly 30% of those above the age of 75 (Smith et al. 2001). Although comprising only 4% of the total retinal area, the macula contains the densest population of the photosensitive nerve cells called photoreceptors and is responsible for high acuity vision. The photoreceptors are supported by a thin monolayer of pigmented epithelial cells (RPE cells). Underneath the RPE layer is the choroid plexus, a network of fenestrated capillaries that provide oxygen and nutrients to the retina. Located between the RPE and the choriocapillaris is the Bruch's membrane (BM), an elastin- and collagen-rich extracellular matrix that regulates exchange of biomolecules, nutrients and metabolic waste (Booij et al. 2010). AMD is characterized by changes in the Bruch's membrane, choriocapillaris and retinal pigment epithelium (RPE) that gradually impair photoreceptor viability.

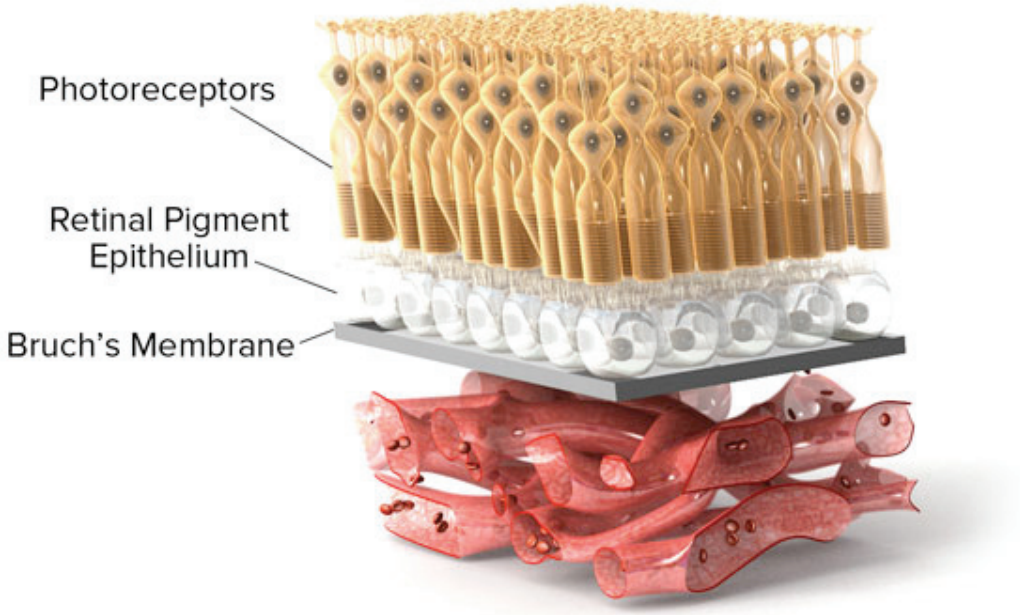

Figure 1.1: The photoreceptor/RPE/Bruch's membrane complex. Adapted from *scienceofamd.org*

Clinically, AMD can be classified into the "dry" form and the "wet" or neovascular form. The hallmark of dry AMD is the accumulation of ophthalmoscopically visible yellow acellular deposits between the retinal pigment epithelium and the Bruch's membrane known as "drusen". Drusen can be classified as small (<63 μm in diameter with discrete margins), medium (63–124 μm) or large (>125 μm with indistinct edges). Large drusen and increased total drusen area are primarily associated with increased risk of progression to advanced stages of the disease (Wang et al. 2003). Advanced AMD is characterized by either complete loss of the supporting RPE layer in the macular region (geographic atrophy) or abnormal growth of choroidal blood vessels ("wet" AMD; see below). Pigmentary changes in the macular RPE layer (both

hypo- and hyperpigmentation) can also be encountered within the spectrum of clinical characteristics of dry AMD. Based on total drusen area and the presence/absence of pigmentary anomalies, the Age-Related Eye Disease Study (AREDS) has developed a nine-step severity scale to define risk categories for development of advanced AMD (Davis et al. 2005).

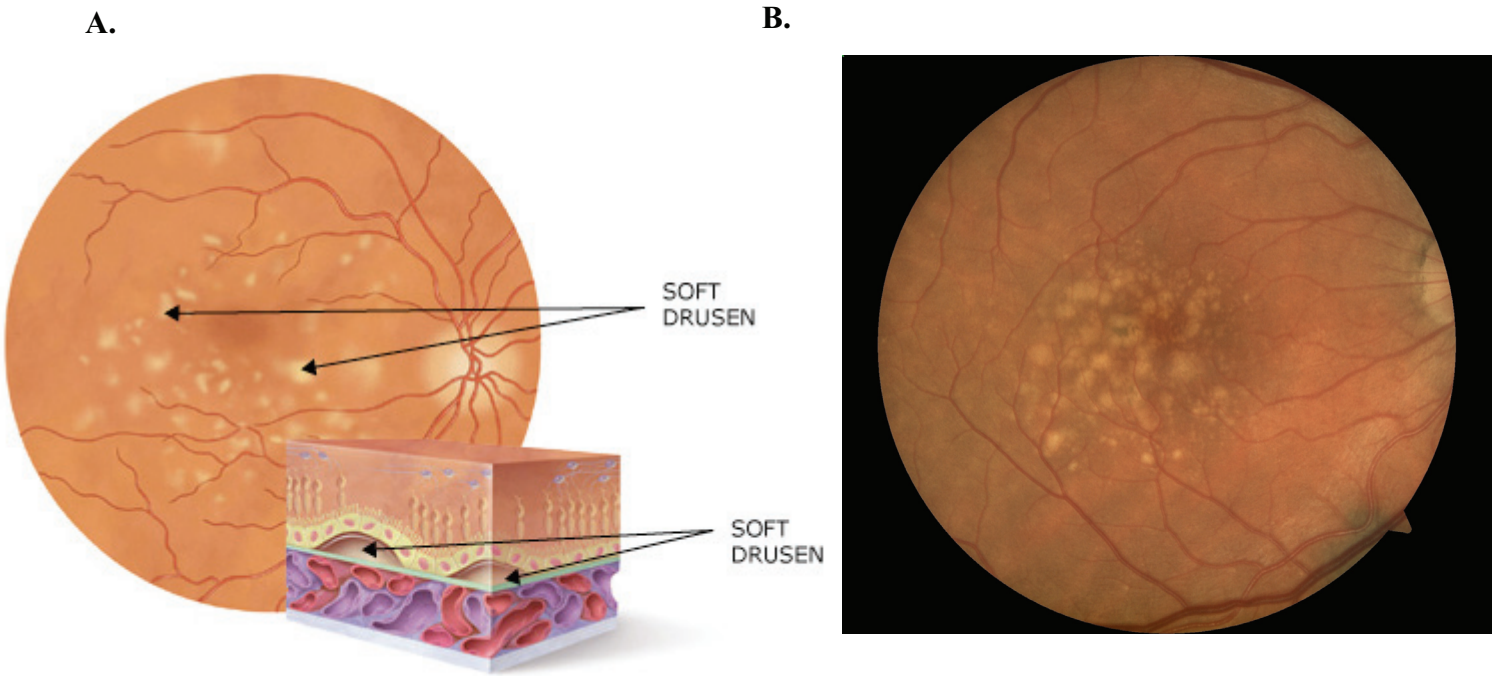

Figure 1.2: Drusen in dry age-related macular degeneration. A) Illustration of soft drusen located between the RPE and the choiroid. Adapted from *amdalliance.org*; B) Representative fundus image from a patient characterized by large drusen and pigmentary changes (*courtesy of Dimopoulos IS*).

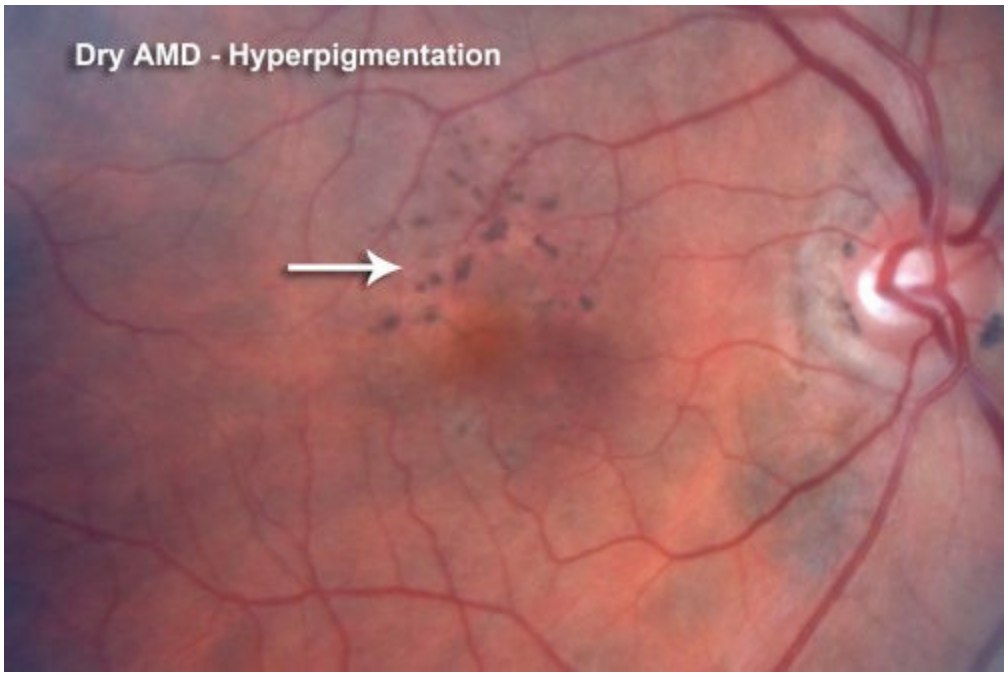

Figure 1.3: Hyperpigmentation in age-related macular degeneration. Adapted from *retinagallery.com*

The "wet" or neovascular form of AMD is considered an advanced form of the disease. Although constituting 10 percent of all AMD cases, advanced dry AMD (geographic atrophy) and neovascular AMD are responsible for 90 percent of vision loss attributed to AMD (Ferris et al. 1984). The designation of "wet" or neovascular AMD implies the abnormal presence of fluid in the intraretinal or subretinal space that is produced by a newly formed neovascular tissue. The process is commonly referred to as choroidal neovascularization (CNV) because the neovascular tissue originates from the choroidal vasculature. Abnormal angiogenesis is driven in a molecular level by vascular endothelial growth factor (VEGF). Uncontrolled VEGF expression results in the growth of immature new blood vessels that are tortuous and lack pericytes resulting in fragility and

propensity to exudation (Qazi et al. 2009). If left untreated, CNV can lead to formation of a disciform scar, a fibrotic scar that causes severe and irreversible central vision loss.

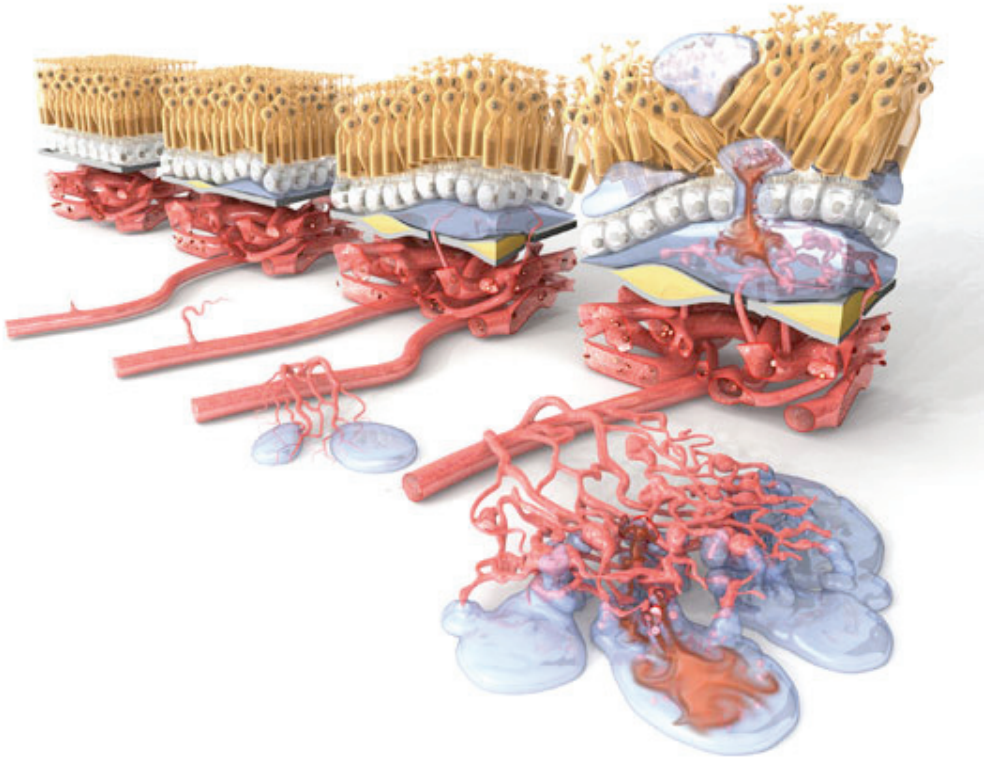

Figure 1.4: Abnormal blood vessel growth in neovascular age-related macular degeneration (AMD). Adapted from *scienceofamd.org*

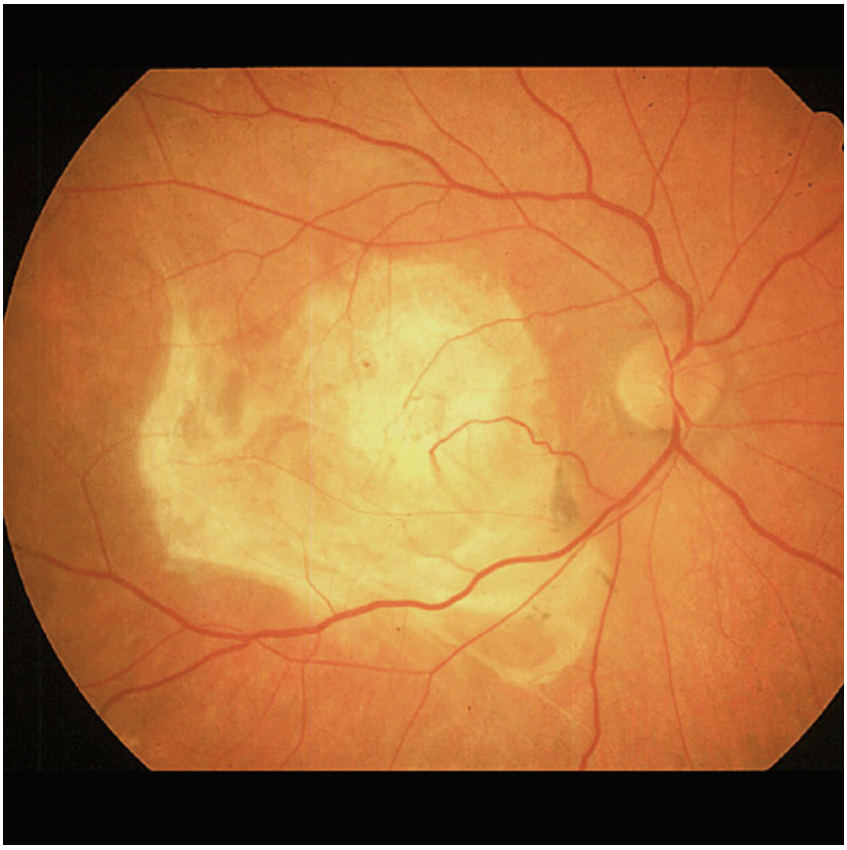

Figure 1.5: Disciform scar secondary to age-related macular degeneration. Adapted from *eyepathologist.com*

1.2) Genetics in Age-related Macular Degeneration (AMD)

Age-related macular degeneration (AMD) is nowadays recognized as a heterogeneous, multifactorial disease, resulting from the interplay of genetic components and environmental factors. Significant progress has been made in the past decade in identifying genetic susceptibility loci for AMD. These gene variants hold promise in developing risk prediction models with high accuracy that can be used effectively in the clinical setting. Risk models are focused on predicting disease development, progression and response to treatment, paving the

way towards personalized medicine in AMD. Genetic linkage studies suggested disease susceptibility loci on chromosomes 1q25-31 and 10q26 (Majewski et al. 2003; Fisher et al. 2005), followed by genome-wide association studies (GWAS), which identified a robust panel of gene variants contributing to the disease.

1.2A) The Complement cascade genes

A series of reports in 2005, including the first successful genome-wide association study (GWAS), found a significant association between AMD and certain polymorphisms in the complement factor H (CFH) gene, which encodes an important regulator of the alternative pathway of the complement system. Risk-conferring and protective CFH haplotypes have been described (Hageman et al., 2005; Klein et al., 2005; Edwards et al. 2005; Haines et al. 2005). Risk-haplotypes in CFH can increase the lifelong risk of developing the disease up to 5-fold (Sofat et al. 2012). Gene alleles in other components or regulators of the alternative complement pathway have been shown to significantly modify AMD risk. These include variants in the complement component 2 (C2) (Gold et al. 2006), complement component 3 (C3) (Yates et al. 2007), complement factor B (CFB) (Gold et al. 2006), and complement factor I (CFI) (Fagerness et al. 2009). All these gene variants implicate immunity as a major risk factor in developing AMD.

1.2B) The ARMS2/HTRA1 locus and other Susceptibility Genes

A region on chromosome 10q26 (ARMS2: age-related maculopathy

susceptibility 2) that does not appear to have an obvious role in immunity has also been strongly associated with AMD development. Its effect size is similar to or greater than that seen with *CFH* (Jakobsdottir et al. 2005; Dewan et al. 2006; Yang et al. 2006). The risk-conferring haplotype encompasses two genes: 1) *ARMS2* (the previously hypothetical *LOC387715*), which codes for a primate-specific transcript with hypothetical mitochondrial function; and 2) *HTRA1,* which codes for a multi-functional serine protease. The identity of the gene that confers the higher risk is still controversial. The ARMS2 A69S SNP (rs10490924) leads to a non-synonymous substitution of alanine to serine at position 69 of the hypothetical mitochondrial protein. On the other hand, the SNP rs11200638 at the promoter region of *HTRA1* may confer high risk for AMD development through elevated levels of mRNA and HTRA1 protein levels in human retina (Yang et al. 2006). Variants in the *ARMS2* have also been suggested to modulate the promoter activity of *HTRA1*. It is thus likely that both alleles contribute to increased AMD risk. Associations with a number of additional genes – including the *ABCA4, FIBLN6*, *TLR3* and *SERPING1* genes have been suggested (Allikmets et al. 1997; Schultz et al. 2003; Cho et al. 2009; Ennis et al. 2008), but in most cases these have not been verified/replicated in subsequent studies. Most recently, genes in the high-density lipoprotein (HDL) pathway were discovered to be associated with AMD. These include the hepatic lipase C gene (*LIPC*) (Yu et al. 2011) and the cholesteryl ester transfer protein gene (*CETP*) (Liu et al. 2014). The tissue inhibitor of metalloproteinase 3 (*TIMP3*) gene, which is related to Sorsby's fundus dystrophy (a juvenile-onset form of macular degeneration), has been shown to

raise susceptibility to AMD (Kaur et al. 2010). In the angiogenesis pathway, certain variants of the vascular endothelial growth factor A gene (*VEGFA*) have been strongly associated with the neovascular form of the disease (Huang et al. 2013).

A recent AMD Gene Consortium in 2013 executed a collaborative genome-wide association study, including >17,000 advanced AMD cases and >60,000 controls of European and Asian ancestry (Fritsche et al. 2013). Advanced AMD cases consisted of both geographic atrophy (GA) and choroidal neovascularization (CNV). In addition to twelve previously associated loci, seven new loci reached genome-wide significance for the first time. Implicated genes so far can be clustered into four different biological pathways: a) inflammation and complement system regulation; b) lipid metabolism; c) oxidative stress and extracellular matrix remodeling; and d) angiogenesis. A summary of the 19 associated SNPs is provided in table 1. These 19 loci represent up to 65% of the total genetic contribution to AMD (Fritsche et al., 2013).

SNP	Risk Allele	Chromosome	Nearby Genes (Symbol/Name)		Odds Ratio
rs10490924	T	10	*ARMS2-HTRA1*	Age-related maculopathy susceptibility 2-HtrA serine peptidase 1	2.76 (2.72-2.80)
rs10737680	A	1	*CFH*	Complement factor H	2.43 (2.39-2.47)
rs429608	G	6	*C2-CFB (SKIVL2)*	Complement component 2-Complement factor B (Superkiller viralicidic activity 2-like	1.74 (1.68-1.79)
rs2230199	C	19	*C3*	Complement component 3	1.42 (1.37-1.47)
rs5749482	G	22	*TIMP3/SYN3*	TIMP metallopeptidase inhibitor 3/Synapsin III	1.31 (1.26-1.36)
rs4420638	A	19	*APOE/APOC1*	Apolipoprotein E/Apolipoprotein C1	1.30 (1.24-1.36)
rs1864163	G	16	*CETP*	Cholesteryl ester transfer protein	1.22 (1.17-1.27)
rs943080	T	6	*VEGFA*	Vascular endothelial growth factor A	1.15 (1.12-1.18)
rs13278062	T	8	*TNFRSF10A*	Tumor necrosis factor receptor superfamily, member 10a	1.15 (1.12-1.19)
rs920915	C	15	*LIPC*	Lipase, hepatic	1.13 (1.09-1.17)
rs4698775	G	4	*CFI/CCDC109B*	Complement factor I/Coiled-coil domain containing 109B	1.14 (1.10-1.17)
rs3812111	T	6	*COL10A1*	Collagen, type X, alpha 1	1.10 (1.07-1.14)
rs13081855	T	3	*COL8A1-FILIP1L*	Collagen, type VIII, alpha 1	1.23 (1.17-1.29)
rs3130783	A	6	*IER3-DDR1*	Immediate early response 3-Discoidin domain receptor tyrosine kinase 1	1.16 (1.11-1.20)
rs8135665	T	22	*SLC16A8*	Solute carrier family 16, member 8 (monocarboxylic acid transporter 3)	1.15 (1.11-1.19)
rs334353	T	9	*TGFBR1*	Transforming growth factor, beta receptor 1	1.13 (1.10-1.17)
rs8017304	A	14	*RAD51B*	RAD51 homolog B	1.11 (1.08-1.14)
rs6795735	T	3	*ADAMTS19*	ADAM metallopeptidase with thrombospondin type 1 motif, 9	1.10 (1.07-1.14)
rs9542236	C	13	*B3GALTL*	Beta 1,3 galactosyltransferase-like	1.10 (1.07-1.14)

Table 1.1: Summary of loci reaching genome-wide significance. Modified from *Fritsche et al. (2013)*.

1.3) Genotype-phenotype associations in AMD

Genotype-phenotype association studies seek to refine the association

between variants in key AMD susceptibility genes (predominantly *CFH* and *ARMS2/HTRA1*) and various parameters of the AMD phenotype. Although not establishing causality, these studies identify gene variants highly likely to predispose to more advanced stages of AMD and to be associated with phenotypic indicators of severe disease, such as age at presentation, bilateral disease manifestation, lower visual acuity and rapid progression of disease. Indeed, homozygous patients for high-risk alleles at both *CFH* and *ARMS2* have been associated with a younger age of presentation (Andreoli et al. 2009; Shuler et al. 2008; Leveziel et al. 2010) Chen et al. (2008) reported that the high-risk allele for rs11200638 (*HTRA1*) was more frequently associated with bilateral than unilateral advanced AMD (GA or CNV). In the Blue Mountains Eye Study, a large Australian population-based cohort study of AMD incidence, patients homozygous for the CFH Y402H high-risk allele were significantly more likely to manifest bilateral than unilateral soft drusen (Pai et al. 2009). Leveziel et al. (2008) prospectively evaluated patients homozygous for the low- or high-risk alleles for the CFH Y402H and ARMS2 A69S variants. Homozygosity for high-risk alleles at both loci was associated with a higher incidence of bilateral CNV and disciform scarring as well as lower visual acuity than those homozygous for low-risk alleles at both loci. Seddon et al. (2007) studied a subset of the Age-Related Eye Disease Study (AREDS) cohort followed longitudinally for progression from early or intermediate AMD to advanced AMD and found that the CFH Y402H and ARMS2 A69S high-risk alleles were each independently associated with such progression. Francis et al. (2007) studied various CFH

polymorphisms and haplotypes in three independent populations with AMD. The authors reported a progressively higher frequency of the CFH Y402H high-risk allele with increasing grade of AMD. Eyes characterized as having intermediate AMD (large drusen and/or multiple medium-size drusen) showed a significantly higher frequency of the high-risk allele than those with early AMD (small and/or a few medium-size drusen). Eyes with advanced AMD (GA or CNV) exhibited a significantly higher frequency of the high-risk allele than those with intermediate AMD. All the above studies suggest an association between CFH Y402H and ARMS2 A69S with phenotype severity and AMD progression rate.

1.4) The Electroretinogram (ERG): its role in describing distinct clinical phenotypes

The ability to describe genotype-phenotype associations depends on having reliable markers of disease. The markers that have been typically used in the association and linkage studies of AMD are the size and extent of drusen, for the early form of the disease, and occurrence of choroidal neovascularization or central geographic atrophy for the late stage of the disease. An objective marker that is derived from genetically controlled physiologic processes would greatly assist not only in establishment of genotype-phenotype associations, but also in the discovery of the remaining 35% genetic contribution to AMD. The electroretinogram (ERG) represents a good example of such an objective marker.

1.4A) Electroretinogram (ERG)

The full-field electroretinogram (ERG) is a mass electrical response of the retina to brief flashes of light. The flash elicits an ERG waveform recorded at the cornea level via conducting electrodes. Recording electrodes consist of Dawson-Trick-Litzkow type (DTL) fiber electrodes with references electrodes placed on the lateral edge of the orbital bone. The ground electrode (gold surface electrode) is usually centered on the forehead, one inch above the upper eyebrow line. The acquired waveform displays two distinct components: the negative a-wave followed by the positive b-wave. The a-wave represents hyperpolarizing photoreceptors activity and the b-wave is thought to reflect ON-bipolar cell depolarization and Muller cell activity (Miller and Dowling, 1970). A-wave amplitudes are measured from baseline to the trough of the negative a-wave peak, whereas b-waves from the a-wave trough to the following peak of the b-wave. The time from flash onset to the through of the a-wave and to the b-wave peak are referred to as the a-wave implicit time and b-wave implicit time, respectively.

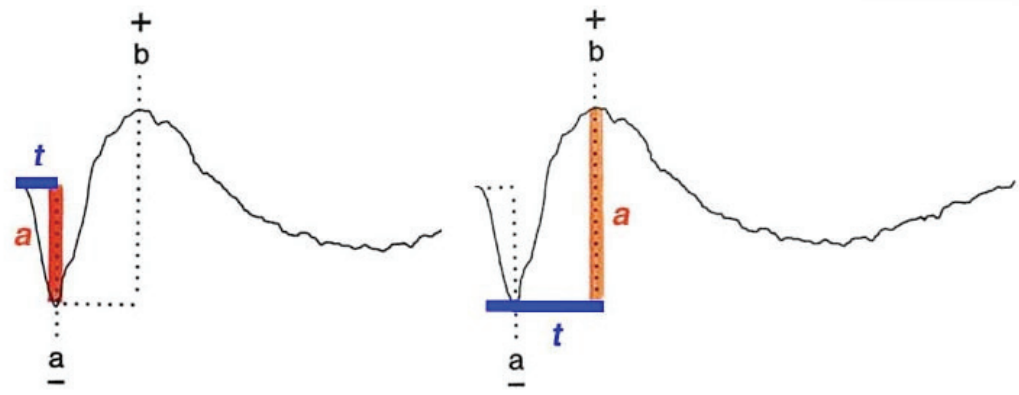

Figure 1.6: Amplitude and implicit time measurements of the ERG waveform. A-wave (left); b-wave (right). Adapted from *webvision.med.utah.edu*

Several ERG protocols can be employed to dissect cone and rod pathways. Background illumination can be used to desensitize rod cells and record cone-driven responses. Rod-driven responses can be elicited following a period of dark adaptation (20min) to sensitize rods. Dim flashes of light are then used that are sub-threshold to the cones. At higher flash strengths, mixed responses (both cone and rod contribution) can be recorded from the dark-adapted retina. By controlling variables such as background illumination, flash intensity and wavelength, it is possible not only to isolate rod- from cone-driven responses but to distinguish pre- from post-synaptic contribution as well. Thus, the ERG is an invaluable tool for detecting changes in distinct physiologic pathways of the retinal visual system.

1.4B) The Oscillatory Potential Component (OPs)

Another distinct component of the human ERG is the oscillatory potential (OP) response. OPs are small rhythmic wavelets seen on the ascending limb of the b-wave under both dark- and light-adapted conditions. They are most easily recorded is mesopic (dim) adaptational conditions when the retina is stimulated with short-duration, high-intensity flashes that bleach a negligible amount of photopigment (Wachtmeister 1998). Although their exact origin remains unspecified up to this point, findings favor the conclusion that they reflect neuronal synaptic activity in inhibitory feedback pathways initiated by interplexiform cells and/or amacrine cells in the inner retina (Wachtmeister and Dowling, 1978). Affected parameters of the oscillatory response have been linked to underlying inner retina dysfunction (Wachtmeister 1998), especially loss of integrity in the retinal microcirculation (Brown 1968).

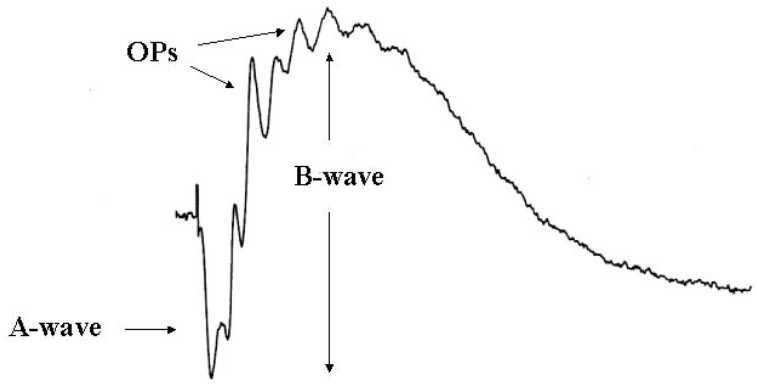

Figure 1.7: The Oscillatory potentials (OPs) of the ERG waveform. Adapted from *webvision.med.utah.edu*

There are various human retinal disorders that show attenuated OP responses as a characteristic ERG feature: diabetic retinopathy (Kizawa et al. 2006; Bresnick and Palta 1987; van der Torren and Mulder 1993; Li et al. 1992), retinopathy of prematurity (Akula et al. 2007), central retinal vein occlusion (Yu et al. 1998; Huang et al. 2001) and primary open-angle glaucoma (Halopigian et al. 2000). Furthermore, a number of drugs given in high doses or for long periods of time can cause retinal toxicity and affect OPs and other components of the ERG. Vigabatrin, a pediatric seizure medication, is a classic example of a drug that can lead to dramatic changes in oscillatory potentials through impacting GABAergic amacrine cells in the inner plexiform layer (Westallet al. 2003).

Treatment of neovascular AMD with prolonged VEGF blockade has raised concerns about potential retinal toxicity. Several lines of evidence indicate an important role for endogenous VEGF in the maintenance and function of adult retina neuronal cells, such as the photoreceptors and the Müller cells (Saint-Geniez et al. 2008). Chronic inhibition of VEGF-A function in normal adult animals has been shown to lead to a significant loss of retinal ganglion cells (Nishijima et al. 2007). In addition, changes in retinal nerve fiber layer thickness have been reported in treated eyes of patients with unilateral neovascular AMD (Martinez-de-la-Casa et al. 2012). Whether prolonged VEGF blockade definitely affects inner retina function remains to be elucidated.

1.4C) The Electroretinogram (ERG) in AMD

Historically, due to the regional macular dysfunction typifying AMD, the full-field ERG has not been used in the study of AMD progression. Since the macula represents only 5% of the whole retinal surface area, dysfunctions confined to this region do not result in impaired full field ERG responses (Van Lith GHM 1976). The multifocal ERG has been developed specifically to assess regional function, such as from the macula, but it is limited to cone-driven responses. Past full field ERG studies have shown conflicting findings in AMD, most likely reflecting the complex nature of the disease. These findings include a global reduction in retinal function (Walter et al. 1999) and a generalized cone dysfunction in subgroups of AMD patients (Ronan et al. 2006). The authors of these studies suggested that "using standardized full field ERG to identify a more homogeneous subgroup of AMD patients with panretinal dysfunction will aid in better characterizing subtypes clinically and is likely to be valuable in identifying new genes contributing to AMD". (Ronan et al. 2006)

1.5) Aim of Thesis I

The first aim of the current thesis is to use extensive electrophysiological testing (ERG) to identify distinct AMD phenotypes. The focus will extend beyond standard clinical protocols, including assessment of OPs, dark adaptation dynamics and phototransduction kinetics.

1.6) Anti-VEGF therapeutics in neovascular (wet) AMD

Responsiveness to treatment is an alternative classification method for AMD patients. Over the past decade, vascular endothelial growth factor (VEGF)-targeting therapies have become the mainstay of treatment for neovascular (wet) AMD. The *VEGF-A* gene consists of eight exons on chromosome 6p21. Alternate gene splicing can generate 6 isoforms: $VEGF_{121}$, $VEGF_{145}$, $VEGF_{165}$, $VEGF_{183}$, $VEGF_{189}$ and $VEGF_{206}$. $VEGF_{165}$ is the predominant pathologic isoform. The VEGF-A protein product is a dimeric glycoprotein that interacts with two tyrosine kinase receptors, VEGFR-1 (FLT-1) and VEGFR-2 (KDR) located primarily on endothelial cells (Kovach et al. 2012; Ferrara N. 2004). Pegaptanib (Macugen; Eyetech, Palm Beach Gardens, FL) was the first anti-VEGF therapy approved by FDA for the treatment of neovascular AMD in 2004. It is a pegylated aptamer that selectively binds to one VEGF isoform, $VEGF_{165}$. As an aptamer (nucleic acid–based molecule) it is less immunogenic than any other protein-based binding molecule. Its shorter half-life and rapid elimination are the main disadvantages compared to antibodies or Fab fragments. Bevacizumab (Avastin; Genentech/Roche, South San Francisco) is a full-length, humanized, monoclonal IgG antibody with two VEGF-A binding sites that inhibits all identified VEGF isoforms. In 2004, FDA approved bevacizumab for the treatment of metastatic colon cancer (Ferrara N. 2004). The first reported case of intravitreal administration of bevacizumab occurred in 2005 and led to complete resolution of subretinal fluid after a single injection (1mg) (Rosenfeld et al. 2005). Since then

there has been widespread adoption of this off-label therapy for neovascular AMD. Another protein-based binding molecule was approved in 2006 for treatment of neovascular AMD. Ranibizumab (Lucentis; Genentech/Roche, South San Francisco) is a recombinant humanized monoclonal antibody fragment (Fab) that binds to and inhibits all identified VEGF isoforms. It was genetically engineered to have 100 times the binding affinity of bevacizumab. Due to the absence of the Fc segment, ranibizumab exhibits: 1) shorter systemic half-life than bevacizumab, even though both agents are identified in systemic circulation after intravitreal administration (Gaudreault et al. 2005); and 2) better retinal penetration (Ferrara et al. 2006).

The efficacy and safety of ranibizumab for patients with different choroidal neovascular membrane lesion types has been demonstrated in pivotal phase III trials, MARINA (Rosenfeld et al. 2006) and ANCHOR (Brown et al. 2006).

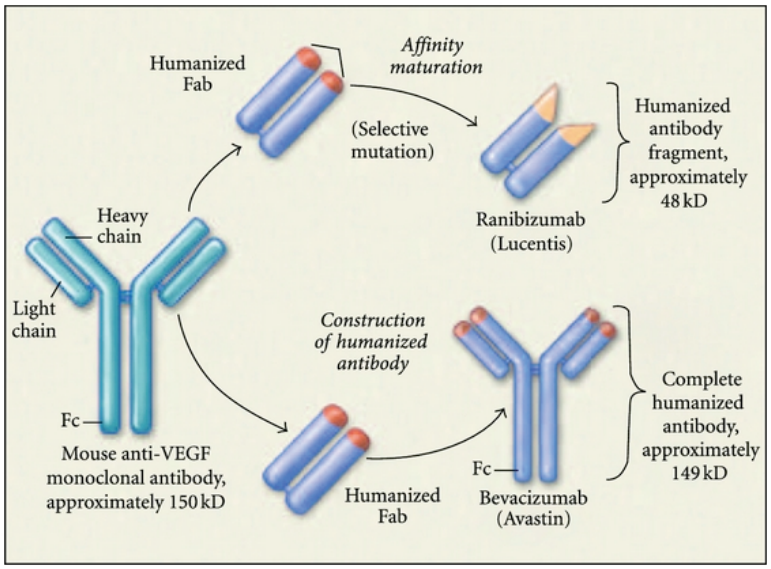

Figure 1.8: The anti-VEGF agents Ranibizumab (Lucentis) and Bevacizumab (Avastin). Ranibizumab is a recombinant humanized monoclonal antibody fragment, whereas bevacizumab a recombinant humanized IgG antibody. Adapted from *Kovach et al. (2013).*

In 2011, FDA approved an additional anti-VEGF agent for the treatment of neovascular macular degeneration. Afibercept VEGF Trap-Eye (EYLEA; Regeneron, Tarrytown, NY, USA) is a soluble fusion protein that inhibits the activity of the VEGF-A and VEGF-B molecules as well as the placental growth factor (PlGF). It is a soluble fusion protein consisting of key receptor domains of VEGFR-1 and VEGFR-2 fused to a constant Fc region of IgG1. VEGF-Trap has stronger affinity to circulating VEGF than either anti-VEGF monoclonal antibodies and that translates into smaller effective doses and potentially a more prolonged biologic effect. VEGF-Trap binds on top of VEGF to the placental growth factor (PlGF). PlGF is found in human neovascular membranes and is

upregulated in experimental mouse models of CNV (Rakic et al. 2003). Efficacy and safety outcomes with afibercept 2mg every 8 weeks have been shown to be comparable to ranibizumab 0.5mg every 4 weeks in two similarly designed, phase-3 studies (VIEW1, VIEW 2) (Heier et al. 2012).

Although many anti-VEGF options exist, no single study reports universal response to anti-VEGF therapies. Research efforts have lately sought to determine whether this response can be genetically determined.

1.7) Genetic markers for AMD treatment outcomes

Pharmacogenetics constitutes an evolving research discipline in ophthalmology. The earliest ophthalmic pharmacogenetic reports involved the treatment of open-angle glaucoma (Schwartz et al. 2005; Sakurai et al. 2007). The discipline seeks to explain inter-patient variability in response to medications by investigating genotype-phenotype interplay. There is now a growing body of data concerning various treatments for age-related macular degeneration (AMD). Pharmacogenetics enable physicians to prescribe individualized treatments based on the patient's genetic background. Identification of protective genetic factors may assist their clinical judgment on overall prognosis. Variations in the treatment aspects of efficacy and toxicity would allow clinicians to move from the current "trial-and-error" treatment approach to personalized medicine based on predicted drug responses. Drug usage in individuals who are susceptible to genotyped-based adverse reactions may be through this way avoided. Protective

haplotypes may also be found which may be efficacious during treatment of the choroidal neovascularization stage. Given the large number of people who are currently at risk to develop CNV and so will require anti-VEGF treatment in the future, understanding of the potential pharmacogenetic relationship is needed to best guide the use and maximize the benefits of these expensive and highly effective interventions.

1.7.A) Pharmacogenetics of AREDS vitamins

Klein et al (2008) investigated potential differences in responsiveness to AREDS vitamins supplementation by doing a retrospective analysis on the data acquired through the large scale Age-Related Eye Disease Study (AREDS) cohort. The authors reported that patients with the "low-risk TT genotype" in CFH Y402H showed greater reduction (68%) in AMD progression compared with those with the "high-risk CC genotype" (11%) from antioxidant and zinc treatment (Klein et al. 2008). No significant associations with AMD progression were seen for the *ARMS2* A69S variant. Their results are an important beginning for the application of pharmacogenetics for personalized medicine for ocular diseases.

As Klein and colleagues acknowledge, an alternative explanation for their findings is that "*the high-risk CC genotype and treatment assignment may reflect disease progression rather than a treatment effect from antioxidants plus zinc*" (Klein et al. 2008). This alternative explanation is supported by a similar

observation that patients with the CFH CC genotype did not respond favorably to intravitreal bevacizumab compared with those patients with the CFH TC and TT genotypes. [See next chapter]. The CFH CC genotype appears to provide prognostic information about disease progression that is not substantially impacted by the currently available treatments.

1.7.B) Pharmacogenetics of Anti-VEGF agents

Some early studies reported that an individual's genetic variation might affect response to bevacizumab and ranibizumab for neovascular AMD. Homozygosity for the high risk Y402H polymorphism in the *CFH* gene (CC genotype) was associated with greater visual acuity loss following treatment with intravitreal bevacizumab (Brantley et al. 2007). This finding was confirmed in a prospective study with twice the number of subjects, where the risk CC genotype was associated with worse visual outcomes (Nischler et al. 2011). In studies with ranibizumab, the TC and TT genotype required fewer injections over a 9-month period. Patients with the CC genotype were 37% more likely to require additional intravitreal injections (Lee et al. 2009). A recent meta-analysis by Chen et al. (2012) showed that the rs1061170 polymorphism in the *CFH* gene was a strong predictor of anti-VEGF treatment response of neovascular AMD. Two of the largest pharmacogenetic studies so far though failed to support these initial associations. A cohort of patients participating in the Comparison of AMD Treatments Trial (CATT) was genotyped for high-risk gene variants in the *CFH*,

ARMS2/HTRA1 and *C3* genes. No association was found between clinical measures of responsiveness to anti-VEGF agents (bevacizumab or ranibizumab) and genotype (Hagstrom et al. 2013). Similarly, the IVAN study (trial of alternative treatments to Inhibit VEGF in Age-related choroidal Neovascularization) showed a lack of genetic association with response to VEGF inhibition therapy (Lotery et al. 2013).

For *ARMS2/HTRA1* and *VEGF*, pharmacogenetic reports have provided inconsistent results to draw firm conclusions. A series of studies found no association between high-risk polymorphisms in *ARMS2/HTRA1* and treatment response with anti-VEGF therapies (Brantley et al. 2007; Kloeckener-Gruissem et al. 2011; McKibbin et al. 2012; Orlin et al. 2012). On the other hand, two studies associated homozygosity for the TT risk allele at *ARMS2* rs10490924 with worse visual outcomes after ranibizumab (Teper et al. 2010) or bevacizumab treatment (Tian et al. 2012). In addition, Abedi et al. (2013) suggested that the HTRA1 promoter SNP (rs11200638) might influence treatment response, a finding not replicated by other groups (McKibbin et al. 2012; Kloeckener-Gruissem et al. 2011; Imai et al., 2010). Polymorphisms in the *VEGF* genes and their receptors (*VEGFR*) have also been investigated as candidate predictors of anti-VEGF treatment response. A trend towards better visual outcomes after ranibizumab therapy has been observed for patients carrying the risk genotype (CC) at rs1413711 of *VEGF* (McKibbin et al. 2012). A higher frequency of the T risk allele for the VEGFA-rs943080 polymorphism has also been associated with poor response to anti-VEGF therapy (Zhao et al. 2013). The rs943080 TT genotype has

also been associated with higher VEGFA expression in human lymphocytes cells compared to the CC genotype. Other studies failed to show any significant correlation between VEGF polymorphisms and treatment response (Boltz et al. 2012; Kloeckener-Gruissem et al. 2011). In the case of VEGF receptors, a polymorphism in the *VEGFR2/KDR* gene was recently found to significantly influence visual outcome in 366 patients receiving ranibizumab treatment (Hermann et al. 2013).

Another approach taken by various groups is to examine the cumulative effect of risk alleles at different loci to create models involving multiple genes. Kloeckener-Gruissem et al. (2011) genotyped 309 patients receiving ranibizumab treatment for neovascular AMD for high-risk SNPs in eight genes: *CFH* (Y402H; rs1061170), *ARMS2* (A69S; rs10490924), *VEGF* (rs699947, rs833069), *VEGFR2/KDR* (rs2071559, rs7671745), *LPR5* (rs3736228) and *FZD4* (rs10898563) (FZD4: frizzled-4; involved in retinal vascular development). Pairwise analysis revealed that patients with a combinational genotype of AG at *CFH* together with CT at *FZD4* had significantly higher chance of better visual outcomes. In a similar study, Smailhodzic et al. (2012) studied 420 eyes receiving ranibizumab treatment and determined the number of risk alleles each patient carried in *CFH*, *ARMS2* and *VEGF*. Those patients without the high-risk alleles in *CFH* and *ARMS2* gained ten letters in visual acuity tests compared to zero letters for those carrying all four risk alleles. By adding *VEGF* into the model, the authors found that patients with all six-risk alleles in *CFH, ARMS2* and *VEGF* lost on average ten letters, suggesting a cumulative effect of the risk alleles with a

poorer response rate to treatment. This multi-SNP approach seems to yield statistically superior results compared to any single SNP analysis done up to this point. AMD is a genetically complex disease and it seems highly likely that predicting treatment response will be genetically complex as well.

1.8) Aim of Thesis II

The second aim of this thesis is to combine genetic information from multiple disease susceptibility loci to better explain differential response to anti-VEGF therapy in neovascular AMD.

BIBLIOGRAPHY

Abedi F, Wickremasinghe S, Richardson AJ, Islam AF, Guymer RH, Baird PN. Genetic influences on the outcome of anti-vascular endothelial growth factor treatment in neovascular age-related macular degeneration. Ophthalmology. 2013 Aug;120(8):1641-8.

Akula JD, Mocko JA, Moskowitz A, Hansen RM, Fulton AB. The oscillatory potentials of the dark-adapted electroretinogram in retinopathy of prematurity. *Invest Ophthalmol Vis Sci.* 2007 Dec;48(12):5788-97.

Allikmets R, Shroyer NF, Singh N, Seddon JM, Lewis RA, Bernstein PS, Peiffer A, Zabriskie NA, Li Y, Hutchinson A, Dean M, Lupski JR, Leppert M. Mutation of the Stargardt disease gene (ABCR) in age-related macular degeneration. Science. 1997 Sep 19;277(5333):1805-7.

Andreoli MT, Morrison MA, Kim BJ, Chen L, Adams SM, Miller JW, DeAngelis MM, Kim IK. Comprehensive analysis of complement factor H and LOC387715/ARMS2/HTRA1 variants with respect to phenotype in advanced age-related macular degeneration. Am J Ophthalmol. 2009 Dec;148(6):869-74.

Boltz A, Ruiß M, Jonas JB, Tao Y, Rensch F, Weger M, Garhöfer G, Frantal S, El-Shabrawi Y, Schmetterer L. Role of vascular endothelial growth factor polymorphisms in the treatment success in patients with wet age-related macular degeneration. Ophthalmology. 2012 Aug;119(8):1615-20.

Booij JC, Baas DC, Beisekeeva J, Gorgels TG, Bergen AA. The dynamic nature of Bruch's membrane. Prog Retin Eye Res. 2010 Jan;29(1)

Brantley MA Jr, Fang AM, King JM, Tewari A, Kymes SM, Shiels A. Association of complement factor H and LOC387715 genotypes with response of exudative age-related macular degeneration to intravitreal bevacizumab. Ophthalmology. 2007 Dec;114(12):2168-73.

Brantley MA Jr, Fang AM, King JM, Tewari A, Kymes SM, Shiels A. Association of complement factor H and LOC387715 genotypes with response of exudative age-related macular degeneration to intravitreal bevacizumab. Ophthalmology. 2007 Dec;114(12):2168-73.

Bresnick GH, Palta M. Oscillatory potential amplitudes. Relation to severity of diabetic retinopathy. Arch Ophthalmol. 1987 Jul;105(7):929-33.

Brown DM, Kaiser PK, Michels M, Soubrane G, Heier JS, Kim RY, Sy JP, Schneider S; ANCHOR Study Group. Ranibizumab versus verteporfin for neovascular age-related macular degeneration. N Engl J Med. 2006 Oct 5;355(14):1432-44.

Brown KT. The eclectroretinogram: its components and their origins. Vision Res. 1968 Jun;8(6):633-77.

Chen H, Yang Z, Gibbs D, Yang X, Hau V, Zhao P, Ma X, Zeng J, Luo L, Pearson E, Constantine R, Kaminoh Y, Harmon J, Tong Z, Stratton CA, Cameron DJ, Tang S, Zhang K. Association of HTRA1 polymorphism and bilaterality in advanced age-related macular degeneration. Vision Res. 2008 Feb;48(5):690-4.

Chen H, Yu KD, Xu GZ. Association between variant Y402H in age-related macular degeneration (AMD) susceptibility gene CFH and treatment response of AMD: a meta-analysis. PLoS One. 2012;7(8):e42464.

Cho Y, Wang JJ, Chew EY, Ferris FL 3rd, Mitchell P, Chan CC, Tuo J. Toll-like receptor polymorphisms and age-related macular degeneration: replication in three case-control samples. Invest Ophthalmol Vis Sci. 2009 Dec;50(12):5614-8.

Davis MD, Gangnon RE, Lee LY, Hubbard LD, Klein BE, Klein R, Ferris FL, Bressler SB, Milton RC; Age-Related Eye Disease Study Group. The Age-Related Eye Disease Study severity scale for age-related macular degeneration: AREDS Report No. 17. Arch Ophthalmol. 2005 Nov;123(11):1484-98.

Dewan A, Liu M, Hartman S, Zhang SS, Liu DT, Zhao C, Tam PO, Chan WM, Lam DS, Snyder M, Barnstable C, Pang CP, Hoh J. HTRA1 promoter polymorphism in wet age-related macular degeneration. Science. 2006 Nov 10;314(5801):989-92.

Edwards AO, Ritter R 3rd, Abel KJ, Manning A, Panhuysen C, Farrer LA. Complement factor H polymorphism and age-related macular degeneration. Science. 2005 Apr 15;308(5720):421-4. Epub 2005 Mar 10.

Ennis S, Jomary C, Mullins R, Cree A, Chen X, Macleod A, Jones S, Collins A, Stone E, Lotery A. Association between the SERPING1 gene and age-related macular degeneration: a two-stage case-control study. Lancet. 2008 Nov 22;372(9652):1828-34.

Fagerness JA, Maller JB, Neale BM, Reynolds RC, Daly MJ, Seddon JM. Variation near complement factor I is associated with risk of advanced AMD. Eur J Hum Genet. 2009 Jan;17(1):100-4.

Ferrara N, Damico L, Shams N, Lowman H, Kim R. Development of

ranibizumab, an anti-vascular endothelial growth factor antigen binding fragment, as therapy for neovascular age-related macular degeneration. Retina. 2006 Oct;26(8):859-70.

Ferrara N. Vascular endothelial growth factor: basic science and clinical progress. Endocr Rev. 2004 Aug;25(4):581-611.

Ferris FL 3rd, Fine SL, Hyman L. Age-related macular degeneration and blindness due to neovascular maculopathy. Arch Ophthalmol. 1984 Nov;102(11):1640-2.

Fisher SA, Abecasis GR, Yashar BM, Zareparsi S, Swaroop A, Iyengar SK, Klein BE, Klein R, Lee KE, Majewski J, Schultz DW, Klein ML, Seddon JM, Santangelo SL, Weeks DE, Conley YP, Mah TS, Schmidt S, Haines JL, Pericak-Vance MA, Gorin MB, Schulz HL, Pardi F, Lewis CM, Weber BH. Meta-analysis of genome scans of age-related macular degeneration. Hum Mol Genet. 2005 Aug 1;14(15):2257-64.

Francis PJ, Schultz DW, Hamon S, Ott J, Weleber RG, Klein ML. Haplotypes in the complement factor H (CFH) gene: associations with drusen and advanced age-related macular degeneration. PLoS One. 2007 Nov 28;2(11):e1197. Miller RF, Dowling JE. Intracellular responses of the Müller (glial) cells of mudpuppy retina: their relation to b-wave of the electroretinogram. J Neurophysiol. 1970 May;33(3):323-41.

Fritsche LG, Chen W, Schu M, et al. Seven new loci associated with age-related macular degeneration. Nat Gen. 2013; 45: 433–439.

Gaudreault J, Fei D, Rusit J, Suboc P, Shiu V. Preclinical

pharmacokinetics of Ranibizumab (rhuFabV2) after a single intravitreal administration. Invest Ophthalmol Vis Sci. 2005 Feb;46(2):726-33.

Gold B, Merriam JE, Zernant J, Hancox LS, Taiber AJ, Gehrs K, Cramer K, Neel J, Bergeron J, Barile GR, Smith RT; AMD Genetics Clinical Study Group, Hageman GS, Dean M, Allikmets R. Variation in factor B (BF) and complement component 2 (C2) genes is associated with age-related macular degeneration. Nat Genet. 2006 Apr;38(4):458-62. Epub 2006 Mar 5.

Hageman GS, Anderson DH, Johnson LV, Hancox LS, Taiber AJ, Hardisty LI, Hageman JL, Stockman HA, Borchardt JD, Gehrs KM, Smith RJ, Silvestri G, Russell SR, Klaver CC, Barbazetto I, Chang S, Yannuzzi LA, Barile GR, Merriam JC, Smith RT, Olsh AK, Bergeron J, Zernant J, Merriam JE, Gold B, Dean M, Allikmets R. A common haplotype in the complement regulatory gene factor H (HF1/CFH) predisposes individuals to age-related macular degeneration. Proc Natl Acad Sci U S A. 2005 May 17;102(20):7227-32.

Hagstrom SA, Ying GS, Pauer GJ, Sturgill-Short GM, Huang J, Callanan DG, Kim IK, Klein ML, Maguire MG, Martin DF; Comparison of AMD Treatments Trials Research Group. Pharmacogenetics for genes associated with age-related macular degeneration in the Comparison of AMD Treatments Trials (CATT). Ophthalmology. 2013 Mar;120(3):593-9.

Haines JL, Hauser MA, Schmidt S, Scott WK, Olson LM, Gallins P, Spencer KL, Kwan SY, Noureddine M, Gilbert JR, Schnetz-Boutaud N, Agarwal A, Postel EA, Pericak-Vance MA. Complement factor H variant increases the risk of age-related macular degeneration. Science. 2005 Apr 15;308(5720):419-21.

Heier JS, Brown DM, Chong V, Korobelnik JF, Kaiser PK, Nguyen QD, Kirchhof B, Ho A, Ogura Y, Yancopoulos GD, Stahl N, Vitti R, Berliner AJ, Soo Y, Anderesi M, Groetzbach G, Sommerauer B, Sandbrink R, Simader C, Schmidt-Erfurth U; VIEW 1 and VIEW 2 Study Groups. Intravitreal aflibercept (VEGF trap-eye) in wet age-related macular degeneration. Ophthalmology. 2012 Dec;119(12):2537-48.

Hermann MM, van Asten F, Muether PS, Smailhodzic D, Lichtner P, Hoyng CB, Kirchhof B, Grefkes C, den Hollander AI, Fauser S. Polymorphisms in Vascular Endothelial Growth Factor Receptor 2 Are Associated with Better Response Rates to Ranibizumab Treatment in Age-related Macular Degeneration. Ophthalmology. 2013 Dec 20. pii: S0161-6420(13)01056-7.

Holopigian K, Greenstein VC, Seiple W, Hood DC, Ritch R. Electrophysiologic assessment of photoreceptor function in patients with primary open-angle glaucoma. J Glaucoma. 2000 Apr;9(2):163-8.

Huang C, Xu Y, Li X, Wang W. Vascular endothelial growth factor A polymorphisms and age-related macular degeneration: a systematic review and meta-analysis. Mol Vis. 2013 Jun 2;19:1211-21.

Huang S, Wu L, Luo T, et al. The electroretinogram in patients with retinal vascular occlusion. *Yan Ke Xue Bao.* 2001 Mar;17(1):50-3.

Imai D, Mori K, Horie-Inoue K, Gehlbach PL, Awata T, Inoue S, Yoneya S. CFH, VEGF, and PEDF genotypes and the response to intravitreous injection of bevacizumab for the treatment of age-related macular degeneration. J Ocul Biol Dis Infor. 2010 Jun;3(2):53-9.

Jakobsdottir J, Conley YP, Weeks DE, Mah TS, Ferrell RE, Gorin MB. Susceptibility genes for age-related maculopathy on chromosome 10q26. Am J Hum Genet. 2005 Sep;77(3):389-407.

Kaur I, Rathi S, Chakrabarti S. Variations in TIMP3 are associated with age-related macular degeneration. Proc Natl Acad Sci U S A. 2010 Jul 13;107(28)

Kizawa J, Machida S, Kobayashi T, Gotoh Y, Kurosaka D. Changes of oscillatory potentials and photopic negative response in patients with early diabetic retinopathy. Jpn J Ophthalmol. 2006 Jul-Aug;50(4):367-73.

Klein ML, Francis PJ, Rosner B, Reynolds R, Hamon SC, Schultz DW, Ott J, Seddon JM. CFH and LOC387715/ARMS2 genotypes and treatment with antioxidants and zinc for age-related macular degeneration. Ophthalmology. 2008 Jun;115(6):1019-25.

Klein RJ, Zeiss C, Chew EY, Tsai JY, Sackler RS, Haynes C, Henning AK, SanGiovanni JP, Mane SM, Mayne ST, Bracken MB, Ferris FL, Ott J, Barnstable C, Hoh J. Complement factor H polymorphism in age-related macular degeneration. Science. 2005 Apr 15;308(5720):385-9. Epub 2005 Mar 10.

Kloeckener-Gruissem B, Barthelmes D, Labs S, Schindler C, Kurz-Levin M, Michels S, Fleischhauer J, Berger W, Sutter F, Menghini M. Genetic association with response to intravitreal ranibizumab in patients with neovascular AMD. Invest Ophthalmol Vis Sci. 2011 Jul 1;52(7):4694-702.

Kovach JL, Schwartz SG, Flynn HW Jr, Scott IU. Anti-VEGF Treatment Strategies for Wet AMD. J Ophthalmol. 2012;2012:786870.

Lee AY, Raya AK, Kymes SM, Shiels A, Brantley MA Jr.

Pharmacogenetics of complement factor H (Y402H) and treatment of exudative age-related macular degeneration with ranibizumab. Br J Ophthalmol. 2009 May;93(5):610-3.

Leveziel N, Puche N, Richard F, Somner JE, Zerbib J, Bastuji-Garin S, Cohen SY, Korobelnik JF, Sahel J, Soubrane G, Benlian P, Souied EH. Genotypic influences on severity of exudative age-related macular degeneration. Invest Ophthalmol Vis Sci. 2010 May;51(5):2620-5.

Leveziel N, Zerbib J, Richard F, Querques G, Morineau G, Fremeaux-Bacchi V, Coscas G, Soubrane G, Benlian P, Souied EH. Genotype-phenotype correlations for exudative age-related macular degeneration associated with homozygous HTRA1 and CFH genotypes. Invest Ophthalmol Vis Sci. 2008 Jul;49(7):3090-4.

Li X, Sun X, Hu Y, Huang J, Zhang H. Electroretinographic oscillatory potentials in diabetic retinopathy. An analysis in the domains of time and frequency. Doc Ophthalmol. 1992;81(2):173-9.

Liu K, Chen LJ, Lai TY, Tam PO, Ho M, Chiang SW, Liu DT, Young AL, Yang Z, Pang CP. Genes in the High-Density Lipoprotein Metabolic Pathway in Age-Related Macular Degeneration and Polypoidal Choroidal Vasculopathy. Ophthalmology. 2014 Jan 3.

Lotery AJ, Gibson J, Cree AJ, Downes SM, Harding SP, Rogers CA, Reeves BC, Ennis S, Chakravarthy U; Alternative Treatments to Inhibit VEGF in Patients with Age-Related Choroidal Neovascularisation (IVAN) Study Group. Pharmacogenetic associations with vascular endothelial growth factor inhibition

in participants with neovascular age-related macular degeneration in the IVAN Study. Ophthalmology. 2013 Dec;120(12):2637-43.

Majewski J, Schultz DW, Weleber RG, Schain MB, Edwards AO, Matise TC, Acott TS, Ott J, Klein ML. Age-related macular degeneration--a genome scan in extended families. Am J Hum Genet. 2003 Sep;73(3):540-50.

Martinez-de-la-Casa JM, Ruiz-Calvo A, Saenz-Frances F, Reche-Frutos J, Calvo-Gonzalez C, Donate-Lopez J, Garcia-Feijoo J. Retinal nerve fiber layer thickness changes in patients with age-related macular degeneration treated with intravitreal ranibizumab. Invest Ophthalmol Vis Sci. 2012 Sep 14;53(10):6214-8.

McKibbin M, Ali M, Bansal S, Baxter PD, West K, Williams G, Cassidy F, Inglehearn CF. CFH, VEGF and HTRA1 promoter genotype may influence the response to intravitreal ranibizumab therapy for neovascular age-related macular degeneration. Br J Ophthalmol. 2012 Feb;96(2):208-12.

Nischler C, Oberkofler H, Ortner C, Paikl D, Riha W, Lang N, Patsch W, Egger SF. Complement factor H Y402H gene polymorphism and response to intravitreal bevacizumab in exudative age-related macular degeneration. Acta Ophthalmol. 2011 Jun;89(4):e344-9.

Nishijima K, Ng YS, Zhong L, Bradley J, Schubert W, Jo N, Akita J, Samuelsson SJ, Robinson GS, Adamis AP, Shima DT. Vascular endothelial growth factor-A is survival factor for retinal neurons and a critical neuroprotectant during the adaptive response to ischemic injury. Am J Pathol. 2007 Jul;171(1):53-67.

Orlin A, Hadley D, Chang W, Ho AC, Brown G, Kaiser RS, Regillo CD,

Godshalk AN, Lier A, Kaderli B, Stambolian D. Association between high-risk disease loci and response to anti-vascular endothelial growth factor treatment for wet age-related macular degeneration. Retina. 2012 Jan;32(1):4-9.

Pai AS, Mitchell P, Rochtchina E, Iyengar S, Wang JJ; Blue Mountains Eye Study. Complement factor H and the bilaterality of age-related macular degeneration. Arch Ophthalmol. 2009 Oct;127(10):1339-44.

Qazi Y, Maddula S, Ambati BK. Mediators of ocular angiogenesis. J Genet. 2009 Dec;88(4):495-515.

Rakic JM, Lambert V, Devy L, Luttun A, Carmeliet P, Claes C, Nguyen L, Foidart JM, Noël A, Munaut C. Placental growth factor, a member of the VEGF family, contributes to the development of choroidal neovascularization. Invest Ophthalmol Vis Sci. 2003 Jul;44(7):3186-93.

Ronan S, Nusinowitz S, Swaroop A, Heckenlively JR. Senile panretinal cone dysfunction in age-related macular degeneration (AMD): a report of 52 AMD patients compared to age-matched controls. Trans Am Ophthalmol Soc. 2006; 104: 232–240.

Rosenfeld PJ, Brown DM, Heier JS, Boyer DS, Kaiser PK, Chung CY, Kim RY; MARINA Study Group. Ranibizumab for neovascular age-related macular degeneration. N Engl J Med. 2006 Oct 5;355(14):1419-31.

Rosenfeld PJ, Moshfeghi AA, Puliafito CA. Optical coherence tomography findings after an intravitreal injection of bevacizumab (avastin) for neovascular age-related macular degeneration. Ophthalmic Surg Lasers Imaging. 2005 Jul-Aug;36(4):331-5.

Saint-Geniez M, Maharaj AS, Walshe TE, Tucker BA, Sekiyama E, Kurihara T, Darland DC, Young MJ, D'Amore PA. Endogenous VEGF is required for visual function: evidence for a survival role on müller cells and photoreceptors. PloS One. 2008;3(11):e3554.

Sakurai M, Higashide T, Takahashi M, Sugiyama K. Association between genetic polymorphisms of the prostaglandin F2alpha receptor gene and response to latanoprost. Ophthalmology. 2007 Jun;114(6):1039-45.

Schultz DW, Klein ML, Humpert AJ, Luzier CW, Persun V, Schain M, Mahan A, Runckel C, Cassera M, Vittal V, Doyle TM, Martin TM, Weleber RG, Francis PJ, Acott TS. Analysis of the ARMD1 locus: evidence that a mutation in HEMICENTIN-1 is associated with age-related macular degeneration in a large family. Hum Mol Genet. 2003 Dec 15;12(24):3315-23.

Schwartz SG, Puckett BJ, Allen RC, Castillo IG, Leffler CT. Beta1-adrenergic receptor polymorphisms and clinical efficacy of betaxolol hydrochloride in normal volunteers. Ophthalmology. 2005 Dec;112(12):2131-6.

Seddon JM, Francis PJ, George S, Schultz DW, Rosner B, Klein ML. Association of CFH Y402H and LOC387715 A69S with progression of age-related macular degeneration. JAMA. 2007 Apr 25;297(16):1793-800.

Shuler RK Jr, Schmidt S, Gallins P, Hauser MA, Scott WK, Caldwell J, Agarwal A, Haines JL, Pericak-Vance MA, Postel EA. Peripheral reticular pigmentary change is associated with complement factor H polymorphism (Y402H) in age-related macular degeneration. Ophthalmology. 2008 Mar;115(3):520-4.

Smailhodzic D, Muether PS, Chen J, Kwestro A, Zhang AY, Omar A, Van de Ven JP, Keunen JE, Kirchhof B, Hoyng CB, Klevering BJ, Koenekoop RK, Fauser S, den Hollander AI. Cumulative effect of risk alleles in CFH, ARMS2, and VEGFA on the response to ranibizumab treatment in age-related macular degeneration. Ophthalmology. 2012 Nov;119(11):2304-11.

Smith W, Assink J, Klein R, Mitchell P, Klaver CC, Klein BE, Hofman A, Jensen S, Wang JJ, de Jong PT. Risk factors for age-related macular degeneration: Pooledfindings from three continents. Ophthalmology. 2001 Apr;108(4):697-704.

Sofat R, Casas JP, Webster AR, Bird AC, Mann SS, Yates JR, Moore AT, Sepp T, Cipriani V, Bunce C, Khan JC, Shahid H, Swaroop A, Abecasis G, Branham KE, Zareparsi S, Bergen AA, Klaver CC, Baas DC, Zhang K, Chen Y, Gibbs D, Weber BH, Keilhauer CN, Fritsche LG, Lotery A, Cree AJ, Griffiths HL, Bhattacharya SS, Chen LL, Jenkins SA, Peto T, Lathrop M, Leveillard T, Gorin MB, Weeks DE, Ortube MC, Ferrell RE, Jakobsdottir J, Conley YP, Rahu M, Seland JH, Soubrane G, Topouzis F, Vioque J, Tomazzoli L, Young I, Whittaker J, Chakravarthy U, de Jong PT, Smeeth L, Fletcher A, Hingorani AD. Complement factor H genetic variant and age-related macular degeneration: effect size, modifiers and relationship to disease subtype. Int J Epidemiol. 2012 Feb;41(1):250-62.

Teper SJ, Nowinska A, Pilat J, Palucha A, Wylegala E. Involvement of genetic factors in the response to a variable-dosing ranibizumab treatment regimen for age-related macular degeneration. Mol Vis. 2010 Dec 7;16:2598-604.

Tian J, Qin X, Fang K, Chen Q, Hou J, Li J, Yu W, Chen D, Hu Y, Li X.

Association of genetic polymorphisms with response to bevacizumab for neovascular age-related macular degeneration in the Chinese population. Pharmacogenomics. 2012 May;13(7):779-87.

van der Torren K, Mulder P. Comparison of the second and third oscillatory potentials with oscillatory potential power in early diabetic retinopathy. Doc Ophthalmol. 1993;83(2):111-8.

Van Lith GHM. The macular function in the ERG. Doc Ophthalmol Proc Ser. 1976; 10: 405–415.

Wachtmeister L, Dowling JE. The oscillatory potentials of the mudpuppy retina. Invest Ophthalmol Vis Sci. 1978 Dec;17(12):1176-88.

Wachtmeister L. Oscillatory potentials in the retina: what do they reveal. Prog Retin Eye Res. 1998 Oct;17(4):485-521.

Walter P, Widder RA, Luke C, et al. Electrophysiologic abnormalities in age-related macular degeneration. Graefes Arch Clin Exp Ophthalmol. 1999; 237: 962–968.

Wang JJ, Foran S, Smith W, Mitchell P. Risk of age-related macular degeneration in eyes with macular drusen or hyperpigmentation: the Blue Mountains Eye Study cohort. Arch Ophthalmol. 2003 May;121(5):658-63.

Westall CA, Nobile R, Morong S, Buncic JR, Logan WJ, Panton CM. Changes in the electroretinogram resulting from discontinuation of vigabatrin in children. Doc Ophthalmol. 2003 Nov;107(3):299-309.

Yang Z, Camp NJ, Sun H, Tong Z, Gibbs D, Cameron DJ, Chen H, Zhao Y, Pearson E, Li X, Chien J, Dewan A, Harmon J, Bernstein PS, Shridhar V,

Zabriskie NA, Hoh J, Howes K, Zhang K. A variant of the HTRA1 gene increases susceptibility to age-related macular degeneration. Science. 2006 Nov 10;314(5801):992-3.

Yates JR, Sepp T, Matharu BK, Khan JC, Thurlby DA, Shahid H, Clayton DG, Hayward C, Morgan J, Wright AF, Armbrecht AM, Dhillon B, Deary IJ, Redmond E, Bird AC, Moore AT; Genetic Factors in AMD Study Group. Complement C3 variant and the risk of age-related macular degeneration. N Engl J Med. 2007 Aug 9;357(6):553-61.

Yu M, Liang X, Wen F, Wu DZ, Luo T. Analysis of oscillatory potentials of flash electroretinogram in frequency domain and time domain in retinal vein occlusion. *Yan Ke Xue Bao.* 1998 Sep;14(3):176-81, 144.

Yu Y, Reynolds R, Fagerness J, Rosner B, Daly MJ, Seddon JM. Association of variants in the LIPC and ABCA1 genes with intermediate and large drusen and advanced age-related macular degeneration. Invest Ophthalmol Vis Sci. 2011 Jun 28;52(7):4663-70.

Zhao L, Grob S, Avery R, Kimura A, Pieramici D, Lee J, Rabena M, Ortiz S, Quach J, Cao G, Luo H, Zhang M, Pei M, Song Y, Tornambe P, Goldbaum M, Ferreyra H, Kozak I, Zhang K. Common variant in VEGFA and response to anti-VEGF therapy for neovascular age-related macular degeneration. Curr Mol Med. 2013 Jul;13(6):929-34.

Chapter 2. ELECTROPHYSIOLOGICAL ABNORMALITIES IN AGE-RELATED MACULAR DEGENERATION[1]

INTRODUCTION

AMD is the leading cause of blindness in the elderly of the Western world (Friedman et al. 2004). Since the prevalence of AMD is expected to increase from 1.75 million individuals to 2.95 million individuals by 2020 (Thylefors B. 1998), it is essential to delineate the pathophysiological events that take place prior to vision loss in AMD. Early-stage AMD is characterized by changes in the Bruch's membrane, choriocapillaris and RPE that gradually impair photoreceptor viability. Late-stage AMD, on the other hand, is characterized by complete loss of the supporting RPE layer (geographic atrophy, most advanced form of dry AMD) in the macular region and/or abnormal growth of choroidal blood vessels (neovascular AMD, also called wet AMD). Although representing only 10% of all AMD cases, these advanced forms are responsible for 90% of the vision loss attributed to AMD (Ferris et al. 1984).

The risk factors involved in progression to advanced AMD include age, smoking history, and diet (more specifically antioxidant and omega-3 fatty acid intake) (Meleth et al. 2009). In addition, several genetic determinants have been

---

[1] A version of this chapter has been published:
Dimopoulos IS, Tennant M, Johnson A, Fisher S, Freund PR, Sauvé Y. Subjects with unilateral neovascular AMD have bilateral delays in rod-mediated phototransduction activation kinetics and in dark adaptation recovery. *Invest Ophthalmol Vis Sci.* 2013 Aug 5;54(8):5186-95.

identified (Gorin MB 2012). These include polymorphisms in genes involved in regulation of complement activity, lipid metabolism, extracellular matrix remodeling, and angiogenesis (Fritsche et al. 2013).

The role of the alternate complement pathway appears crucial to disease pathogenesis and progression (Farwick et al. 2009). Activated complement components have been reported to correlate with disease stage in both the vitreous and the serum of patients with AMD (Loyet et al. 2012; Scholl et al. 2008). Together with previous evidence from psychophysical tests (Steinmetz et al. 1993; Jackson et al. 2002; Polyak SL 1941), these findings suggest that AMD may be a systemic disease manifesting locally in the aging macula (Loyet et al. 2012). We can, therefore, hypothesize that the pathological and functional alterations could extend beyond the macula, and involve the whole retina.

Numerous studies have relied on full-field ERG as a mean to assess functional changes across the whole retina. The ERG represents a mass response from the neural retina elicited by flashes of various intensities and wavelengths, under specific light adaptation levels. By controlling these variables, it is possible to isolate rod- from cone-driven contribution, as well as to distinguish pre- from postsynaptic activity of the mass potential response. Historically, due to the regional macular dysfunction typifying AMD, full-field ERG has not been used in the study of AMD progression. Since the macula represents only 5% of the whole retinal surface area, dysfunction confined to this region does not result in impaired full-field ERG response (Van Lith GHM 1976). The multifocal ERG has been developed specifically to assess regional function, such as from the macula, but it

is limited to cone-driven responses. Past full-field ERG studies have shown conflicting findings in AMD, most likely reflecting the complex nature of the disease. These findings include a global reduction in retinal function (Walter et al. 1999) and a generalized cone dysfunction in subgroups of AMD patients (Ronan et al. 2006). An increasing number of studies point to an early-onset rod dysfunction that precedes cone dysfunction in AMD (Steinmetz et al. 1993; Jackson et al. 2002; Jackson and Owsley 2000). Jackson et al. (2004) extensively studied the phototransduction activation and deactivation kinetics of rods as a function of AMD progression. Although neither the activation and deactivation kinetics were affected in dry AMD (Jackson et al. 2004, 2006) the wet form was characterized by a dramatic delay of rod inactivation kinetics.

The purpose of our study was to investigate panretinal rod and cone function in both eyes of individuals with already established neovascular AMD in a single eye. The rationale for choosing this population was that wet AMD in one eye represents the most reliable risk factor for the fellow eye (dry AMD) to progress to the neovascular form (Barbazetto et al. 2010). We predicted that ERG recordings from these high-risk individuals would reveal dysfunctions involving the whole retina in both eyes, therefore challenging the widely accepted notion of a disease confined to the macula.

MATERIAL AND METHODS

This study received ethics approval from the Health Research Ethics Board (Biomedical Panel) of the University of Alberta. All procedures conformed to the Code of Ethics of the World Medical Association (Declaration of Helsinki). ERG recordings were done with the understanding and written consent of each subject after detailed explanation of the nature and possible consequences of the study. All data were analyzed in an aggregated fashion.

Patients

Patients from the Alberta Retina Clinic (ARC) were invited to participate in this study. Twenty-five subjects (mean age: 73.6, SD: 8.9) with unilateral neovascular macular degeneration (Age-Related Eye Disease Study [AREDS] severity scale: 11b (Davis et al. 2005); definite end-stage disease) were recruited in the study. Absence of wet AMD in the fellow eye was confirmed by OCT. All subjects were undergoing treatment in their neovascular eye with intravitreal injections of anti-VEGF agents. The number of injections did not differ among subjects (mean: 11 monthly injections). Subjects with cataracts or previous ocular surgery (with the exception of cataract surgery) were excluded. Other exclusion criteria included diagnosis of diabetic retinopathy, glaucoma, ocular hypertension or optic neuropathy, and any history of medication known to be toxic to the retina or optic nerve (deferoxamine, chloroquine, tamoxifen, chlorpromazine, phenothiazines, chronic systemic steroid use of more than 10 mg per day, and ethambutol). Eleven of the AMD subjects had undergone bilateral cataract surgery with intraocular lens placement. Data from a group of 18 age-matched (69 ± 5) controls were used

for comparison. Twelve additional pseudophakic control subjects (71 ± 4) were used for the dark-adaptation analysis. Control subjects had best-corrected visual acuity 20/20 or better, with no current or past ocular history and their fundus appearance was free of drusen or pigmentary anomalies (AREDS scale: step 1).

Fellow eye dry AMD severity grading

Modified three-field 30° stereoscopic color fundus photographs were acquired after dilation using a Visucam NM Pro (Visucam, Zeiss, Germany) fundus camera. Non-neovascular fellow eyes were evaluated for dry AMD severity based on the 9-step AREDS severity scale (Davis et al. 2005) which combines a six-step drusen area scale with a five-step pigmentary abnormality scale. All grading was performed by an independent former Wisconsin Reading Center grader (JA), masked to patient characteristics and ERG recording. For grouping and comparison purposes, eyes with AREDS scale scores of 1 to 3 were characterized as early AMD (AMD1), 4 to 6 as intermediate (AMD2), and 7 to 9 as advanced (AMD3). Subjects in AMD3 group had extensive areas of decreased pigment up to 0.5 DA (disc area) and/or noncentral geographic atrophy. Representative examples for each group are provided in Figure 2.1

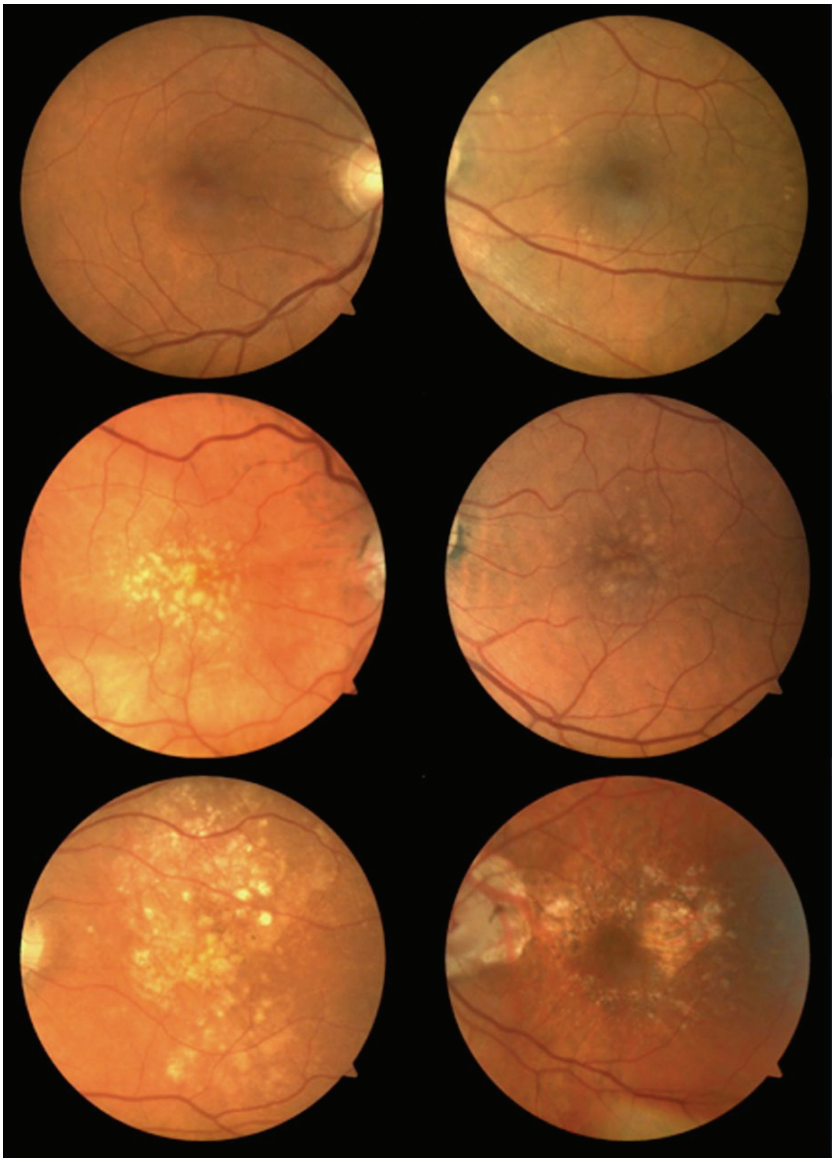

Figure 2.1: Representative dry AMD fundus photographs. Images from the fellow eyes of patients with unilateral neovascular AMD. Top row: Eyes classified as AMD1 had several hard drusen or a few intermediate size drusen. Middle row: Eyes classified as AMD2 had large, soft drusen or several intermediate size drusen with increased pigmentation. Bottom row: Eyes classified as AMD3 had large drusen with extensive areas of depigmentation up to 0.5DA. Noncentral geographic atrophy was included in this category.

ERG recordings

The subjects underwent bilateral full-field ERG recordings (Espion E^2system; Diagnosys LLC, Lowell, MA) in accordance with International Society for Clinical Electrophysiology of Vision (ISCEV) standard protocols (Marmor et al. 2009) and supplemented by custom-made analytical protocols described below. Pupils were dilated using two drops of 1% Tropicamide applied on the corneal surface of each eye. Testing lasted 1.5 hours and began after full mydriasis was achieved (>6.5 mm pupil diameter); full mydriatic effect of the eye drops was confirmed in all subjects after the end of the testing period. Recording electrodes consisted of Dawson-Trick-Litzkow type (DTL) fiber electrodes with references electrodes (gold surface electrode, F-E5GH-60; Grass Technologies, West Warwick, RI) placed on the lateral edge of the orbital bone. The ground electrode (gold surface electrode) was centered on the forehead, 1 inch above the upper eyebrow line. All stimuli consisted of white flashes generated by a xenon bulb (6500°K color temperature, 10 μs duration) unless specifically noted. Calibration of light levels was achieved using an IL1700 photometer (International Light Technologies, Inc., Peabody, MA) equipped with either a photopic or scotopic filter (McCullough et al. 2010).

Amplitudes and implicit times of the a- and b-waves were measured by strictly adhering to the standards provided by the ISCEV (Marmor et al. 2009). B/A wave ratios were examined only when both a- and b-waves exceeded criterion response (10 μV). Criterion amplitudes were set at 10 μV, a magnitude below which the signal could not be clearly distinguished from background noise. For all traces

obtained, both a- and b-waves were clearly distinguishable when exceeding 10 μV in amplitude; both their amplitude and implicit times could be measured accurately.

Photopic ERG

Pure cone-driven responses were studied under photopic conditions (30 cd/m^2, measured at the corneal surface), by presenting single white flashes (as described above) with increasing time-integrated luminances along 11 stepwise increments: −1.63, −1.22, −0.81, −0.42, −0.02, 0.38, 0.88, 1.37, 1.89, 2.39, and 2.86 photopic log cd s/m^2 (logarithm of candela seconds/meters square). Time interval between each step was 10 seconds and each stimulus was presented two to six times at 5-second intervals (six times for steps 1–8, two times for steps 9–11). Responses to flashes of a given strength were averaged at each step. Amplitudes and implicit times of the a- and b-waves were measured as described above.

Dark-adaptation

Subjects were dark adapted for 20 minutes after conclusion of the photopic ERG recordings. Bleaching conditions were identical in all study subjects as previously published (Freund et al. 2011) and consisted of a 10-minute exposure to 30 cd/m^2 background in addition to the last six sets of bright flashes (steps 9–11) of an average of 2.38 photopic log cd s/m^2 each. Consistency of this bleaching regimen among groups was confirmed by the observation that normalized pure rod b-wave amplitudes recorded at time zero (just after transition from light to

dark-adapted background) were 5% to 10% of the fully dark-adapted values. To study the process of dark adaptation, the amplitude of the pure rod b-wave was assessed every 120 seconds (starting at $t = 0$ minutes, 11 steps in total) using the standard ISCEV dim flash of −2.04 log cd s/m^2. Each step consisted of five repeats with 5-second intervals between them. Responses were averaged at each step.

Dark-adapted ERG

Dark-adapted subjects were stimulated using 16 flashes of increasing strengths(−5.22, −4.70, −4.22, −3.70, −3.22, −2.82, −2.44, −2.04, −1.63, −1.22, −0.81, −0.42, −0.02, 0.38, 0.88, and 1.37 scotopic log cd s/m^2), each averaged three to five times. To allow for maximal rod recovery between consecutive flashes, interstimuli intervals were increased from 4 seconds at the lowest stimulus strength up to 60 seconds at the highest stimulus strength (Pepperberg et al. 1996).

To isolate rod photoresponses, photopic ERG responses were subtracted from the mixed dark-adapted responses elicited by stimuli of the same intensities; this exercise was applied for the responses elicited by the three highest intensity stimuli (0.38, 0.88, and 1.37 scotopic log cd s/m^2). For each subject, these isolated rod responses were fitted to the following equation to describe the response (R) as function of flash intensity (I), and time (t), based on the Hood and Birch formulation (Hood and Birch 1994) of the Lamb and Pugh model (Lamb and Pugh 1992):

$$R(I,t) = [1 - \exp\{-I \cdot S \cdot (t - t_d)^2\}] \cdot Rm_{P3}$$

where S is sensitivity, t_d is the delay before onset of the a-wave, and Rm_{P3} is the maximum amplitude (Figure 2.2). All curve fits were performed using Igor Pro (Wavemetrics, Inc., Lake Oswego, OR) and satisfied a least-squares goodness-of-fit criterion (R^2) of at least 0.90. Best-fit variables S and Rm_{P3} were calculated and transformed to log values for data analysis.

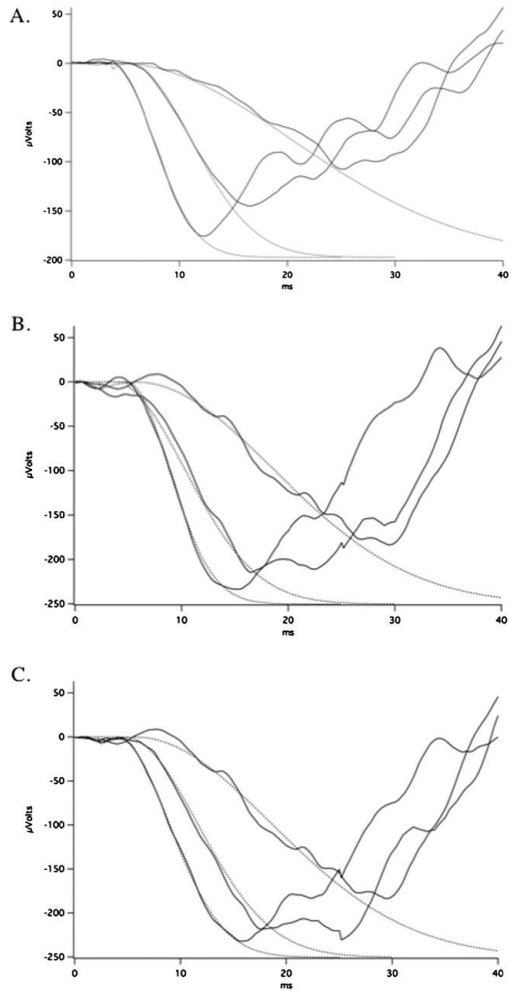

Figure 2.2: Fitting of rod-isolated ERG a-wave leading edge. Representative ERG recordings (solid curves) and best fit (dashed curves) from an age-matched non-AMD eye (A), dry AMD eye (B), and wet AMD eye (C) (same patient for

[B, C]) elicited by white flash stimuli ranging in energy from 0.93 to 3.36 log phot td-s; note that a tight fit was obtained independently of the stimulus intensity and state of the eye (non-, dry, or wet AMD).

Statistics

Statistical significance between groups was assessed using repeated-measures ANOVA with the Greenhouse-Geisser correction for sphericity. Post hoc analyses were done between the individual groups and at individual stimulus strengths or time points using the Bonferroni technique for multiple comparisons. Graphpad Prism was used for one-way ANOVA, linear regression, and correlation analyses (Graphpad Software, Inc., La Jolla CA). SPSS was used for the repeated-measures ANOVA (SPSS, Inc., Chicago, IL). Significance was set at P less than 0.05. Data points on graphs represent mean ± 95% confidence interval (95% CI).

RESULTS

Light-adapted responses

Figures 2.3A through 3E provide the intensity-response curves for the photopic a- and b-waves. There were no differences in any of the related parameters (amplitude, implicit time, and b/a ratio) among groups. For instance, in all subjects, the b-wave luminance response function followed the pattern of the previously described "photopic hill" (Rufiange et al. 2003): initial amplitude increase as a function of flash strength increments, peaking halfway along the *x*-axis, followed by a nadir (this pattern was named due to its resemblance to a

“hill”). The peak of this “photopic hill” always occurred at the same light strength independently of the group.

The maximal b-wave amplitude (b_{max}) was recorded with a flash intensity of 7.67 cd s/m^2 photopic units. This intensity was selected as it preceded the onset of the photopic hill in all subjects. To test whether maximal b-wave amplitude was related to macular phenotype severity, a subgroup analysis was performed. Scatter plots of cone b-wave amplitudes in all subgroups are illustrated in Figure 2.3F. Even though no overall group mean difference was reported ($P = 0.15$), 19 of 45 eyes had values below the 2.5% percentile of our control data set. Subjects with AMD3 features in the fellow eye (displaying morphological features of nonexudative AMD and extensive areas of hypopigmentation or noncentral geographic atrophy) were more likely to fall into this category.

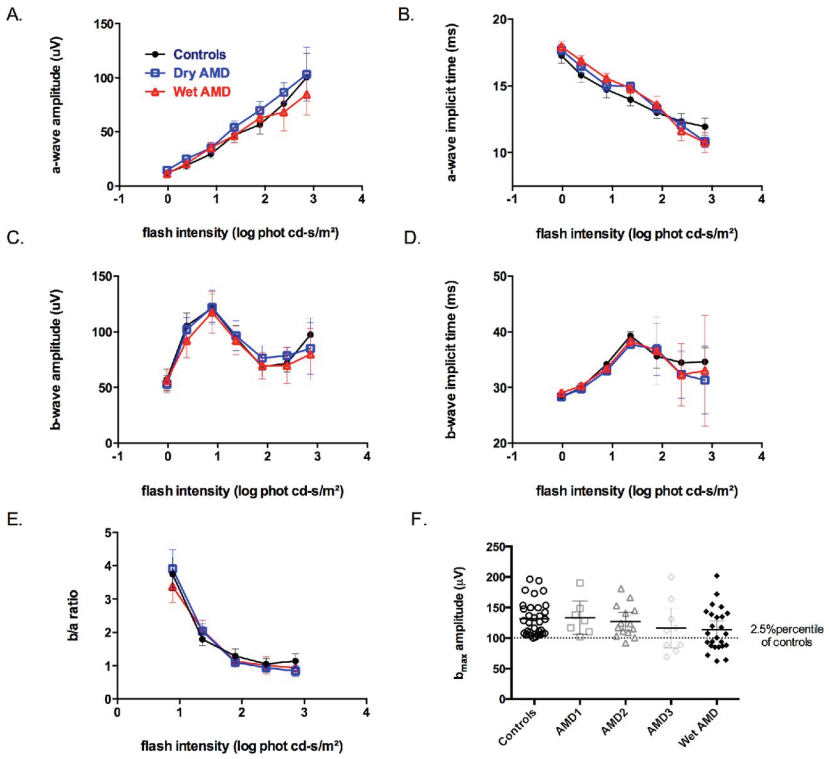

Figure 2.3: Pure cone-driven ERG responses. Stimuli ranging in intensity from −0.02 to 2.86 photopic log cd s/m2. Intensity responses for a-wave amplitude (A) and implicit time (B) as well as for b-wave amplitude (C) and implicit time (D), and finally for b/a ratio (E) are provided for the three eye groups studied: controls (black), dry AMD (blue), and wet AMD (red). (F) Maximal b-wave amplitudes were calculated for each eye per group; dry AMD eyes were divided into three severity levels: AMD1, AMD2, and AMD3.

Dark adaptation

During the 20-minute dark adaptation, there was a progressive increase between five- and six-fold in pure rod b-wave amplitude for all groups (Figure 2.4). Due to significant interindividual variability in fully recovered amplitudes at $t = 20$ (coefficient of variation > 30%), normalized values at each time point were used for all subjects (Figure 2.4). Averaged data points were fitted to a sigmoid function of the form:

$$y = \frac{base + \max}{1 + \exp\left(\frac{thalf - t}{t_{10}}\right)},$$

where y represents normalized b-wave amplitude; *base* represents normalized pure rod b-wave amplitude values at the beginning of the dark adaptation ($t = 0$); *thalf* represents the time to reach half the maximum normalized amplitude value (0.5); t represents time, and t_{10} represents the inverse slope as measured at 10 minutes (at which point linearity of the sigmoid curve was optimal). This inverse slope has the dimensions of time. All curves met a goodness of fit (R^2) of at least 0.95.

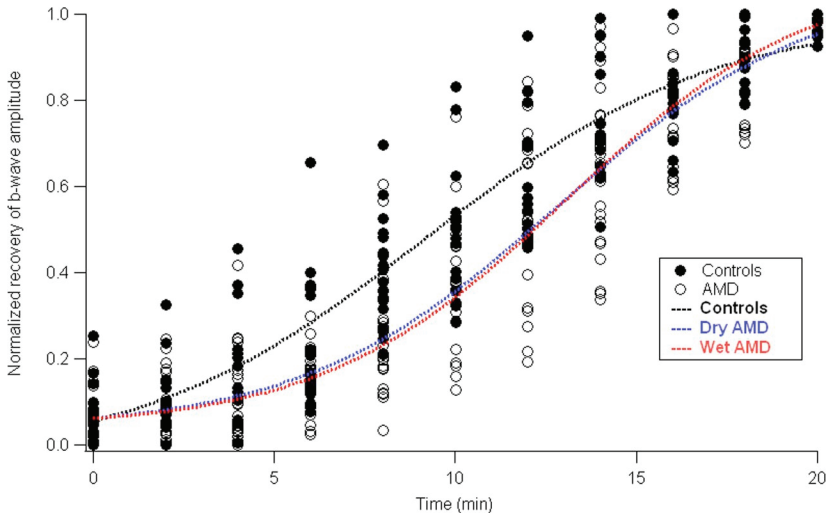

Figure 2.4: Dark adaptation curves. Raw data. To ensure optimal clarity of the individual data points (*circles*), data from both eyes of all respective AMD subjects were pooled (*hollow black circles*); the rationale for this grouping was to distinguish values of control eyes from those of AMD eyes. The *y*-axis represents the pure rod b-wave amplitude normalized against amplitude at 20 minutes of dark adaptation; *x*-axis represents time in minutes following transition from light to dark adaptation. *Fitted lines* (*all dashed*): controls (*black*), dry AMD (*blue*), and wet AMD (*red*).

Best-fit parameters for *thalf* and *rate* were calculated for all groups (Figure 2.5). Base values were identical for all three groups (0.04 ± 0.02 for non-AMD eyes, 0.04 ± 0.02 for dry AMD eyes, and 0.04 ± 0.02 for neovascular AMD eyes). Therefore, the marginal rod contribution prior to beginning dark adaptation was not affected by AMD status. Best-fit coefficient values for *thalf,* the time to reach

half of the fully recovered pure rod b-wave amplitude (obtained at the end of the dark adaptation, i.e., $t = 20$ minutes), were significantly higher ($P < 0.0001$) in AMD eyes. These were estimated to be 9 ± 0.4 minimum for the non-AMD group, 13 ± 0.4 for the dry AMD eyes, and 13 ± 0.3 for the wet AMD eyes. In addition, the slope parameter of the fitted curve (*rate*) was reduced compared to controls ($P = 0.0008$), implying a delay in recovery (not illustrated). The dynamic of recovery was equally delayed in both neovascular (wet AMD) and their fellow eyes (dry AMD). Inclusion of all subjects or subanalysis limited to pseudophakic subjects yielded similar results. As such, to eliminate potential contributions of various levels of lens opacification, we restricted data presentation to subjects with artificial lenses in both eyes ($n = 12$ AMD and $n = 11$ control subjects).

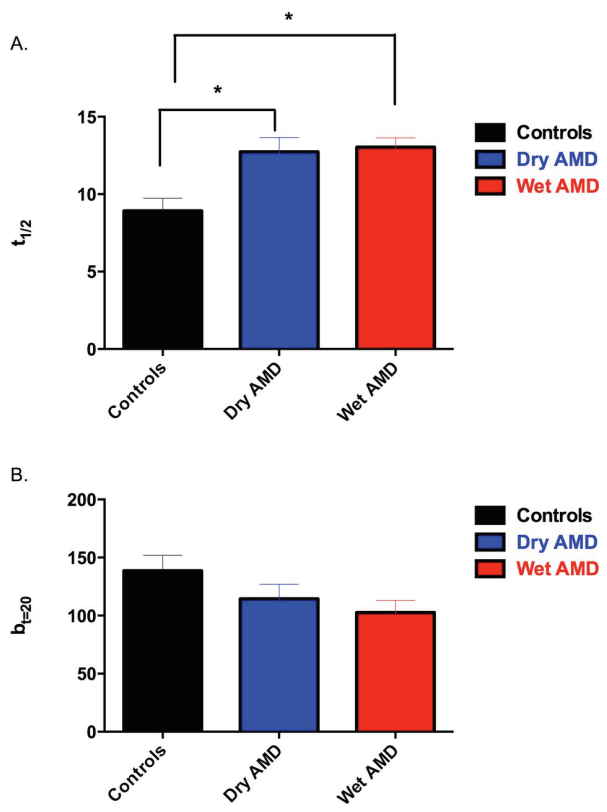

Figure 2.5: Dark adaptation results. Time to reach 50% recovery of pure rod b-wave amplitude (**A**) and amplitude reached at 20 minutes of dark adaptation (**B**).*Asterisk* indicates that there was a statically significant difference for time to reach 50% recovery, between control and dry AMD eyes as well as between controls and wet AMD eyes ($P < 0.05$). Amplitudes of the pure rod b-wave recorded at 20 minutes of dark adaptation were not different among the three eye groups. Controls (*black*), dry AMD (*blue*), and wet AMD (*red*). *Error bars* represent SD.

Dark-adapted responses

Figures 2.6A through 2.6E provide the intensity-response curves for the dark-adapted mixed a- and b-waves. Neither a- or b-wave response curves showed any significant differences among the three groups with regard to amplitude (repeated measures ANOVA *P* values 0.65 and 0.31, respectively). Within the range of stimulus intensity tested, the mean maximal recorded mixed a-wave amplitude was −211 ± 45 in non-AMD eyes versus 211 ± 52 in nonneovascular fellow eyes and 207 ± 45 in neovascular eyes. Mean maximal b-wave values were 329 ± 76, 319 ± 70, and 311 ± 70, respectively. There was no difference noted between neovascular and fellow eyes (Wilcoxon matched-pairs signed rank test: $P = 0.20$ for maximal a-wave and $P = 0.38$ for maximal b-wave).Implicit times were significantly delayed for both a- and b-waves throughout all stimulus intensities tested. Delays were more pronounced for a-waves ($P < 0.0001$). For more accurate determination of a-wave parameters, implicit time measurement was carried out at the highest available intensity (1.37 photopic log cd s/m^2). Such high-intensity stimuli are now recommended by ISCEV in routine testing since they yield a larger a-wave with improved definition and lack of double trough (Marmor et al. 2009). Mean implicit time of the maximal mixed a-wave was 14 ± 1 in non-AMD eyes, 16 ± 1 in dry AMD fellow eyes, and 16 ± 1 in wet AMD eyes (analysis of variance: *F* statistic 33.19, $P < 0.0001$).

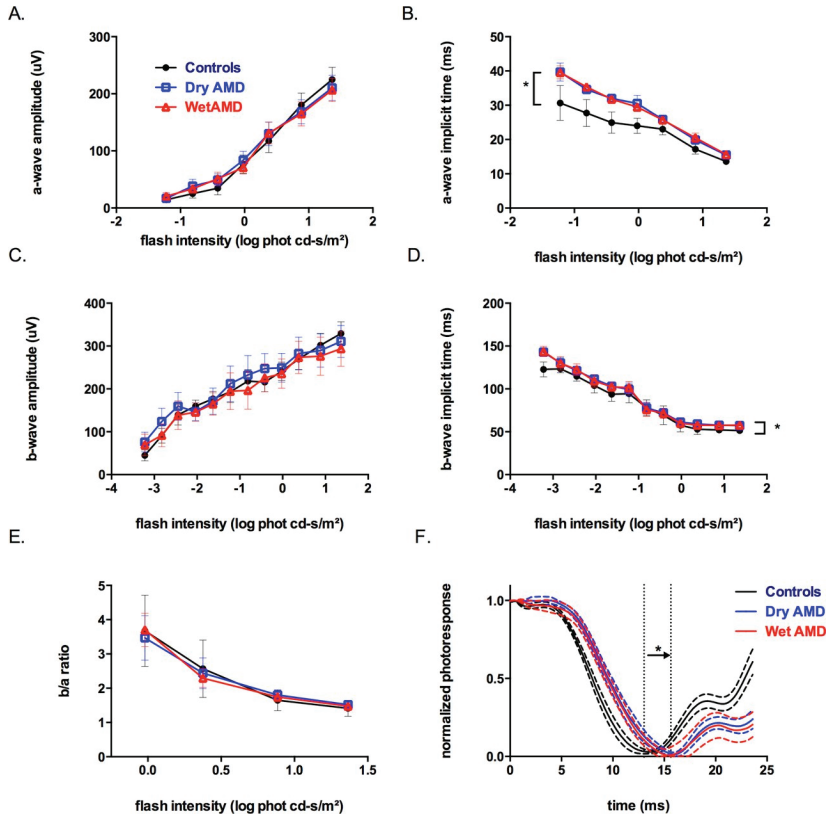

Figure 2.6: Mixed rod-cone–driven ERG responses. Responses elicited following 20 minutes of dark adaptation under a scotopic background with 16 flashes of increasing strengths encompassing −5.22 to 1.37 scotopic log cd s/m2. Intensity responses for a-wave amplitude (A) and implicit time (B) as well as for b-wave amplitude (C) and implicit time (D), and finally for b/a ratio (E) are provided for the three eye groups studied: controls (black), dry AMD (blue), and wet AMD (red). (F) Averages (±95% confidence intervals, dashed lines) of normalized mixed a-waves elicited by the highest intensity stimulus (1.37 scotopic log cd s/m2). The asterisk denotes a significant shift in implicit time ("shift to the right" as pointed by the arrow) between control eyes and eyes with either dry or wet AMD ($P < 0.05$). Controls (black), dry AMD (blue), and wet AMD (red).

B-wave implicit times were also significantly different among the three groups of eyes for all intensities tested (repeated measures ANOVA: $P = 0.02$). The mean implicit time of b-waves at their maximal amplitude was equally delayed in both eyes of AMD subjects when compared to non-AMD eyes (52 ± 6 for non-AMD eyes compared to 57 ± 7 for the neovascular and 58 ± 7 for the non-neovascular fellow eyes; analysis of variance: F statistic 8.4, $P < 0.004$).

To further investigate the origin of the delays in a-wave implicit times in AMD versus non-AMD eyes, normalization of the a-wave function was performed for each response elicited at the highest stimulus intensity. Such an approach allows controlling for interindividual differences in a-wave amplitude. Normalized photoresponses provide an estimate of the time course of cGMP-channel closure (Breton et al. 1994) through the following equation:

$$1 - \left[\frac{a(t)}{a_{\max}} \right] = F(t)$$

where a_{max} represents the maximal a-wave amplitude and $F(t)$ represents the function of cGMP-activated current as a fraction of resting (dark) level. Group averages with 95% CIs (dashed lines) of normalized photoresponses are provided in Figure 2.6F. Results from fitting of the a-wave leading edge indicate that phototransduction activation kinetics were significantly delayed in both eyes of AMD subjects (to a similar extent) when compared to non-AMD eyes.

Phototransduction activation kinetics in rods

To address whether rod-mediated activity accounts for these observed delays in AMD versus age-matched non-AMD eyes, parameters of activation of the rod photoresponse (RmP_3, S, and t_d) were estimated using the Hood and Birch modification of the Lamb and Pugh model (see Methods section). Table 2.1 summarizes all estimated rod-mediated ERG parameters. Maximum amplitude of the rod photoresponse (RmP_3) did not differ among the three groups of eyes (P = 0.9580), whereas sensitivity (S) log values and time delay (t_d) showed significant differences. Mean log$S$ was estimated to be 0.98 ± 0.19 in non-AMD eyes, 0.79 ± 0.18 in neovascular eyes, and 0.78 ± 0.26 in nonneovascular eyes, yielding differences between AMD and non-AMD (P = 0.0039). Significance remained when comparison was limited to AMD subjects with intraocular lenses (P = 0.005). The time delay (t_d) parameter was allowed to vary in the ERG response model rather than kept constant. On average it was estimated to be approximately 0.6 to 0.7 seconds higher in some AMD subjects (3.84 ± 0.53 vs. 4.47 ± 0.69) (see section below).

Table 2.1: Rod-mediated ERG parameters.

	Age-Matched Controls, n = 25	Dry AMD, n = 20	Wet AMD, n = 18	P Value
log$S$	0.92 (0.19)	0.78 (0.26)	0.79 (0.18)	0.0039
log$S$/IOL	0.98 (0.14)	0.78 (0.16)	0.79 (0.17)	0.0072
log Rm_{P3}	2.27 (0.08)	2.28 (0.12)	2.27 (0.10)	0.9580
t_d	3.84 (0.53)	4.47 (0.69)	4.37 (0.61)	0.002

Values in brackets represent SD.

Fellow eye macular phenotype and rod-mediated ERG parameters

To investigate whether maculopathy severity level in the non-neovascular fellow eye was related to any of the rod-mediated ERG parameters, a subgroup analysis of variance was performed (n = 6 eyes AMD1; n = 8 AMD2, and n = 6 in AMD3 group; see Methods section). Subjects in the AMD3 group tended to have extensive areas of decreased pigment up to 0.5 DA and/or noncentral geographic atrophy. Scatter plots of log$S$, log Rm_{P3}, and t_d values are illustrated in Figure 2.7 for all groups. In terms of sensitivity *(S)*, post hoc analysis with Bonferroni correction for multiple comparisons, yielded, interestingly, significance only for the AMD3 subgroup for both their non-neovascular and neovascular eyes (P = 0.002 for both). Rm_{P3} did not vary significantly among subgroups (P = 0.67). Time delay (*td*) was the most variable ERG parameter and remained significant only in the AMD2 group (P = 0.029) when correction for multiple comparisons was applied.

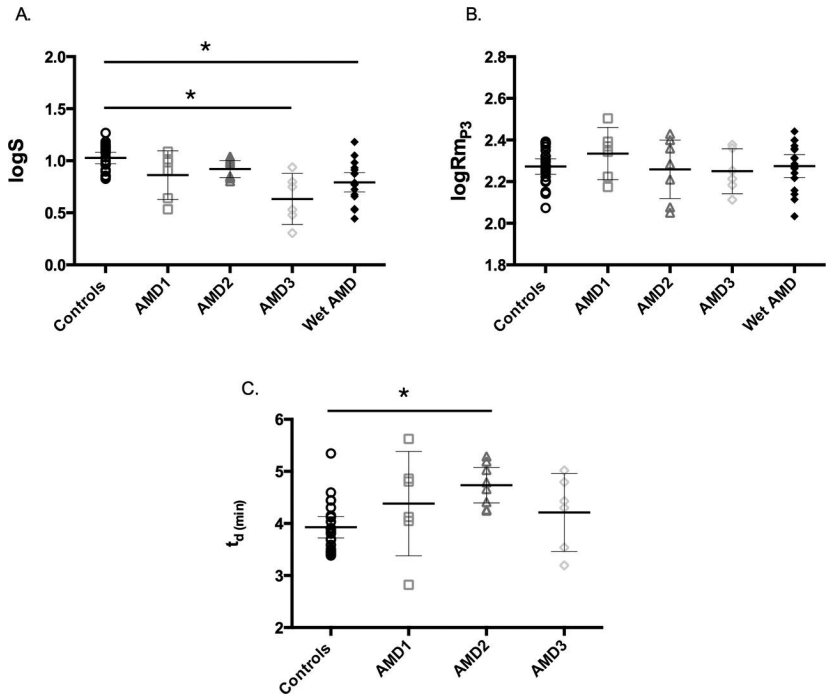

Figure 2.7: Phototransduction activation parameters. Obtained from fitting the leading edge of the isolated rod a-wave: (**A**) log sensitivity (log*S*); (**B**) maximal amplitude (log RmP_3); (**C**) delay before onset (t_d). *Asterisk* indicates statistically significant differences between groups.

DISCUSSION

Our full-field ERG results indicate that a subset of AMD patients undergo dysfunction affecting both rod- and cone-driven retinal processing that span beyond the macula, across the whole retina. For instance, delayed recovery of the pure rod b-wave following partial rod bleaching was noted in both eyes of patients with unilateral wet AMD. These results provide the first objective evidence of a

whole retina-based impairment of dark adaptation. Abnormalities of dark adaptation in AMD have been documented primarily through psychophysical studies in the past (Owsley et al. 2007). Various groups have explored the validity of relying on the pure rod b-wave amplitude as an objective complement to psychophysical dark adaptation tests with success. Adrian (1945) first showed that the b-wave was reduced substantially after large bleaches and that it gradually recovered with time. Karpe and Tansley (1948) and Fulton and Rushton (1978) also reported that the time course of b-wave amplitude recovery corresponds closely to the recovery of the visual threshold, measured psychophysically. Rod outer segments contain the photosensitive visual pigment known as rhodopsin, which consists of a visual chromophore (11-*cis* retinal) covalently bound to a rod specific protein, opsin. Absorption of photons by pigments results in photoisomerization of the chromophore to all-*trans*-retinal and generation of free opsin. Recycling of retinal to its 11-*cis* form and regeneration of rhodopsin is achieved through a well-characterized retinal pigment epithelium (RPE) pathway called retinoid visual cycle (Saari JC 2000; Lamb and Pugh 2004). Despite differences in the psychophysical and ERG experiments, two consecutive works by Cameron et al. (2006) and Ruseckaite et al. (2011) showed that both methods extract a common time course for the main component of rod sensitivity recovery (commonly referred to as "S2" component). Lamb and Pugh (2004) reviewed a wide range of evidence indicating that this component represents in molecular terms "unregenerated opsin." Our results suggest that the time course of rod b-wave amplitude recovery is delayed in both eyes of patients with unilateral

neovascular (wet) AMD. Reasons underlying this defect remain to be explored. Since the component measured to assess dark adaptation was the pure rod b-wave, changes directly affecting its generation (depolarization of ON type bipolar cells by rods) must be examined.

Saari et al. (1998) suggested that all-*trans* retinal released by bleaching may have an effect itself in reducing rod bipolar cell sensitivity. It is known that large bleaches lead to the formation of millimolar levels of all-*trans* retinal in the outer segments (Saari et al. 1998) and that all-*trans* retinal leads to closure of cyclic nucleotide-gated ion channels of photoreceptor outer segments (Dean et al. 2002; McCabe et al. 2004; Horrigan et al. 2005) and blocks the calcium channels of the synaptic terminal (Vellani et al. 2000). Either of these mechanisms would be expected to be associated with desensitization of the rod bipolar cell response.

Another possibility might be related to the loss of DHA that has been suggested to occur in AMD (Liu et al. 2010). Lower retina DHA levels have been associated with decreased binding affinity of IRBP (interphotoreceptor retinoid binding protein) (Chen et al. 1996). IRBP is a key transport protein involved in photopigment regeneration, and contains high-affinity DHA-binding sites for chromophores. Alterations in retinal lipid content may also impede the efficiency of the RPE visual cycle and therefore account, at least in part, for the observed delays in dark adaptation. Furthermore, other factors likely to delay the processing of visual cycle retinoids in AMD could be intrinsic abnormalities of the RPE cell layer itself. Several lines of evidence suggest that excessive accumulation of lipofuscin by RPE cells is significant in terms of the etiology of AMD (Sparrow et

al. 2003). Delayed rod dark adaptation is a common feature in patients with Stargardt's disease, an inherited juvenile form of macular degeneration that is characterized by excessive accumulation of lipofuscin and shares several phenotypic similarities with the dry form of AMD (Fishman et al. 1991). To further decipher the exact origin of the observed rod dark-adaptation delays, more experiments are undoubtedly required. A key aspect involves relying on a double-flash approach as a means to isolate the photoresponse (also called PIII component) and examine its contribution to the reported panretinal defects. Previous double-flash recordings in AMD subjects by Jackson et al. (2006) showed a significant delay in rod inactivation kinetics in late stages of AMD. We therefore must consider the possibility that the dark-adaptation delays (as measured by recording the pure rod b-wave) are caused, at least in part, by presynaptic events in photoreceptors and RPE.

Our study also provides additional evidence for panretinal defects in AMD: implicit times of dark-adapted a- and b-waves were prolonged in both dry and wet AMD eyes. Occurrence of such defects in both types of AMD suggests an underlying panretinal dysfunction that precedes the onset of neovascularization. Mechanisms responsible for increased implicit times can be related to generalized ischemia or overt activation of inflammation affecting the health of the entire neural retina. It is widely known that fellow eyes of advanced AMD patients are at the highest risk of developing choroidal neovascularization (CNV). The role of ischemia in the development of CNV has been well established. Systematic decrease in choroidal circulatory parameters has been observed with an increase

in the severity of AMD features associated with risk for the development of CNV (Grunwald et al. 2005). Pathological changes, such as drusen accumulation and thickening of Bruch's membrane, increase the distance between the choriocapillaris and the retina, reduce the oxygen flux to the photoreceptors, and induce hypoxia in these cells (Stefánsson et al. 2011). It is plausible that the ERG delays measured from the entire retina might predict the onset of CNV development in the fellow eye. Analogously, increased cone b-wave implicit times in 30 Hz flicker electroretinography have been associated with ocular neovascularization in cases of central retinal vein occlusion (Larsson et al. 2001; Roy et al. 1997). It would be relevant to prospectively follow this cohort of patients to address this hypothesis. Of interest, we examined whether there was an association between the number of injections (mean: 11 monthly injections) and the degree of panretinal dysfunction as assessed with the ERG, and found there was none among the 25 unilateral wet AMD subjects we studied. However, we cannot exclude that repeated intravitreal delivery of anti-VEGF agents may have impaired photoreceptor function, not only in eyes with wet AMD but also in fellows eyes via a systemic delivery (Matsuyama et al. 2011).

Overt activation of inflammation could also account for the observed delays in implicit times. Systemic and vitreal activation of the alternative complement pathway has been associated with genetic variants of CFH. Certain CFH haplotypes are known to confer high risk for developing advanced forms of the disease. A possible genotype-based association with a distinct ERG phenotype may exist. Such a genetic association might even be stronger in the subset of

patients who exhibit a complementary generalized cone dysfunction. Such a subgroup has been consistently described even in earlier forms of the disease by Ronan et al. (2006) and Ladewig et al. (2003) and not only restricted to subjects with advanced morphologic changes in the retina, as reported in our study.

To investigate further whether implicit time delays in AMD are of receptoral or postreceptoral origin, we assessed rod-mediated parameters of phototransduction activation. Reduced sensitivity was observed only in those AMD patients with advanced nonexudative morphology in the fellow eye, such as extensive area of RPE depigmentation. Jackson et al. (2004) studied rod-mediated responses during the early stages of the disease and found no abnormalities. Their results showed that among all macular phenotypic characteristics, increased retinal pigment had the least association with decreased sensitivity of activation. Several groups have reported a strong correlation between intermediate to advanced macular phenotypes and peripheral retinal involvement, as manifested through the presence of drusen and reticular pigment near the equator. Lewis et al. (1985) first described the histopathology of peripheral reticular pigment and showed an association with macular degenerative abnormalities. Intriguingly, Seddon et al. (2009) associated peripheral retinal involvement with certain CFH genotypes (CFHrs1410996 variant and CFHY402H). Even though whole retina phenotype assessment and genotyping were not within the scope of our study, these reports provide further support that a distinct genotype may underlie certain ERG characteristics.

BIBLIOGRAPHY

Adrian ED. The electric response of the human eye. J Physiol. 1945; 29; 104: 84–104.

Barbazetto IA, Saroj N, Shapiro H, Wong P, Ho AC, Freund KB. Incidence of new choroidal neovascularization in fellow eyes of patients treated in the MARINA and ANCHOR trials. Am J Ophthalmol. 2010; 149: 939–946.

Breton ME, Schueller AW, Lamb TD, Pugh EN. Analysis of ERG a-wave amplification and kinetics in terms of the G-protein cascade of phototransduction. Invest Ophthalmol Vis Sci. 1994; 35: 295–309.

Cameron AM, Mahroo OA, Lamb TD. Dark adaptation of human rod bipolar cells measured from the b-wave of the scotopic electroretinogram. J Physiol. 2006; 575: 507–526.

Chen Y, Houghton L, Brenna J, Noy N. Docosahexaenoic acid modulates the interactions of the interphotoreceptor retinoid-binding protein with 11-cis-retinal. J Biol Chem. 1996; 271: 20507–20515.

Davis MD, Gangnon RE, Lee LY, et al. The Age-Related Eye Disease Study severity scale for age-related macular degeneration: AREDS Report No. 17. Arch Ophthalmol. 2005; 123: 1484–1498.

Dean DM, Nguitragool W, Miri A, McCabe SL, Zimmerman AL. All-trans-retinal shuts down rod cyclic nucleotide-gated ion channels: a novel role for photoreceptor retinoids in the response to bright light? Proc Natl Acad Sci U S A. 2002; 99: 8372–8377.

Farwick A, Dasch B, Weber BHF, Pauleikhoff D, Stoll M, Hense HW. Variations in five genes and the severity of age-related macular degeneration: results from the Muenster aging and retina study. Eye. 2009; 23: 2238–2244.

Ferris FL III, Fine SL, Hyman L. Age-related macular degeneration and blindness due to neovascular maculopathy. Arch Ophthalmol. 1984; 102: 1640–1642.

Fishman GA, Farbman JS, Alexander KR. Delayed rod dark adaptation in patients with Stargardt's disease. Ophthalmology. 1991; 98: 957–962. Web

Freund PR, Watson J, Gilmour GS, Gaillard F, Sauvé Y. Differential changes in retina function with normal aging in humans. Doc Ophthalmol. 2011; 122: 177–190.

Friedman DS, O'Colmain BJ, Muñoz B, et al. Prevalence of age-related macular degeneration in the United States. Arch Ophthalmol. 2004; 122: 564–572.

Fritsche LG, Chen W, Schu M, et al. Seven new loci associated with age-related macular degeneration. Nat Gen. 2013; 45: 433–439.

Fulton AB, Rushton WA. The human rod ERG: correlation with psychophysical responses in light and dark adaptation. Vision Res. 1978; 18: 793–800.

Gorin MB. Genetic insights into age-related macular degeneration: controversies addressing risk, causality, and therapeutics. Mol Aspects Med. 2012; 33: 467–486.

Grunwald JE, Metelitsina TI, Dupont JC, Ying GS, Maguire MG. Reduced foveolar choroidal blood flow in eyes with increasing AMD severity. Invest Ophthalmol Vis Sci. 2005; 46: 1033–1038.

Hood DC, Birch DG. Rod phototransduction in retinitis pigmentosa: estimation and interpretation of parameters derived from the rod a-wave. Invest Ophthalmol Vis Sci. 1994; 35: 2948–2961.

Horrigan DM, Tetreault ML, Tsomaia N, et al. Defining the retinoid binding site in the rod cyclic nucleotide-gated channel. J Gen Physiol. 2005; 126: 453–460.

Jackson GR, McGwin G, Phillips JM, Klein R, Owsley C. Impact of aging and age-related maculopathy on activation of the a-wave of the rod-mediated electroretinogram. Invest Ophthalmol Vis Sci. 2004; 45: 3271–3278.

Jackson GR, McGwin G, Phillips JM, Klein R, Owsley C. Impact of aging and age-related maculopathy on inactivation of the a-wave of the rod-mediated electroretinogram. Vis Res. 2006; 46: 1422–1431.

Jackson GR, Owsley C. Scotopic sensitivity during adulthood. Vis Res. 2000; 40: 2467–2473.

Jackson GR, Owsley C, Curcio CA. Photoreceptor degeneration and dysfunction in aging and age-related maculopathy. Ageing Res Rev. 2002; 1: 381–396.

Karpe G, Tansley K. The relationship between the change in the electroretinogram and the subjective dark-adaptation curve. J Physiol. 1948; 107: 272–279.

Ladewig M, Kraus H, Foerster MH, Kellner U. Cone dysfunction in patients with late-onset cone dystrophy and age-related macular degeneration. Arch Ophthalmol. 2003; 121: 1557–1561.

Lamb TD, Pugh EN Jr. A quantitative account of the activation steps involved in phototransduction in amphibian photoreceptors. J Physiol. 1992; 449: 719–758.

Lamb TD, Pugh EN Jr. Dark adaptation and the retinoid cycle of vision. Prog Retin Eye Res. 2004; 23: 307–380.

Larsson J, Andréasson S. Photopic 30 Hz flicker ERG as a predictor for rubeosis in central retinal vein occlusion. Br J Ophthalmol. 2001; 85: 683–685.

Lewis H, Straatsma BR, Foos RY, Lightfoot DO. Reticular degeneration of the pigment epithelium. Ophthalmology. 1985; 92: 1485–1495. Web

Liu A, Chang J, Lin Y, Shen Z, Bernstein PS. Long-chain and very long-chain polyunsaturated fatty acids in ocular aging and age-related macular degeneration. J Lipid Res. 2010; 51: 3217–3229.

Loyet KM, Deforge LE, Katschke KJ, et al. Activation of the alternative complement pathway in vitreous is controlled by genetics in age-related macular degeneration. Invest Ophthalmol Vis Sci. 2012; 53: 6628–6637.

Marmor MF, Fulton AB, Holder GE, Miyake Y, Brigell M, Bach MISCEV. Standard for full-field clinical electroretinography (2008). Doc Ophthalmol. 2009; 118: 69–77.

Matsuyama K, Ogata N, Matsuoka M, Wada M, Nishimura T, Takahashi K. Effects of intravitreally injected bevacizumab on vascular endothelial growth factor in fellow eyes. J Ocul Pharmacol Ther. 2011; 27: 379–383.

McCabe SL, Pelosi DM, Tetreault M, et al. All-trans-retinal is a closed-state inhibitor of rod cyclic nucleotide-gated ion channels. J Gen Physiol. 2004; 123: 521–531.

McCulloch DL, Hamilton R. Essentials of photometry for clinical electrophysiology of vision. Doc Ophthalmol. 2010; 121: 77–84.

Meleth AD, Reed GF, Sperduto RD, Clemons TE, Sangiovanni JP, Agro E. Omega-3 long-chain polyunsaturated fatty acid intake and 12-y incidence of neovascular age-related macular degeneration and central geographic atrophy. AREDS report 30, a prospective cohort study from the Age-Related Eye Disease Study. Am J Clin Nutr. 2009; 90: 1601–1607.

Owsley C, McGwin G, Jackson GR, Kallies K, Cone- Clark M. and rod-mediated dark adaptation impairment in age-related maculopathy. Ophthalmology. 2007; 114: 1728–1735.

Pepperberg DR, Birch DG, Hofmann KP, Hood DC. Recovery kinetics of human rod phototransduction inferred from the two-branched alpha-wave saturation function. J Opt Soc Am. 1996; 13: 586–600.

Polyak SL. The Retina. Chicago: University of Chicago Press; 1941. Search Google Scholar

Ronan S, Nusinowitz S, Swaroop A, Heckenlively JR. Senile panretinal cone dysfunction in age-related macular degeneration (AMD): a report of 52

AMD patients compared to age-matched controls. Trans Am Ophthalmol Soc. 2006; 104: 232–240.

Roy MS, Mackay CJ, Gouras P. Cone ERG subnormality to red flash in central retinal vein occlusion: a predictor of ocular neovascularisation? Eye. 1997; 11: 335–341.

Rufiange M, Dassa J, Dembinska O, et al. The photopic ERG luminance-response function (photopic hill): method of analysis and clinical application. Vision Res. 2003; 43: 1405–1412.

Ruseckaite R, Lamb TD, Pianta MJ, Cameron AM. Human scotopic dark adaptation: comparison of recoveries of psychophysical threshold and ERG b-wave sensitivity. J Vis. 2011; 11: 1–16.

Saari JC, Garwin GG, Van Hooser JP, Palczewski K. Reduction of all-trans-retinal limits regeneration of visual pigment in mice. Vis Res. 1998; 38: 1325–1333.

Saari JC. Biochemistry of visual pigment regeneration: the Friedenwald lecture. Invest Ophthalmol Vis Sci. 2000; 41: 337–348.

Scholl HPN Issa Charbel P, Walier M, et al. Systemic complement activation in age-related macular degeneration. PloS ONE. 2008; 3: e2593.

Seddon JM, Reynolds R, Rosner B. Peripheral retinal drusen and reticular pigment: association with CFHY402H and CFHrs1410996 genotypes in family and twin studies. Invest Ophthalmol Vis Sci. 2009; 50: 586–591.

Sparrow JR, Cai B, Fishkin N, et al. A2E, a fluorophore of RPE lipofuscin: can it cause RPE degeneration? Adv Exp Med Biol. 2003; 533: 205–211.

Stefánsson E, Geirsdóttir A, Sigurdsson H. Metabolic physiology in age related macular degeneration. Prog Ret Eye Res. 2011; 30: 72–80.

Steinmetz RL, Haimovici R, Jubb C, Fitzke FW, Bird AC. Symptomatic abnormalities of dark adaptation in patients with age-related Bruch's membrane change. Br J Ophthalmol. 1993; 77: 549–554.

Thylefors B. A global initiative for the elimination of avoidable blindness. Am J Ophthalmol. 1998; 125: 90–93.

Van Lith GHM. The macular function in the ERG. Doc Ophthalmol Proc Ser. 1976; 10: 405–415.

Vellani V, Reynolds AM, McNaughton PA. Modulation of the synaptic Ca2+ current in salamander photoreceptors by polyunsaturated fatty acids and retinoids. J Physiol. 2000; 529: 333–344.

Walter P, Widder RA, Luke C, et al. Electrophysiologic abnormalities in age-related macular degeneration. Graefes Arch Clin Exp Ophthalmol. 1999; 237: 962–968.

Chapter 3. OSCILLATORY POTENTIALS IN AGING AND IN AGE-RELATED MACULAR DEGENERATION: TREATMENT IMPLICATIONS[2]

INTRODUCTION

The full-field ERG is widely used to assess retina function (Creel D. 2001). The ERG trace consists of several distinct light-driven components, with the a-wave, b-wave and OPs constituting the major ones. There are many lines of evidence supporting that the a-wave essentially reflects activity at the presynaptic photoreceptor level (Lamb and Pugh 2006) whereas the b-wave corresponds largely to post synaptic ON bipolar and Müller cell activity (Stockton and Slaughter 1989). Coinciding with the b-wave are the OPs, which reflect activity from the inner retina (Wachtmeister L. 1998). Based on pharmacological manipulations, OPs are generated from the light-driven activation of negative feedback pathways between amacrine cells, retinal ganglion cells and bipolar cells (Guité et al. 1990; Dong et al. 2004).

The traditional approach to characterizing OP properties involves band-pass filtering to remove low frequency components such as the a- and b-waves. Individual OP peaks can then be identified in the time domain and trough-to-peak amplitudes and implicit times determined. An alternative representation of the power spectrum of OPs in the frequency domain can be achieved by applying Fast

[2] A version of this chapter has been submitted for publication:
Dimopoulos IS, Freund PR, Redel T, Dornstauder B, Gilmour G, Sauvé Y. Simultaneous precocious changes in rod and cone-driven inner retinal function in the aging human retina. *Invest Ophthalmol Vis Sci.*

Fourier Transform (FFT) analysis. The FFT analysis only retrieves the global frequency content of the OP signal, excluding time-related variations. Morlet wavelet transform (MWT) is a novel application that allows complex information to be dissected into elementary forms at different temporal positions and scales and then reconstructed with high precision. Wavelet transform of a function can be seen as an "improved" version of the Fast Fourier Transform (FFT) in that it allows analyzing non-stationary signals (such as the ERG) in addition to stationary ones. This approach, when applied to the human ERG, opens up a new analytical dimension of the ERG that can be applied to age-related changes in the healthy and diseased retina.

Numerous studies have documented age-related changes in the outer nuclear layer (ONL) of healthy human retinas (Jackson et al. 1999; Pandas-Jonas et al. 1995; Gartner and Henkind 1981). Curcio et al. (1993) described a preferential loss of parafoveal rods in aged retinas, which led us to rely on the full-field ERG as a means to assess age-related changes in rod- versus cone-driven retina function in humans. We previously showed that the dark-adapted a-wave but not b-wave was reduced in amplitude with age (Freund et al. 2011). These results are in agreement with the potential occurrence of compensatory post-receptoral changes, in response to decreased photoreceptoral input, associated with b-wave amplitude preservation. From an anatomical perspective, these functional changes could reflect the sprouting of ON bipolar cell dendrites as characterized in the healthy aging retina; these dendrites expand into the outer nuclear layer, a dendrite free region in young healthy retinas (Liets et al. 2006).

It is plausible that the retina undergoes such plasticity in its interplexiform circuitry prior to the detection of rod and cone dysfunction by using other methods. To validate this hypothesis, we sought to identify precocious compensatory changes in the inner retina of intermediate-aged healthy individuals (40-59y); for comparison purposes, younger (20-39y) and older (60-82y) groups were similarly studied. We extensively characterized OPs over a wide range of flash strengths using traditional and novel analytical methods. In addition, we relied for the first time on MWT to simultaneously quantify the frequency, peak time and power spectrum of the OP components of the human ERG. Recording and analyzing OPs, as done in this paper, provides a highly sensitive approach for the early detection of age-related functional changes in the human retina. If such changes occur, these must be taken into account as being part of an age-dependent baseline when screening for pathologies affecting the inner retina such as diabetic retinopathy, central vein occlusion and glaucoma.

METHODS

Subjects

Sixty-three healthy human subjects were studied. Inclusion criteria consisted of no ocular pathology (current or previous) and best corrected visual acuity of 20/20. These individuals were split into three groups according to age: 20-39 years (n=26; mean age±SD: 24.6±4), 40-59 years (n=21; 52.1±5), and 60-82 (n=16; 65.8±5). To compare the two OP extraction methods in pathological states, we further included five subjects with unilateral neovascular age-related

macular degeneration (AMD) undergoing intravitreal anti-VEGF therapy, as well as two subjects presenting with treatment-naïve unilateral serous pigment epithelial detachment (sPED). In each case, the fellow non-neovascular eye served as an internal control to identify potential inner retina dysfunction in the neovascular eye. All fellow eyes were classified as having intermediate dry AMD, defined by the presence of either many medium-sized drusen or one or more large drusen. This study received ethics approval from the "Health Research Ethics Board (Biomedical Panel)" of the University of Alberta (license #6194). All procedures conformed to the Code of Ethics of the World Medical Association (Declaration of Helsinki) and were done with the understanding and written consent of each participant.

ERG recordings

Subjects underwent bilateral full-field ERG recordings. Stimulus presentation, amplification (0.1 to 300 Hz bandpass, without notch filtering) and digital data acquisition were provided by the Espion E^2 system (Diagnosys LLC, Lowell MA 01854, U.S.A.). Digitization rate was set at 1 kHz for all tests, with the exception of 5 kHz for scotopic intensity responses for which a higher rate was used in order to optimize definition of fast events such as the leading edge of the saturated a-wave. Dawson-Trick-Litzkow (DTL) type recording electrodes were placed below the limbus between the inferior eyelid and sclera in both eyes; reference electrodes (gold surface electrode; F-E5GH-60, Grass Technologies, West Warwick, RI 02893, U.S.A.) were placed on the lateral edge of the orbital

bone. A ground electrode (gold surface electrode) was placed in the center of the forehead, one inch above the eyebrows. Pupils were dilated by applying two drops of tropicamide 1% on each cornea twenty minutes prior to starting the recording session; pupil size (6.4±0.5 mm average diameter) remained unchanged between age groups); full dilation was confirmed after the end of the testing period. The visual stimuli consisted of flashes administered in a full-field Ganzfeld by a xenon bulb of 6,500ºK color temperature, (10 µs duration); light levels were calibrated with an IL1700 photometer (International Light Technologies Inc., Peabody, MA 01960, U.S.A.) equipped with either a photopic or scotopic filter.

Photopic ERG

Subjects were initially light-adapted (background of 30 cd/m^2, measured at the corneal surface) with the purpose of saturating rods to record cone-driven ERG responses. White flashes were presented with the following increasing time-integrated luminance along 6 stepwise increments: - 0.02, 0.38, 0.88, 1.37, 1.89 and 2.39 photopic log cd·s/m^2 (logarithm of candela seconds/meters square). The interval between each step was set at 10 s and each stimulus was presented 6 times at 5 s inter-stimulus intervals. Responses were averaged at each step.

Dark-adapted ERG

Following ISCEV (International Society for Clinical Electrophysiology of Vision) standard 20 minute dark adaptation (Marmor et al. 2009), white flashes were presented with the following increasing time-integrated luminance along 4

stepwise increments: (-0.02, 0.38, 0.88, and 1.37 scotopic log cd·s/m^2), each averaged 3–5 times. To allow for maximal rod recovery between consecutive flashes, inter-stimuli-intervals were increased from 15 s at the lowest stimulus strength up to 60 s at the highest stimulus strength.

OP extraction and analysis

A) Isolation of OPs according to ISCEV standards

As specified by ISCEV's "guidelines for calibration of stimulus and recording parameters" (Brigell et al. 1998), a 75-300 Hz digital band-pass was applied to isolate OPs. Under dark-adapted conditions, five peak OP amplitudes (OP1-OP5) and their corresponding implicit times (t1-t5) were measured from the filtered traces (Figure 3.1A). The sum of the first four OP peaks was used to calculate the "summed OP amplitude" (Marmor et al. 2009). Under light-adapted conditions, four peak OP amplitudes (OP1-OP4) and their corresponding implicit times (t1-t4) were measured from the filtered traces (Figure 3.1B). Calculation of summed photopic OPs, always included OPs 1 to 3, and in addition OP4 when it could be elicited under higher stimulus strengths.

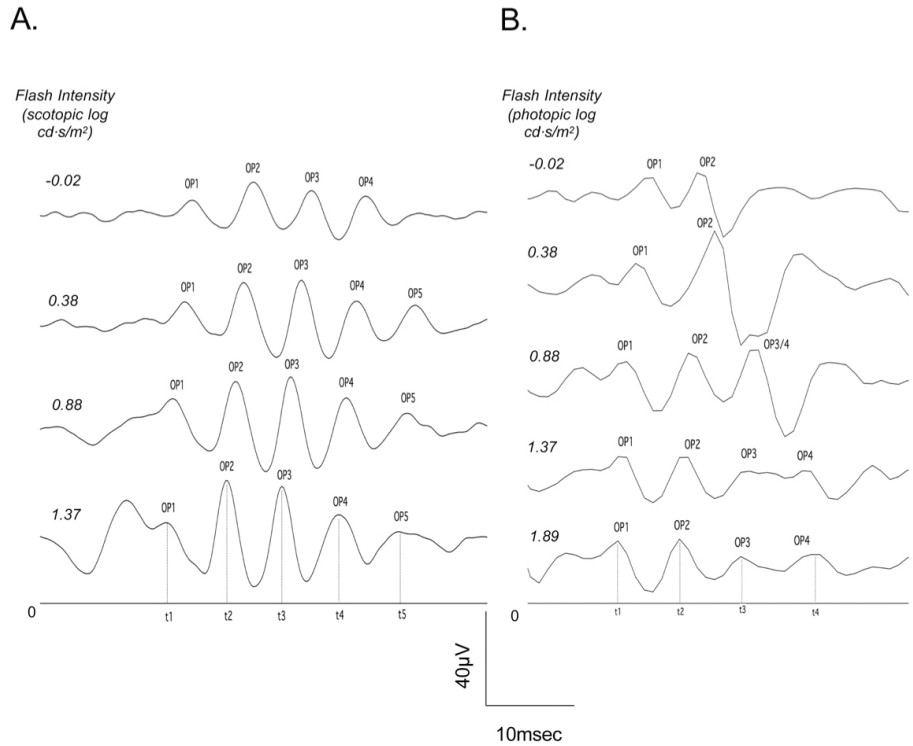

Figure 3.1: Representative filtered luminance-response ERG waveforms. A) Dark-adapted responses showing the five distinct OP peaks (OP1-OP5) and corresponding implicit times (t1-t5). B) Light-adapted responses showing the four distinct OP peaks (OP1-OP4) and corresponding implicit times (t1-t4). The number of measured OP peaks changes as a function of flash strength. Two distinct OP peaks are identified (OP1 and OP2) at lower stimulus strengths (-0.02, 0.38 log cd·s/m2). A third OP ("OP3-4 complex") becomes apparent as the stimulus strength is increased. This OP complex splits and gives rise to two distinct OP peaks (OP3 and OP4) at higher stimulus strengths (>1.37 log cd·s/m2). The horizontal line starts at time point zero (stimulus onset) and represents amplifier calibration at zero microvolt amplitude. Scale bar represents time (x-axis) and amplitude (y-axis).

B) Quantification of OPs with continuous MWT analysis

MWT analysis was adapted from a previous study of rat ERG signals described by Forte et al. (2008). The MWT was used to divide a continuous-time function into smaller or shorter waveforms (wavelets). Unlike Fourier transform, which cannot capture changes in frequency response with respect to time, the continuous MWT allows generating the time-frequency representation of a signal with high resolution in both the frequency and time domains. In general, it has proven particularly useful for the analysis of transient, aperiodic and non-stationary signal features, for both ERG and ECG. The equation of the continuous MWT is given below:

$$X_w(a,b) = \frac{1}{\sqrt{b}} \int_{-\infty}^{\infty} x(t)\psi\left(\frac{t-a}{b}\right) dt, \quad \begin{cases} b > 0 \\ a \in (-\infty, \infty) \end{cases}$$

where *(t)* is the fitted mother wavelet (the Morlet function in this case, see below), *t* the time, *a* the location parameter and *b* the scaling parameter of the wavelet.

By applying changes in the location (*a*) and scaling (*b*) of the mother wavelet, both short duration-high frequency and long duration-low frequency information can be captured simultaneously.

The Morlet wavelet (generated from raw "unfiltered" traces) provides a robust statistical model of the filtered OP waveform (Bui et al. 2002) It is a complex Gabor function composed of a real cosine component and an imaginary sine component multiplied by a Gaussian window (envelope) and is defined by the following equation:

$$\psi(t) = e^{2i\pi f_c t} \; e^{-\frac{t^2}{2}}$$

where f_c is the fundamental frequency of the wavelet determined by the scaling factor b in the wavelet transform, i the square root of -1 and t the time.

Continuous MWT was applied to each of the raw "unfiltered" ERG traces (0.1-300 Hz) to generate a map of the ERG power spectrum in the frequency and time domains and to quantify the three following variables: relative amplitude, oscillation frequency, and implicit time values for the OPs. The wavelet function software used consisted of the Matlab complex Morlet (Mathworks®, Natick, Massachusetts, U.S.A). Raw data were multiplied by half Welch window in order to smoothen the trailing edge of the ERG waveform after 118ms from flash onset. This modification was previously adopted by Forte et al. (2008) to remove terminal artifacts that might contaminate the wavelet analysis. Modified ERG signals were correlated with the Morlet wavelet at every time point. Scaling values were chosen to encompass both the number of steps in frequency measurement and in the envelope of frequencies at which OPs occur (50-300 Hz). Scaling values differed for 1 kHz (light-adapted) and 5 kHz (dark-adapted) samples as scale to frequency conversions are dependent on sample rate. The magnitude of correlation at each point was measured as the complex modulus of the complex wavelet response. Local maxima were located using nearest-neighbor comparison. The largest local maximum in the 50-300 Hz range was considered to be the peak of the OP for dark-adapted responses. For light adapted responses,

largest local maxima were searched in two frequency ranges: 50-100Hz and 100-300Hz. The complex modulus of the maxima was recorded as peak power (arbitrary units). The use of the complex modulus reduces the phase-dependence of the power measurement. The locations of these maxima in the time and frequency domains were recorded as peak time and peak frequency. To generate a wavelet scalogram, magnitudes of correlation coefficients across the ERG signal were expressed as a grayscale, with relative amplitude normalized to the peak value for each exposure. Maximum response appears white.

Statistics

To ensure independence of samples, a single eye per subject was included in the analysis. The included eye was chosen based on the highest recorded a-wave amplitude in the scotopic intensity response series except where there was a clear indication (e.g. excessive voltage noise due to poor electrical contact) to discard the recording in favor of the contralateral eye. Statistical significance between age groups was assessed using repeated-measures ANOVA with the Greenhouse-Geisser correction for sphericity. Posthoc analyses were done between the individual groups and at individual stimulus strengths or time points using the Bonferroni technique for multiple comparisons. GraphPad Prism was used for one-way ANOVA, linear regression, and correlation analyses (GraphPad Software, Inc. La Jolla CA 92037, U.S.A.). SPSS was used for the repeated-measures ANOVA (SPSS Inc. Chicago, Illinois 60606, U.S.A.). Significance was

set at $P<0.05$. Data points on graphs represent mean ± standard error of the mean (SEM).

RESULTS

Scalogram features

Figure 3.2 displays representative examples of wavelet scalograms for a period of 250 ms after flash presentation at t=0 ms. Raw ERG traces have been superimposed on the bottom row scalograms (panels C-D) to determine the origin of each peak. Figure 3.2A shows a representative wavelet trace with a high signal-to-noise ratio. Red triangles point to the peak with the maximum amplitude. In this example, peak OP amplitude occurs at 28 ms with a frequency of ~150 Hz. A small a-wave component occurs at 55 Hz. In Figure 3.2B, a myotonic reflex is seen at t = 125 ms, with the remaining of the trace having low baseline noise level. Figure 3.2C provides an example of wavelet amplitudes in the 50-250 Hz spectrum obtained when presenting a short duration (10 μs) full field flash of 0.88 log cd·s/m^2 strength in the light-adapted human retina. Two distinct peaks of comparable power can be identified. Superimposition of the raw ERG trace reveals that the low frequency band is in close proximity to the peak of the b-wave, while concomitantly the high frequency band peaks during the rising edge of the photopic b-wave.

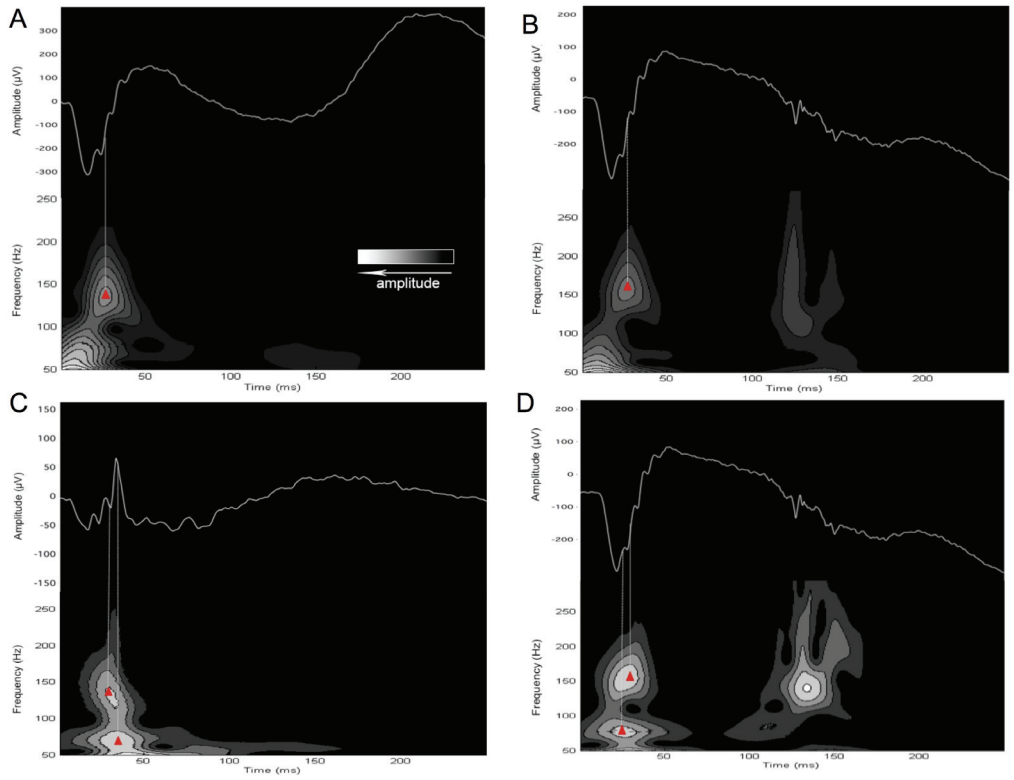

Figure 3.2: Representative examples of ERG traces with MWT scalograms. The y-axis for the scalogram and the ERG trace respectively represent "frequency" and "amplitude" (time zero corresponds to stimulus onset). Correlation magnitudes of the ERG signal are represented by shades of grey in terms of a scalogram, with relative amplitude normalized to the peak value for each exposure. Panel A shows a wavelet trace essentially deprived of background retina activity. Peak OP amplitude occurs at 28 ms with a frequency of ~150 Hz. A small a-wave-related component is observed at 55 Hz. Panel B illustrates the occurrence of a myotonic reflex (extraocular origin) occurring at 125 ms. Of note, in both panels A and B, the scalogram representation of the OPs is distinct of that from the a-wave, and the timing of the peak of the OP train (red triangle) is

synchronous with the b-wave ascending phase. Panel C shows the scalogram representation of a light-adapted response to a flash of 0.88 log cd·s/m2 strength. Two distinct peaks of comparable power can be identified on the scalogram. Superimposition of the ERG trace reveals that the low frequency band occurs at the same time as the peak of the b-wave. The scalogram allows separation of this low frequency event (bottom red triangle) from a higher frequency event (top red triangle) that occurs during the rising phase of the photopic b-wave. Panel D is the scalogram representation of a dark-adapted response to a mid- strength stimulus (-0.02 log cd·s/m2). Two oscillators are superimposed in time: one corresponding to the second trough of the a-wave (lower triangle with frequency peaking at ~75-80 Hz) and the other one corresponding to OPs on the ascending limb of the b-wave (upper triangle with frequency peaking at ~150-160 Hz). The presence of a myotonic reflex can be noted at 140 ms.

Figure 3.2D consists of a scalogram which appearance is representative of dark-adapted recordings, where ERG waveforms with “double-trough” a-waves are present. A low frequency band with a peak at 75-80 Hz is noted in close proximity to the second trough of the a-wave. A second high frequency peak at 150Hz follows, which coincides with the ascending limb of the b-wave. The early peak has been previously attributed to the first OP (OP1) that coincides with the a-wave and splits it into a double-trough a-wave (Brunette JR 1972; el Azazi and Wachtmeister 1993). To remove the potential influence of a-wave onset on the low-frequency OPs, we conditioned the original ERG waveform (Figure 3.3A) to the lowest voltage before the first a-wave trough (Figure 3.3B) or before the second a-wave trough (Figure 3.3C). Wavelet analysis of such conditioned waveforms revealed that removal of the a-wave prior to the first trough had no effect on the power of the low frequency OPs (Figure 3.3B), whereas removal of the first a-wave trough resulted in a 40% power reduction (Figure 3.3C). High frequency OPs remained unaffected. Therefore, this low-frequency peak can be attributed to the oscillatory system without contamination from the a-wave.

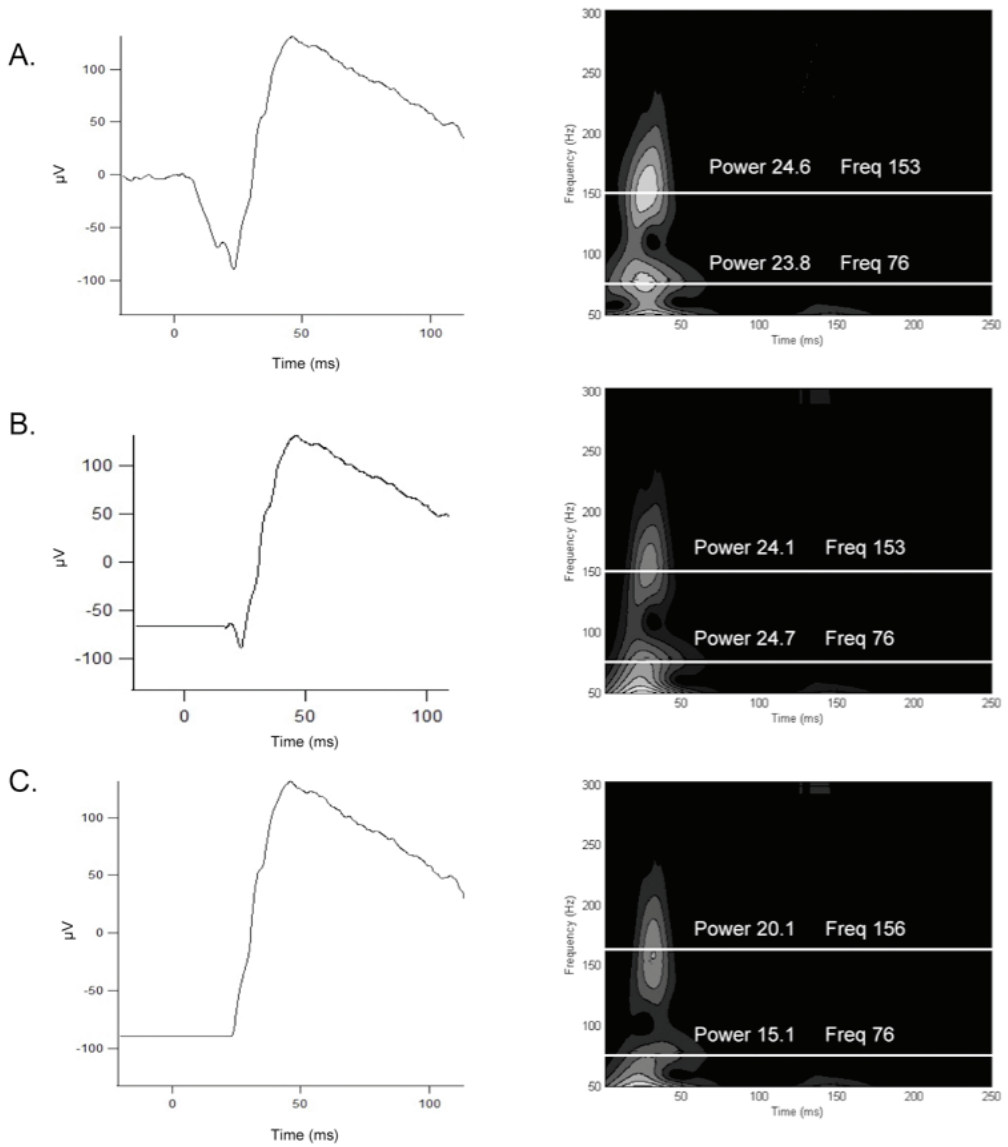

Figure 3.3: Effect of the a-wave onset on dark-adapted OPs. Wavelet analysis after preconditioning the ERG waveform to the lowest voltage before the first (panel B) and the second a-wave trough (panel C). Power of the low frequency band (76Hz) is not altered after removal of the a-wave leading edge (panel B), but becomes significantly reduced once the second a-wave trough has been removed (panel C). The high frequency band remains unaffected. Power units are arbitrary units (complex modulus) and frequency is expressed in Hz.

Dark-adapted responses

A) Band-pass filtering and trough-to-peak analysis

For all age groups, the first four OP peaks (OP1-OP4) grew in amplitude and occurred earlier as stimulus strength increased (Figure 3.4). Aging was associated with a reduction of amplitudes of the first four OP peaks (OP1-OP4, Figure 3.4A-D) in addition to a prolongation of implicit times for all OP peaks (Figure 4G-J). There was no significant effect of stimulus strength on the amplitude of the fifth OP (OP5, Figure 3.4E), although its peak occurred earlier (Figure 3.4K). The calculated summed OP amplitude showed a similar dependency with increased stimulus strength (Figure 3.4F).

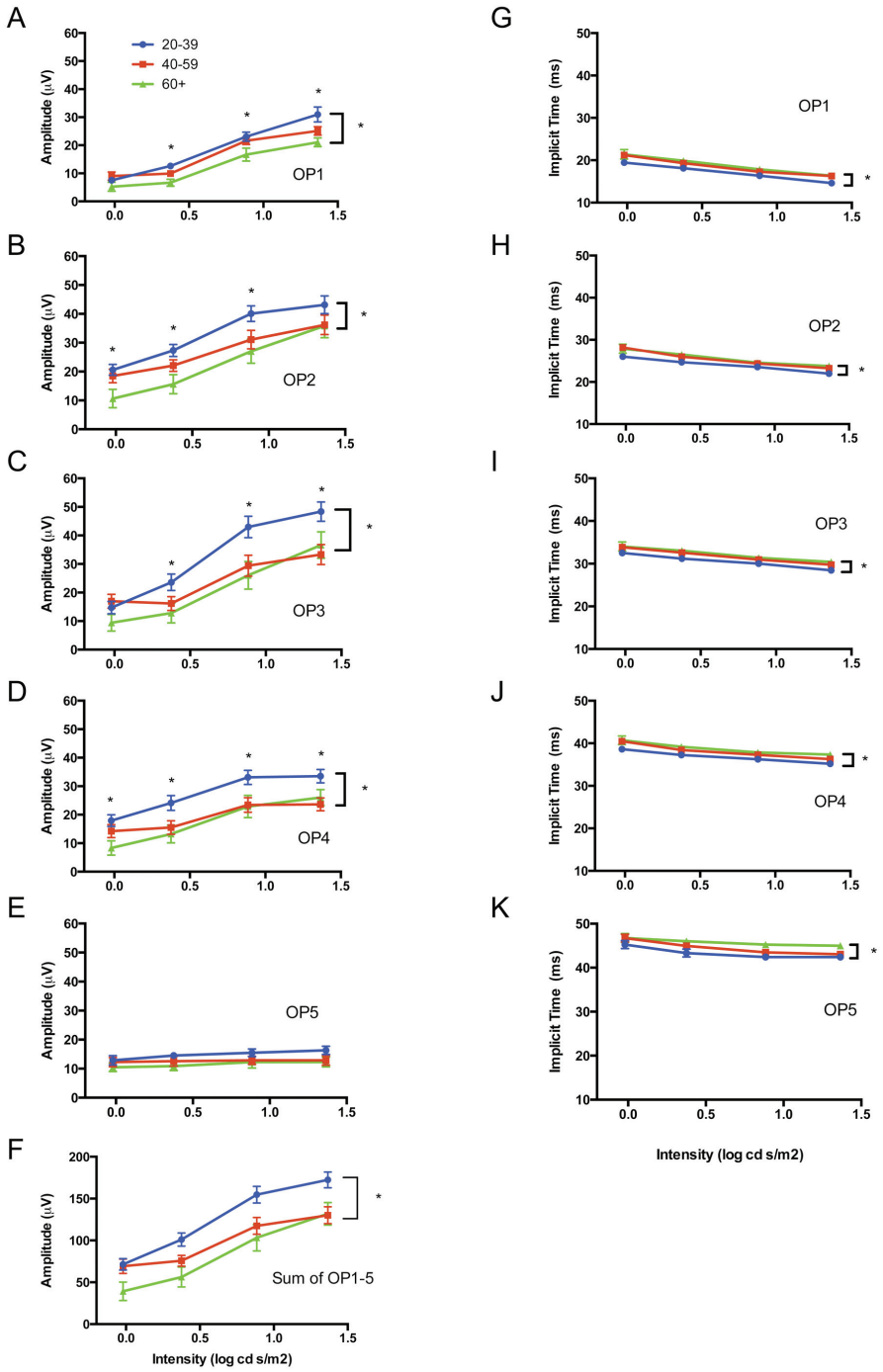

Figure 3.4: Effect of age on dark-adapted OPs. Amplitude and implicit time of the respective OP components as a function of stimulus strength. In all three age groups, amplitude increases and implicit time decreases, respectively, as a function of stimulus strength increments. Amplitudes of OP1 to OP5 are shown in panels A to E, and the summed amplitudes of these respective OPs are shown in

panel F. With the exception of OP5, there is a significant amplitude reduction with age for all individual OP components and summed OP amplitudes. Post-hoc analysis shows differences between the young (blue) and older groups (red and green). Implicit times of OP1 to OP5 (panels G to K) show a similar trend as for amplitudes: there is a significant implicit time prolongation with age for all individual OP components. Asterisks indicate $p<0.05$.

B) Wavelet-derived parameters (amplitude, peak OP time and frequency)

MWT confirmed the relationship (described above) between stimulus strength and peak OP amplitude for all age groups ($p<0.0001$; Figure 3.5); see Figure 3.5A for representative scalograms. Relative amplitudes increased three-fold for the young and two-fold for the older groups from -0.02 log cd·s/m^2 to 1.36 log cd·s/m^2 flash strength. Peak OP time, defined as the location of the peak OP amplitude in the time domain, was decreased as a function of flash strength ($p<0.0001$). Caution was taken to include as OP peaks only local maxima that occurred after the trough of the a-wave. Such a trough was estimated to occur before 27.76 ms and 14.27 ms (*90th percentile*) for the lowest (-0.02 log cd·s/m^2) and highest (1.36 log cd·s/m^2) strength, respectively. Significantly lower peak OP amplitudes ($p<0.001$, Figure 3.5B) and higher peak OP times ($p=0.0028$, Figure 5C) were calculated for the two older groups. Figure 3.5D shows that the peak OP frequency remained unchanged as a function of flash strength for all age groups. One main source of oscillation could be identified for stimulus strengths higher than 0.38 log cd·s/m^2 with a peak at 145-155 Hz. At moderate strengths (-0.02 log cd·s/m^2), a second peak of oscillation with a mean frequency of 77 Hz and onset at 29.1±3.1 ms could be distinguished. This oscillatory peak accounted for 60% of the total observed power in the 50-300Hz frequency range. Potential a-wave contamination was excluded, as discussed previously. As flash strength increased, its peak time occurred earlier and in close proximity to the a-wave trough, making

quantification unreliable without pre-conditioning ERG waveforms to remove the a-wave.

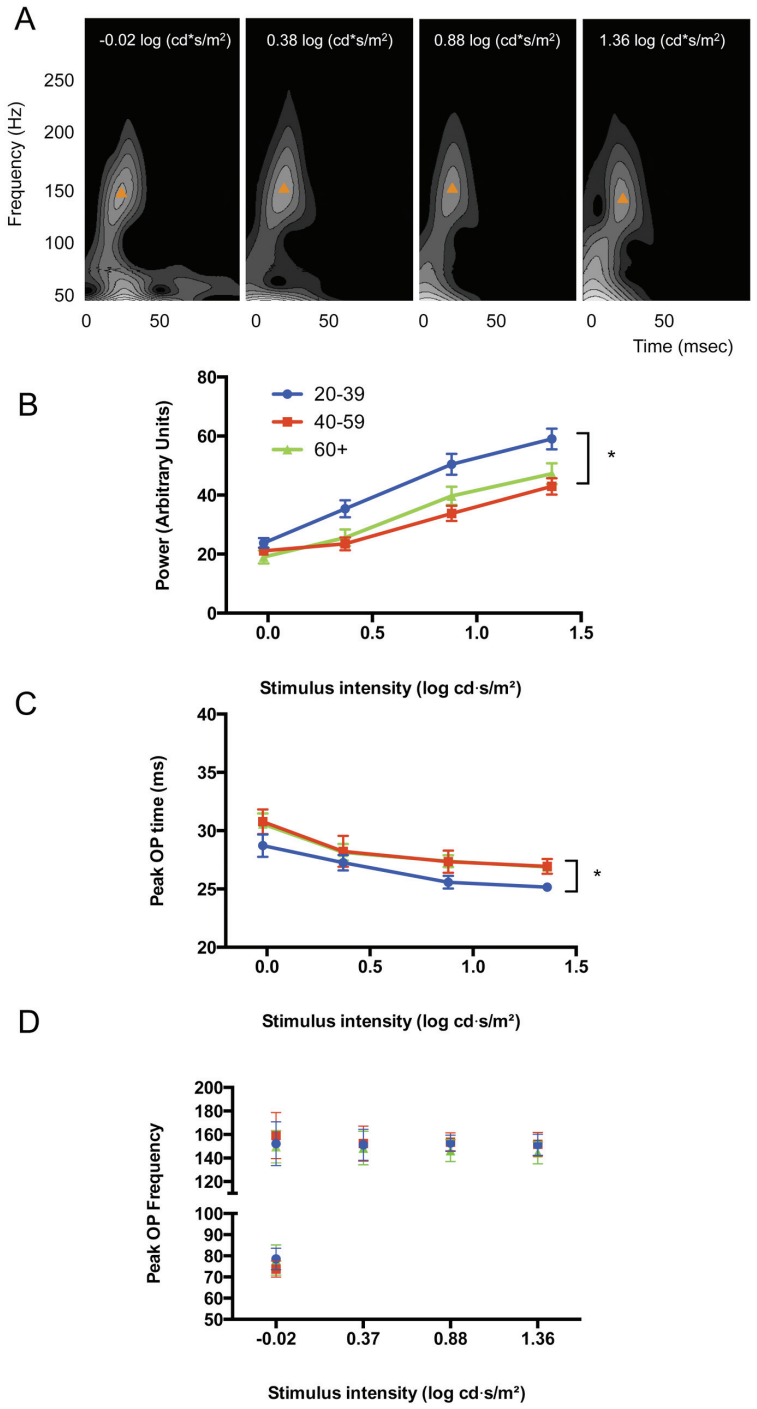

Figure 3.5: Analysis of dark-adapted OPs using MWT. A) Representative examples of MWT scalograms for increasing stimulus strengths; time zero represents visual stimulus onset. Isolation of OP trains from other oscillators allows quantifying distinct peak amplitude, timing and frequency (orange

triangle) for all stimulus strengths. For all age groups, peak OP amplitudes increase (B) and peak OP times decrease (C) as a function of stimulus strength. Peak frequency (D) is independent of stimulus strength, regardless of age. At the lowest stimulus strength (-0.02 log cd·s/m2), a second peak of oscillation can be recorded in synchrony with the a-wave peak (panel D). Lower peak OP amplitudes with delayed implicit times are characteristic of the older groups (red and green) when compared to the young group (blue).

Light-adapted responses

A) Band-pass filtering and trough-to-peak analysis

A more complex picture of OP generation was observed for light-adapted responses (Figure 3.6). The number of measured OP peaks varied as a function of flash strength. At lower strengths (-0.22 and 0.38 log cd·s/m^2), two OP peaks could be distinguished (OP1 and OP2, Figure 3.6A-B). A third OP was evident at 0.88 log cd·s/m^2, which we refer to as "OP3-4 complex" following previous description by Rufiange et al. (2002) (Figure 3.6C). This OP complex would split and give rise to two separate OP peaks (OP3 and OP4, Figure 3.6C-D) at higher strengths (>1.37 log cd·s/m^2). Initially, there was a two-fold increase in the amplitude of OP1 and OP2 for the first two strengths, followed by a plateau phase for OP1 and a decline and plateau phase for OP2 at higher flash strengths. Increased age was associated with amplitude reduction of both OP1 and OP2 (repeated measures ANOVA: $p=0.006$ for OP1 and $p=0.0029$ for OP2), but Bonferroni adjustment for multiple comparisons limited the difference to only OP2 at the 0.38 log cd·s/m^2 flash strength (Figure 3.6B; asterisk denotes significance after Bonferroni correction). The amplitudes of the third and fourth OPs (OP3 and OP4) were not affected by either flash strength or age. The calculated summed OP amplitude showed an initial positive linear growth with increasing flash strength, followed by a plateau phase for higher strengths (>0.88 log cd·s/m^2). Differences among age groups were only significant at the 0.38 log cd·s/m^2 flash strength after Bonferroni adjustment (Figure 3.6E). Peak implicit

times for the first two OPs (OP1 and OP2) were reduced as flash strengths increased ($p<0.0001$). Such dependence was not noted for the late OPs (OP3 and OP4). Peak delays were recorded in both older groups for the first three OP components ($p<0.0001$; Figure 3.6F-H) but not for OP4 (Figure 3.6I).

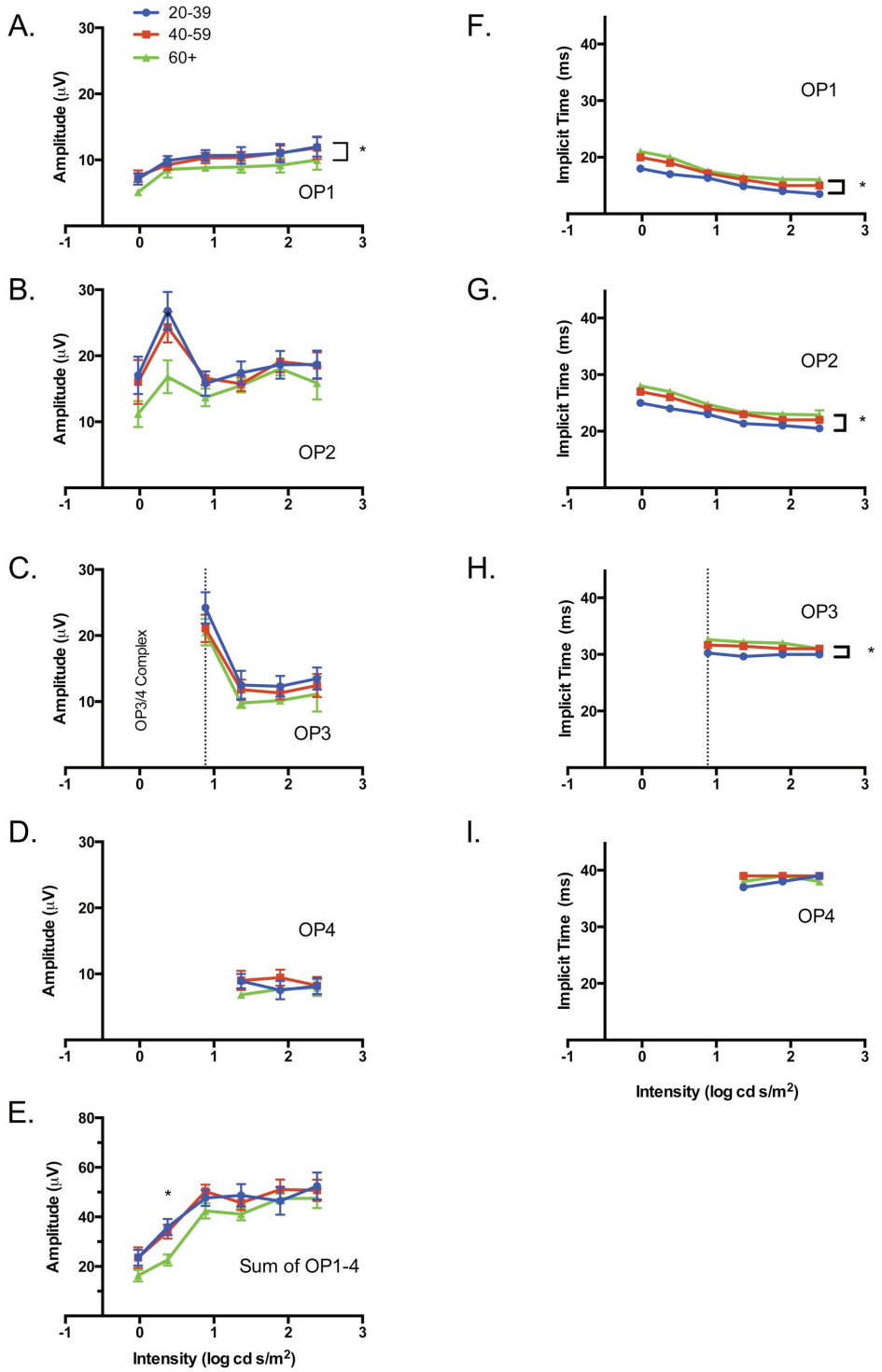

Figure 3.6: Effect of age on light adapted OPs. Amplitude and implicit time of the respective OP components as a function of stimulus strength. The number of measured OP peaks changes as a function of flash strength. There is a significant difference between young (blue) and older (red and green) groups for OP1 and

OP2 amplitudes. The relationship between summed OP amplitude and stimulus strength is best described as an initial linear increase followed by a plateau beginning at 0.88 log cd·s/m2 (panel E). OP1 and OP2 implicit times are inversely proportional to stimulus strength. When comparing the two older groups with the younger one, the first three OP peaks are delayed (panels F-I). Asterisks correspond to $p<0.05$.

3.3.2 Wavelet-derived parameters (amplitude, peak OP time and frequency)

Figure 3.7A shows representative wavelet scalograms for different flash strengths under light-adapted conditions. More than one distinct band of oscillations can be identified in the frequency domain (white arrows). The red triangle highlights the peak with the maximum amplitude. By applying strict power criteria (local peaks within at least 1/3 of the maximum amplitude) and time domain filtering, candidate OP peaks could be more accurately defined. A frequency-domain representation of all candidate OP peaks as a function of flash strength is given in Figure 3.7B. At lower strengths (-0.02 and 0.38 log cd·s/m^2) one oscillatory peak at ~90-100 Hz was the main source of OP power. At higher strengths (0.88 and 1.37 log cd·s/m^2) two distinct bands of oscillations could be noted: a set of high frequency OPs with a peak at 135±6 Hz and a set of low frequency OPs with a peak at 82±7 Hz. As flash strength further increased, the low frequency band could only be recorded in a subset of young individuals. The high frequency band remained the main source of OP power for the rest of the subjects. The location of the OP peaks in the time domain is illustrated in Figure 3.7C. High frequency OP peaks (>120 Hz) were time locked to the onset of early OPs, whereas low frequency OPs (70-100 Hz) gave rise to both early and late OPs. Analysis of variance (ANOVA) was used to analyze differences in OP peak time and amplitude among groups. For older subjects, a significant delay was recorded for most OP peaks (Figure 3.7C; asterisk denotes significance at p=0.05).

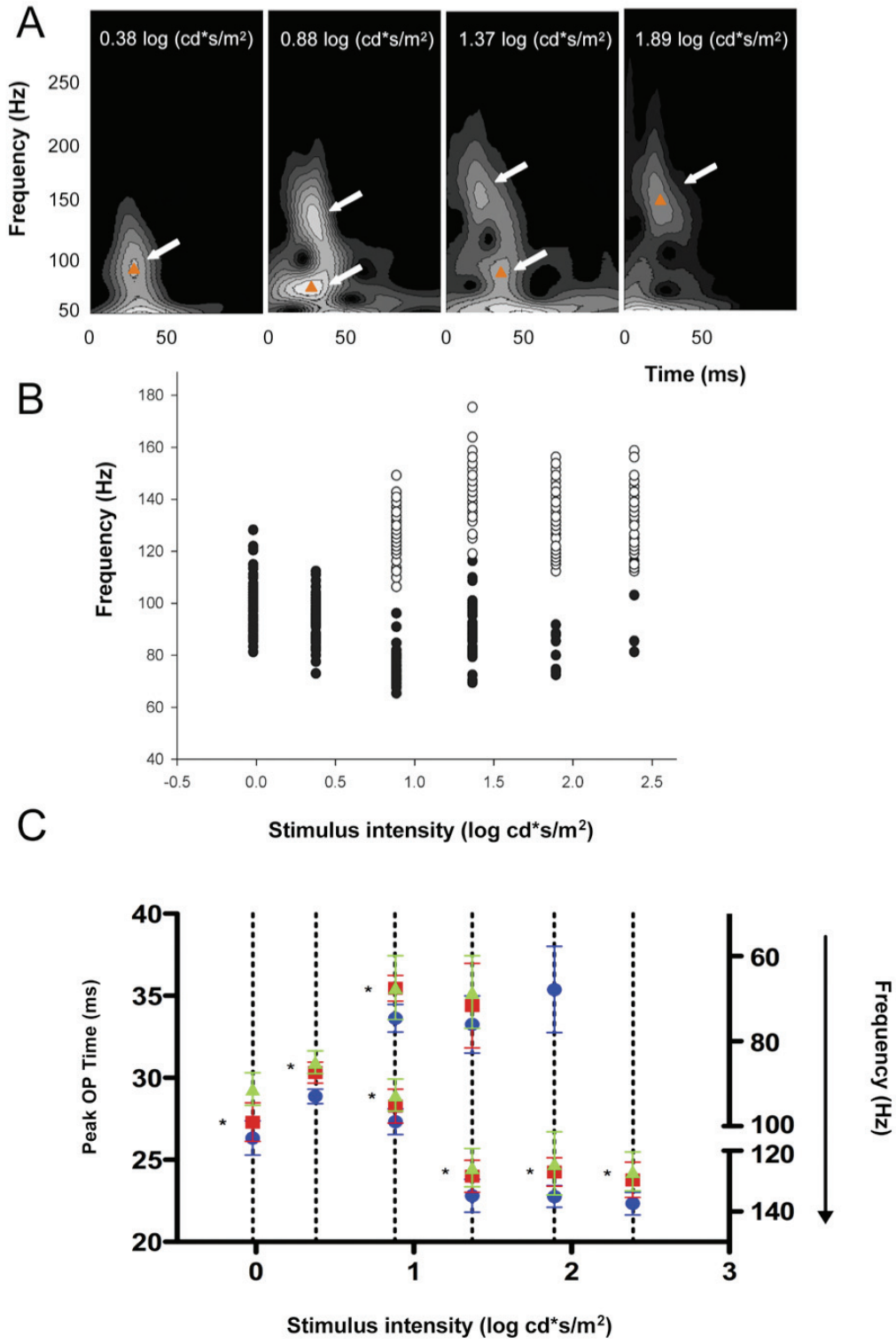

Figure 3.7: Analysis of light-adapted OPs using MWT. A) Representative examples of Morlet wavelet scalograms for increasing stimulus strengths; time

zero represents visual stimulus onset. For a subset of stimulus strengths (middle two scalograms), two distinct oscillatory peaks are identified along the frequency domain (white arrows). The red triangle highlights the peak with the maximum power. B) Segregation of high (hollow circles) and low (filled circles) frequency OP peaks as a function of stimulus strength; aggregated data from all subjects, independently of age. C) Time domain of OP peaks as a function of stimulus strength. High frequency OP peaks (>120 Hz) are elicited prior to their low frequency counterparts (70-100 Hz). When comparing the two older groups (red and green) with the younger group (blue), most of the OP trains are delayed regardless of their peak frequency. Asterisks correspond to $p<0.05$.

Amplitude analysis with frequency segregation revealed a pronounced reduction in peaks of the low frequency spectrum (Figure 3.8A). Contrastingly, the amplitudes of the high frequency OP peaks remained unaffected by age (Figure 3.8B). ANOVA results of wavelet-derived amplitude parameters are summarized in Table 1 for all flash strengths.

Intensity	Low Frequency (70-100 Hz)		High Frequency (>120 Hz)	
(Log cds/m^2)	F-statistic	p-value	F-statistic	p-value
-0.02	6.745	**0.0022**		
0.37	11.92	**<0.0001**		
0.88	13.23	**<0.0001**	0.5840	0.5601
1.37	4.071	**0.0236**	0.4582	0.6343
1.89			1.040	0.3586
2.36			1.163	0.3194

Table 3.1: Comparison of MWT OP peak amplitudes among age groups. Bolded p-values represent significant differences.

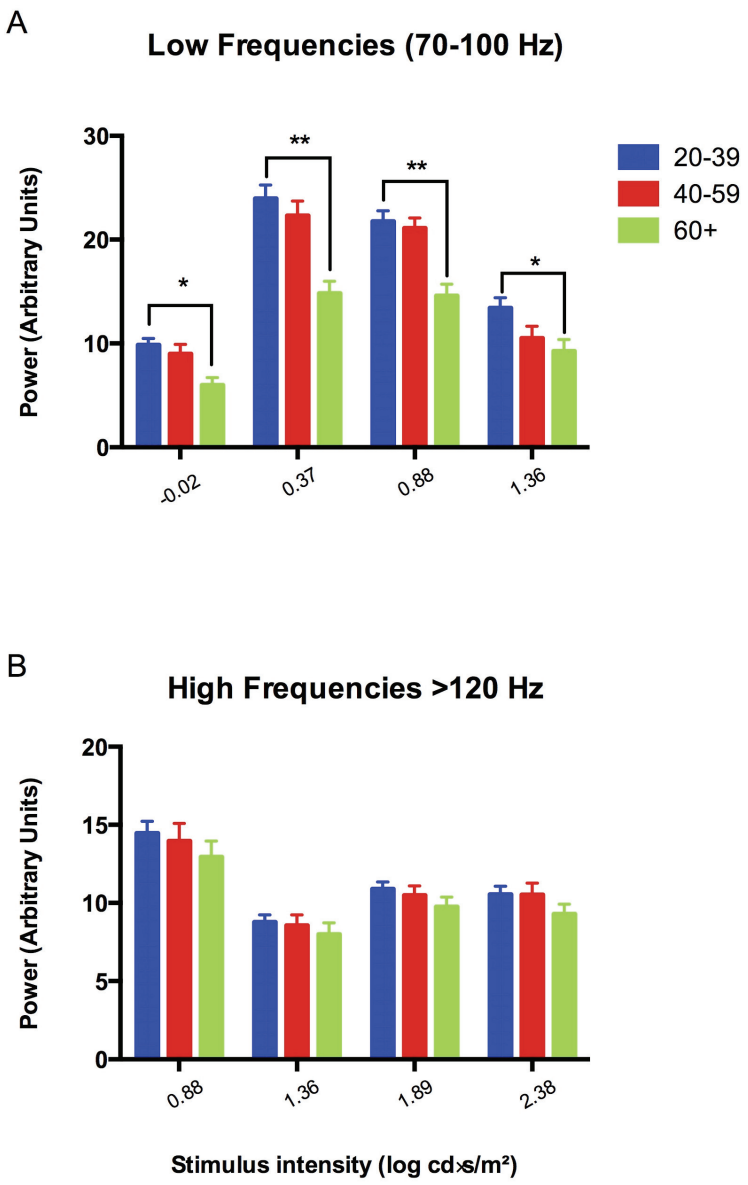

Figure 3.8: Amplitude of the two distinct OPs segregated by frequency. A) Low frequency OP trains have reduced amplitudes in the older groups (red and green) compared to the young group (blue). B) Amplitudes of high frequency OP peaks are unaffected by age. Single and double asterisk correspond to $p<0.05$ and $p<0.0001$, respectively

Comparison of the two OP extraction methods in pathological states

The above findings underline the notion that aging can introduce strong confounding factors when assessing inner retina function through OPs. To compare the ability of the two OP extraction methods to identify defects within the context of an aging-associated retinal disease, we recorded light-adapted ERG luminance-response functions and analyzed OPs from five subjects with unilateral neovascular (wet) age-related macular degeneration treated with intravitreal anti-VEGF agents and two subjects with unilateral large sPED. The sPED cases were included as examples of pathology confined to the outer retinal layers. There was no sign of intra-retinal or sub-retinal fluid and therefore anti-VEGF therapy had not been initiated.

Figure 3.9 shows representative examples of the MWT scalograms with corresponding filtered ERG traces obtained from 3 different patients with unilateral neovascular AMD under anti-VEGF treatment. The fellow non-neovascular (dry) eye served as an internal control to identify potential implications of chronic (>10 monthly ranibizumab injections) VEGF blockade on OP generation. Panels A, D and G illustrate the MWT scalogram of the fellow non-neovascular (dry) eye and panels B, E and H the MWT scalogram of the neovascular (wet) eye. Panels C, F and I show filtered ERG traces from both eyes of each patient. Patient #1 (top row) presented with sub-retinal and intra-retinal fluid. For responses elicited by a flash stimulus of 0.38 log cd·s/m^2, MWT detected a significant reduction in the low frequency OP band power (A: 21.6693, B: 13.8547). Time-amplitude analysis detected no difference in summed or

individual OP measurements (summed OP amplitude A: 24.129, B: 24.477). Patient #2 (middle row) presented with sub-retinal hemorrhage. For responses elicited by a flash stimulus of 0.88 log cd·s/m^2, MWT analysis of the neovascular eye revealed an extinguished high-frequency OP band with a slight decrease in the low-frequency OP power (D: 19.3656, E: 22.0796). Filtered OP analysis (panel F) found significant reduction in the amplitudes of OP2 (almost extinguished) and OP3/4 (-47%). Patient #3 (bottom row) presented with sub-retinal and intra-retinal fluid. For responses elicited by a flash stimulus of 0.88 log cd·s/m^2, MWT detected a preferential loss of the high-frequency band (G: 14.065, H: 7.2719), with relative preservation of the low-frequency OP power (G: 24.4159, H: 28.5706). Time-amplitude analysis (panel I) revealed reduction in the amplitudes of OP2 (-50%) and OP3/4 (-40%). MWT provided evidence that, in this set of patients, chronic VEGF suppression in the neovascular eye led to a selective power reduction of the high frequency oscillators compared to the low frequency. Scalograms generated with MWT revealed very close proximity of the two bands in the time domain. Their timing (26-32ms) coincided with the occurrence of the filtered OP2 and OP3/4 complex. Amplitude reduction in the neovascular eyes was confined to the filtered OP2 and OP3/4 complex peaks.

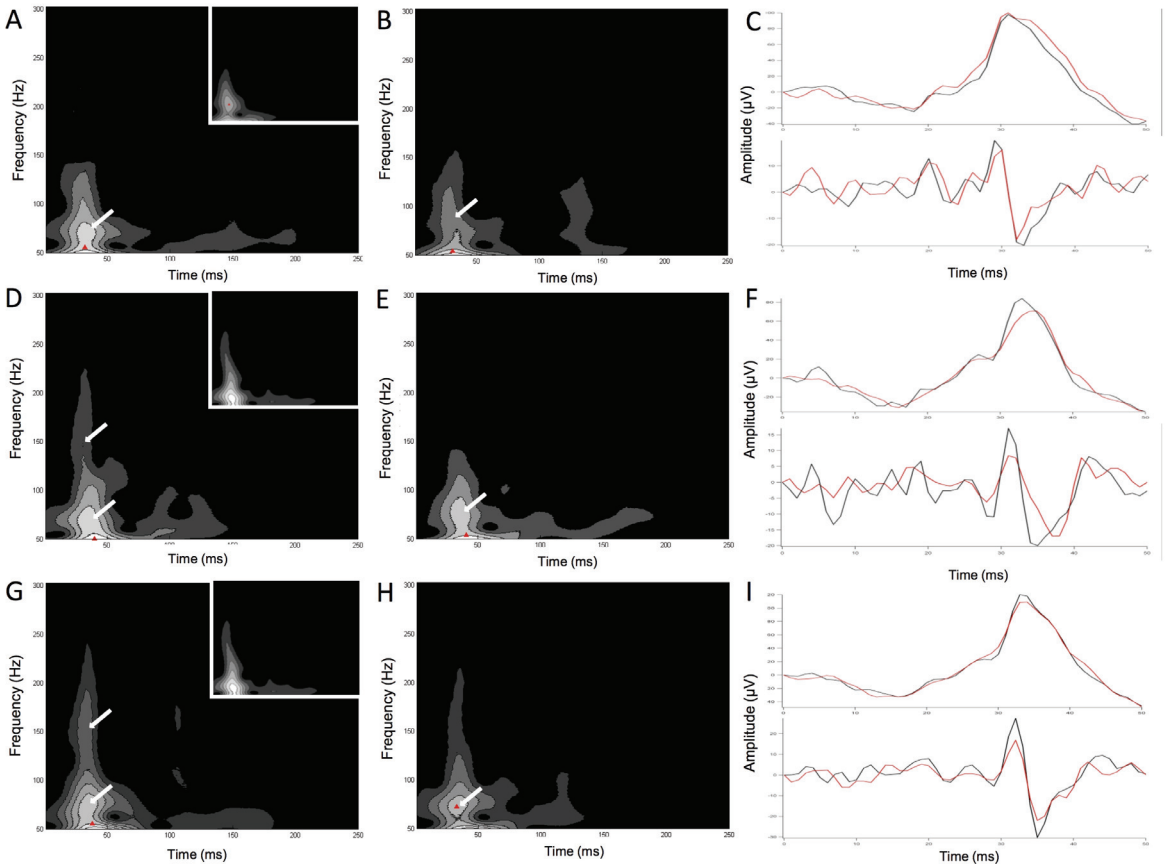

Figure 3.9: OPs in neovascular (wet) AMD. MWT scalograms with unfiltered and filtered ERG traces obtained from patients with unilateral neovascular (wet) AMD under anti-VEGF treatment. Panels A, D and G illustrate the MWT scalogram of the fellow non-neovascular (dry) eye and panels B, E and H the MWT scalogram of the neovascular (wet) eye. A representative example of a normal MWT scalogram for each studied flash strength is given at the top right-hand corner of panels A, D and G. Panels C, F and I show respective unfiltered and filtered ERG traces from both eyes of each patient.

Figure 3.10 shows MWT scalograms with corresponding filtered ERG traces obtained with different flash strengths from a patient diagnosed as having unilateral untreated sPED. Panels A, D and G illustrate the MWT scalogram of the fellow non-neovascular (dry) eye, whereas panels B, E and H the MWT scalogram of the eye with PED. Panels C, F and I show filtered ERG traces from both eyes of the same patient. The top row illustrates responses elicited by a flash stimulus of 0.38 log cd·s/m^2. MWT detected a significant reduction in the low frequency OP band power (A: 17.8148, B: 25.5021). Time-amplitude analysis detected a 25% reduction in OP2. The middle row illustrates responses elicited by a flash stimulus of 0.88 log cd·s/m^2. MWT analysis of the eye with PED revealed a well-preserved high-frequency OP band (D: 8.1851, E: 9.9633) with significant reduction in the low-frequency OP power (D: 16.0634, E: 22.7136). Filtered OP analysis (panel F) identified OP3/4 as the main source of amplitude reduction (-30%). The bottom row illustrates responses elicited by a flash stimulus of 1.36 log cd·s/m^2. Power of the high-frequency band showed no difference between the two eyes. The low frequency OP power was primarily affected (G: 14.6721, H: 20.3739). Time-amplitude analysis (panel I) revealed a universal decline in individual and summed OP amplitudes. In cases of sPED, all of the OP power reduction in MWT originated from the low-frequency oscillators. In terms of filtered OP analysis, the OP2 and OP3/4 complex peaks remained the main source of amplitude reduction.

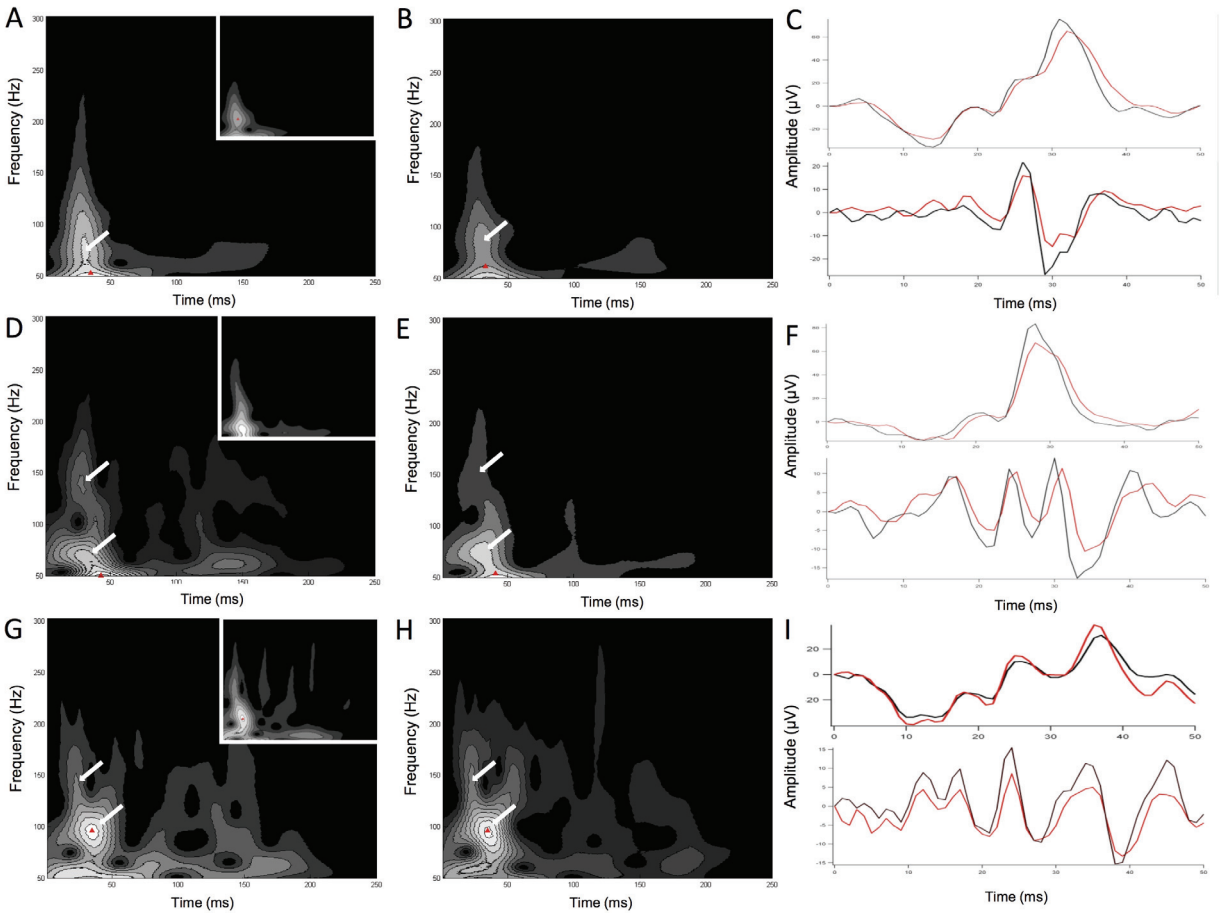

Figure 3.10: OPs in pigment epithelial detachment (PED). MWT scalograms with unfiltered and filtered ERG traces obtained at different flash strengths from a patient with unilateral pigment epithelial detachment (PED). Panels A, D and G illustrate the MWT scalogram of the fellow non-neovascular (dry) eye, whereas panels B, E and H the MWT scalogram of the eye with PED. A representative example of a normal MWT scalogram for each studied flash intensity is given at

the top right-hand corner of panels A, D and G. Panels C, F and I show respective unfiltered and filtered ERG traces from both eyes of the same patient.

DISCUSSION

Previous work on age-related changes in human OPs

To our knowledge, age-related changes in human OPs have been addressed in two main previous studies. In the first study, Kegroat et al. (2001) evaluated individuals aged 75 and older to find amplitude reduction and prolonged implicit times for most OPs recorded under light- and dark-adapted conditions. Our study provided evidence that the inner plexiform layer in the healthy retina undergoes changes much earlier in life (40 years of age) and that most of these changes (especially in dark-adapted OPs) have reached their peak by the age of 60. In fact, changes in amacrine cell function may even precede detection of rod and cone dysfunction by other conventional approaches. Previous analysis of the dark-adapted ERG responses from the same individuals[11] revealed no detectable decline in mixed a- and b-wave amplitude for middle-aged individuals (40-59y). As such, recording and analyzing OPs, as done in this paper, provides a highly sensitive approach for the early detection of age-related functional changes in the human retina. In the second study, Sannita et al. (1989) also examined OPs in a large population of subjects (aged 1 to 84 years) using Ag/AgCl dermal electrodes. The authors reported an initial increase of the OP amplitude from childhood to adulthood, followed by a decrease above 50 years of age. Implicit times for most OPs also increased with age. Although in agreement

with our findings, results from this study should be interpreted cautiously, since all full-field ERG recordings were performed in non-dilated eyes.

Kergoat et al. (2001) also utilized a single strength of light at two separate wavelengths to measure rod- and cone-driven responses and not the wide range of flash strengths used in the current study to reveal dynamics of human OPs. Hancock et al. (2008), on the other hand, studied the intensity-response function of dark-adapted OPs in 5 healthy subjects and reported reduced OP power with faster timing for stimulus strengths 10-fold higher than the ISCEV standard for producing OPs (0.54 log cd·s/m^2). Our results contradict these findings. We were able to record ERG responses across a wide range of white-flash stimulus strengths (-0.02 to 1.37 log cd·s/m^2) under both dark- and light- adapted conditions. Analysis of filtered dark-adapted OP responses showed a clear positive linear relationship with increasing flash strength; no plateau or decline phase was noted for any individual OP components or the summed OP amplitude. In agreement with Hancock et al. (2008), shorter implicit times were found for most OP components as the stimulus strength increased under dark and light adaptation.

OP response attenuation with age

Age-related alterations in crystalline lens density, which reduce retinal luminance in older individuals, should be excluded as a possible explanation for the recorded attenuated OP responses. A sub-analysis restricted to older pseudophakic individuals (n=6) provided further support that the reduced OP

amplitudes and delayed implicit times were of retinal origin. In addition, even though some people develop cataracts during their middle-age years (40s and 50s), these cataracts tend to be very minimal to affect ERG responses. In the present study, attenuated OP responses were recorded already by 40 years of age.

Affected parameters of the oscillatory response have been linked to underlying inner retina dysfunction (Wachtmeister L. 1998), especially loss of integrity in the retinal microcirculation (Brown KT 1968). Such dependence has become clear through studying human retinal disorders that show attenuated OP responses as a characteristic ERG feature: diabetic retinopathy (Kizawa et al. 2006; Bresnick and Palta 1987; van der Torren and Mulder 1993; Li et al. 1992), retinopathy of prematurity (Akula et al. 2007), central retinal vein occlusion (Yu et al. 1998; Huang et al. 2001) and primary open-angle glaucoma (Holopigian et al. 2000). In both proliferative and non-proliferative diabetic retinopathy, individual and summed OP responses are reduced in amplitude and delayed in timing (Li et al. 1992). OP amplitudes have been found to decrease progressively as the retinopathy grade in fundus color photographs and the severity of leakage and capillary non-perfusion in fluorescein angiograms increases (Bresnick and Palta 1987). In primary open angle glaucoma, reduced and delayed OP responses have been reported (Holopigian et al. 2000; Vaegan et. al 1995; Gur et al. 1987; North et al. 2010). Experimental induction of glaucoma in primates has been found to result in selective loss of a low frequency oscillatory component in the multifocal ERG signal. In these studies, reduced OP responses correlated with areas of reduced retinal nerve fiber layer thickness (Rangaswamy et al. 2006; Luo

et al. 2011). An anatomical-functional correlation also exists in humans. Loss of a distinct oscillatory feature in the temporal retina of patients with glaucoma has been shown to lead to asymmetry between nasal and temporal multifocal ERG responses (Fortune et al. 2002). Such changes have been postulated to reflect abnormalities in the inner plexiform layer of the temporal retina, where classic OPs are thought to arise. The documented impairment of inner retinal cell function during the early stages of these diseases seems to closely resemble the age-related pattern of decline seen with our study. OP response attenuation with age could therefore reflect functional changes resulting from either dysfunction/loss of inner retina cells (Gao and Hollyfield 1992; Harman et al. 2000) and/or changes in the inner retinal and choroidal vasculature (Ardeljan and Chan 2013; Hughes et al. 2006).

Evidence of two distinct OP peaks in the human retina

MWT analysis of the human ERG signal allowed simultaneous segmentation of the OP response in the frequency and time domains. This method revealed the existence of more than one oscillator in the dark- and light-adapted human retina. Similar findings were reported in rats by Forte et al. (2008), the original group to detail the MWT application to analyze the dynamics of rat OPs. In their experiments, two clusters of dark-adapted OP bands at 70Hz and 130Hz were identified. For moderate flashes, OP oscillators overlapped in time (50ms). At the highest stimulus strengths, the clusters were 20ms after the flash in the 70Hz band, and 50ms after the stimulus in the 130Hz band. A similar pattern

characterized human dark-adapted OP responses, with bands at 77Hz and 155Hz. At higher strengths, peak time of the low frequency band occurred earlier than the high frequency and in close proximity to the larger and steeper a-wave, making quantification unreliable without pre-conditioning ERG waveforms to remove the a-wave.

In the light-adapted human retina, MWT revealed a dual-band oscillatory system for specific flash strengths. High frequency peaks occurred *earlier* than their low frequency counterparts. Several studies have provided support for an intra-retinal source differentiation of generators of early and late OPs. Pharmacological studies in the mudpuppy retina have related the earlier OPs to the ON component and the later ones to the OFF component of the ERG (Wachtmeister L. 1981). Patients with congenital stationary night blindness, who have defective ON pathways, preferentially lose the first two OPs (early OPs) on the rising edge of the photopic b-wave (Lachapelle et al. 1983). The last OP wavelet of the human ERG is time-locked to stimulus offset (Kojima and Zrenner 1978). It has been suggested previously that the last major OP of the photopic response as well as the i-wave (a post b-wave component recorded under light adaptation in humans, originating, at least in part, from retinal ganglion cells) are generated by the retinal OFF pathway (Lachapelle et al. 1998). In addition, pharmacological disruption of ON and OFF pathways has been shown to differentially affect the OPs in the amphibian retina; GABA-receptor antagonists modulate early OPs, whereas glycine-receptor antagonists affect the late OPs (Wachtmeister L. 1980). Zhou et al. (2007) matched the slow-sequence multifocal

ERG from the macular region of the retina of primates with Gabor functions and showed that OPs fell into two distinct frequency bands: a high frequency band peaking around 150 Hz that contributes to early OPs, and a low frequency band peaking around 80 Hz that contributes to both early and late OPs. In a subsequent study, the OPs at higher frequency were found to be more susceptible to experimental glaucoma (Rangaswamy et al. 2006). Based on the above, the segregation of light-adapted OP responses into two frequency bands separated in time suggests the possibility of ON and OFF system representation. Even in dark-adapted (rod-driven) OP responses, the OFF system may still be represented, since there has been recent evidence of a direct excitation of cone OFF bipolar cells by rod photoreceptors in rodents (Hack et al. 1999).

Luminance dependence of the dual-band frequency oscillatory pattern

In the present study, MWT analysis not only confirmed the existence of a dual-band frequency oscillatory pattern in the light-adapted human retina but also revealed the luminance dependence of this pattern. A plausible explanation for the presence of a stimulus strength threshold for the appearance of the high frequency band could be sought at the complex intensity-response function of the cone-dominated human ERG per se. In response to progressively brighter stimuli, the b-wave of the light-adapted ERG gradually increases in amplitude, reaches a plateau for a narrow range of stimulus strengths and then rapidly decreases with further increments in the flash strength. This unique phenomenon is known as photopic hill (Rufiange et al. 2002; Wali and Leguire 1992). According to Ueno et

al. (2004), the characteristic shape of the photopic hill results from the summation of two events: at higher flash luminance, the ON response amplitude decreases and the positive peak of the OFF response becomes delayed. This is supported by the fact that mathematical modeling of a combination of both ON and OFF cone response curves can produce a hill effect (Hamilton et al. 2007). Intensity-response analysis of light-adapted wavelet derived parameters showed that for low to moderate light stimuli (<0.88 log cd·s/m^2) only the low frequency (80-100 Hz) band could be identified. At these stimulus strengths, OFF bipolar cells (hyperpolarizing type) are known to mostly contribute to the generation of the cone a-wave (Bush and Sieving 1994). Interestingly, the stimulus strength threshold for the appearance of the dual-band frequency pattern coincided with the occurrence of the plateau and decline phase of the photopic hill function (Freund et al. 2011). The relative amplitude of the high frequency band remained stable with further increments of flash strength (~10 arbitrary units of power), whereas the relative amplitude of the low frequency band yielded a characteristic "photopic hill" function (see Figure 3.5). Rufiange et al. (2002) found that the OPs previously associated with the retinal ON pathway (OP1 and OP2) do not appear to show any deterioration as a result of progressively brighter flashes. Contrastingly, brighter flashes led to a complete abolition of the late OPs (mainly OP4) that are generated by the retinal OFF pathway (Nagata M. 1963). Although not proven directly, it can be postulated that the ON and OFF pathways are not only expressed in OP generation but may also possess different frequency spectrum characteristics. In support of this hypothesis, only OP peaks in the low

frequency band showed vulnerability to age-associated decline. Suzuki et al. (1998) reported a higher age-related vulnerability of the OFF compared to ON bipolar cells. Further work will be required to determine whether the distinct groups of oscillators identified by wavelet analysis can be attributed to pharmacologically distinguishable retinal pathways.

Advantage of Morlet Wavelet Transform over time-amplitude analysis

As a potential age-independent marker of inner retina function, the high frequency OP band could be of significant clinical utility, as one could exclude age as a confounder and attribute with higher confidence deterioration to a disease state per se. We compared the two OP analytical methods in the context of an age-associated disease, to investigate what additional information MWT could provide over traditional time-amplitude analysis. Our findings show that eyes with neovascular (wet) AMD treated with anti-VEGF agents had selectively reduced OP power in the high frequency compared to the low frequency band, when compared to the untreated fellow eye. In cases of treatment-naïve sPED, all of the OP power reduction in MWT originated from the low-frequency oscillators. Filtered OPs failed to provide a similar differentiation; in both neovascular AMD and sPED cases, the OP2 and the OP3/4 complex peaks accounted for the recorded amplitude reduction. A possible explanation behind this observation is that, as an approach, time-amplitude analysis relies on the summed amplitude of multiple oscillators. For instance, based on timing, the OP2 and the OP3/4 complex may reflect activity from both the low frequency and high frequency

oscillators. Scalograms generated with MWT in the neovascular AMD eyes show the occurrence of both low and high frequency bands at the very same time (30ms) of occurrence of the OP3/4 complex for a specific flash strength (figure 3.8).

Although outside the scope of the present study, why we see such changes in OPs of neovascular AMD eyes under anti-VEGF treatment remains to be elucidated. The issue of possible inner retina toxicity caused by prolonged VEGF blockade has been previously raised. Several lines of evidence indicate an important role for endogenous VEGF in the maintenance and function of adult retina neuronal cells, such as the photoreceptors and the Müller cells (Saint-Geniez et al. 2008). Chronic inhibition of VEGF-A function in normal adult animals has been shown to lead to a significant loss of retinal ganglion cells (Nishijima et al. 2007). In addition, changes in retinal nerve fiber layer thickness have been reported in treated eyes of patients with unilateral neovascular AMD (Martinez-de-la-Casa et al. 2012).

In conclusion, MWT provides complementary information not obtainable through traditional analytical methods and as such optimizes the differential diagnosis of retinal disorders. Application of this approach to retinal dystrophies with distinct pathway deficits would not only further validate the clinical utility of MWT as a tool, but also provide further insight into the physiological origin of multiple oscillators in the human retina.

BIBLIOGRAPHY

Akula JD, Mocko JA, Moskowitz A, Hansen RM, Fulton AB. The oscillatory potentials of the dark-adapted electroretinogram in retinopathy of prematurity. *Invest Ophthalmol Vis Sci.* 2007 Dec;48(12):5788-97.

Ardeljan D, Chan CC. Aging is not a disease: Distinguishing age-related macular degeneration from aging. *Prog Retin Eye Res.* 2013 Aug 9.

Bresnick GH, Palta M. Oscillatory potential amplitudes. Relation to severity of diabetic retinopathy. *Arch Ophthalmol.* 1987 Jul;105(7):929-33.

Brigell M, Bach M, Barber C, Kawasaki K, Kooijman A. Guidelines for calibration of stimulus and recording parameters used in clinical electrophysiology of vision. Calibration Standard Committee of the International Society for Clinical Electrophysiology of Vision (ISCEV). *Doc Ophthalmol.* 1998;95(1):1-14.

Brown KT. The eclectroretinogram: its components and their origins. *Vision Res.* 1968 Jun;8(6):633-77.

Brunette JR. Double a-waves and their relationships to the oscillatory potentials. *Invest Ophthalmol.* 1972 Apr;11(4):199-210.

Bui BV, Armitage JA, Vingrys AJ. Extraction and modelling of oscillatory potentials. *Doc Ophthalmol.* 2002 Jan;104(1):17-36.

Bush RA, Sieving PA. A proximal retinal component in the primate photopic ERG a-wave. *Invest Ophthalmol Vis Sci.* 1994 Feb;35(2):635-45.

Creel, D. (2011) The electroretinogram: Clinical Applications. Webvision http://webvision.med.utah.edu/book/electrophysiology/the-electroretinogram-clinical-applications/

Curcio CA, Millican CL, Allen KA, Kalina RE. Aging of the human photoreceptor mosaic: evidence for selective vulnerability of rods in central retina. *Invest Ophthalmol Vis Sci.* 1993 Nov;34(12):3278-96.

Dong CJ, Agey P, Hare WA. Origins of the electroretinogram oscillatory potentials in the rabbit retina. *Vis Neurosci.* 2004 Jul-Aug;21(4):533-43.

el Azazi M, Wachtmeister L. The postnatal development of the oscillatory potentials of the electroretinogram V. Relation to the double peaked a-wave. *Acta Ophthalmol (Copenh).* 1993 Feb;71(1):32-8.

Forte JD, Bui BV, Vingrys AJ. Wavelet analysis reveals dynamics of rat oscillatory potentials. J Neurosci Methods. 2008 Mar 30;169(1):191-200.

Fortune B, Bearse MA Jr, Cioffi GA, Johnson CA. Selective loss of an oscillatory component from temporal retinal multifocal ERG responses in glaucoma. *Invest Ophthalmol Vis Sci.* 2002 Aug;43(8):2638-47.

Freund PR, Watson J, Gilmour GS, Gaillard F, Sauvé Y. Differential changes in retina function with normal aging in humans. *Doc Ophthalmol.* 2011 Jun;122(3):177-90.

Gao H, Hollyfield JG. Aging of the human retina. Differential loss of neurons and retinal pigment epithelial cells. *Invest Ophthalmol Vis Sci.* 1992 Jan;33(1):1-17.

Gartner S, Henkind P. Aging and degeneration of the human macula. 1. Outer nuclear layer and photoreceptors. *Br J Ophthalmol.* 1981 Jan;65(1):23-8.

Guité P, Lachapelle P. The effect of 2-amino-4-phosphonobutyric acid on the oscillatory potentials of the electroretinogram. *Doc Ophthalmol.* 1990 Sep;75(2):125-33.

Gur M, Zeevi YY, Bielik M, Neumann E. Changes in the oscillatory potentials of the electroretinogram in glaucoma. *Curr Eye Res.* 1987 Mar;6(3):457-66.

Hack I, Peichl L, Brandstätter JH. An alternative pathway for rod signals in the rodent retina: rod photoreceptors, cone bipolar cells, and the localization of glutamate receptors. Proc Natl Acad Sci U S A. 1999 Nov 23;96(24):14130-5.

Hamilton R, Bees MA, Chaplin CA, McCulloch DL. The luminance-response function of the human photopic electroretinogram: a mathematical model. *Vision Res.* 2007 Oct;47(23):2968-72.

Hancock HA, Kraft TW. Human oscillatory potentials: intensity-dependence of timing and amplitude. *Doc Ophthalmol.* 2008 Nov;117(3):215-22.

Harman A, Abrahams B, Moore S, Hoskins R. Neuronal density in the human retinal ganglion cell layer from 16-77 years. *Anat Rec.* 2000 Oct 1;260(2):124-31.

Holopigian K, Greenstein VC, Seiple W, Hood DC, Ritch R. Electrophysiologic assessment of photoreceptor function in patients with primary open-angle glaucoma. *J Glaucoma.* 2000 Apr;9(2):163-8.

Huang S, Wu L, Luo T, et al. The electroretinogram in patients with retinal vascular occlusion. *Yan Ke Xue Bao.* 2001 Mar;17(1):50-3.

Hughes S, Gardiner T, Hu P, Baxter L, Rosinova E, Chan-Ling T. Altered pericyte-endothelial relations in the rat retina during aging: implications for vessel stability. *Neurobiol Aging.* 2006 Dec;27(12):1838-47.

Jackson GR, Owsley C, McGwin G Jr. Aging and dark adaptation. *Vision Res.* 1999 Nov;39(23):3975-82.

Kergoat H, Kergoat MJ, Justino L. Age-related changes in the flash electroretinogram and oscillatory potentials in individuals age 75 and older. *J Am Geriatr Soc.* 2001 Sep;49(9):1212-7.

Kizawa J, Machida S, Kobayashi T, Gotoh Y, Kurosaka D. Changes of oscillatory potentials and photopic negative response in patients with early diabetic retinopathy. *Jpn J Ophthalmol.* 2006 Jul-Aug;50(4):367-73.

Kojima M, Zrenner E. Off-components in response to brief light flashes in the oscillatory potential of the human electroretinogram. *Albrecht Von Graefes Arch Klin Exp Ophthalmol.* 1978 May 2;206(2):107-20.

Lachapelle P, Little JM, Polomeno RC. The photopic electroretinogram in congenital stationary night blindness with myopia. *Invest Ophthalmol Vis Sci.* 1983 Apr;24(4):442-50.

Lachapelle P, Rousseau S, McKerral M, et al. Evidence supportive of a functional discrimination between photopic oscillatory potentials as revealed with cone and rod mediated retinopathies. *Doc Ophthalmol.* 1998;95(1):35-54.

Lamb TD, Pugh EN Jr. Phototransduction, dark adaptation, and rhodopsin regeneration the proctor lecture. *Invest Ophthalmol Vis Sci.* 2006 Dec;47(12):5137-52.

Li X, Sun X, Hu Y, Huang J, Zhang H. Electroretinographic oscillatory potentials in diabetic retinopathy. An analysis in the domains of time and frequency. *Doc Ophthalmol.* 1992;81(2):173-9.

Liets LC, Eliasieh K, van der List DA, Chalupa LM. Dendrites of rod bipolar cells sprout in normal aging retina. Proc Natl Acad Sci U S A. 2006 Aug 8;103(32):12156-60.

Luo X, Patel NB, Harwerth RS, Frishman LJ. Loss of the low-frequency component of the global-flash multifocal electroretinogram in primate eyes with experimental glaucoma. *Invest Ophthalmol Vis Sci.* 2011 Jun 1;52(6):3792-804.

Marmor MF, Fulton AB, Holder GE, Miyake Y, Brigell M, Bach M; International Society for Clinical Electrophysiology of Vision. ISCEV Standard for full-field clinical electroretinography (2008 update). *Doc Ophthalmol.* 2009 Feb;118(1):69-77.

Martinez-de-la-Casa JM, Ruiz-Calvo A, Saenz-Frances F, Reche-Frutos J, Calvo-Gonzalez C, Donate-Lopez J, Garcia-Feijoo J. Retinal nerve fiber layer thickness changes in patients with age-related macular degeneration treated with intravitreal ranibizumab. Invest Ophthalmol Vis Sci. 2012 Sep 14;53(10):6214-8.

Nagata M. Studies on the photopic ERG of the human retina. *Jpn J Opbthalmol.* 1963;7:96-124

Nishijima K, Ng YS, Zhong L, Bradley J, Schubert W, Jo N, Akita J, Samuelsson SJ, Robinson GS, Adamis AP, Shima DT. Vascular endothelial growth factor-A is survival factor for retinal neurons and a critical neuroprotectant during the adaptive response to ischemic injury. Am J Pathol. 2007 Jul;171(1):53-67.

North RV, Jones AL, Drasdo N, Wild JM, Morgan JE. Electrophysiological evidence of early functional damage in glaucoma and ocular hypertension. *Invest Ophthalmol Vis Sci.* 2010 Feb;51(2):1216-22.

Panda-Jonas S, Jonas JB, Jakobczyk-Zmija M. Retinal photoreceptor density decreases with age. *Ophthalmology.* 1995 Dec;102(12):1853-9.

Rangaswamy NV, Zhou W, Harwerth RS, Frishman LJ. Effect of experimental glaucoma in primates on oscillatory potentials of the slow-sequence mfERG. *Invest Ophthalmol Vis Sci.* 2006 Feb;47(2):753-67.

Rufiange M, Rousseau S, Dembinska O, Lachapelle P. Cone-dominated ERG luminance-response function: the Photopic Hill revisited. *Doc Ophthalmol.* 2002 May;104(3):231-48.

Rufiange M, Rousseau S, Dembinska O, Lachapelle P. Cone-dominated ERG luminance-response function: the Photopic Hill revisited. *Doc Ophthalmol.* 2002 May;104(3):231-48.

Saint-Geniez M, Maharaj AS, Walshe TE, Tucker BA, Sekiyama E, Kurihara T, Darland DC, Young MJ, D'Amore PA. Endogenous VEGF is required for visual function: evidence for a survival role on müller cells and photoreceptors. PloS One. 2008;3(11):e3554.

Sannita WG, Maggi L, Germini PL, Fioretto M. Correlation with age and sex of flash-evoked electroretinogram and retinal oscillatory potentials recorded with skin electrodes. Doc Ophthalmol. 1989 Apr;71(4):413-419.

Stockton RA, Slaughter MM. B-wave of the electroretinogram. A reflection of ON bipolar cell activity. *J Gen Physiol.* 1989 Jan;93(1):101-22.

Suzuki S, Horiguchi M, Tanikawa A, Miyake Y, Kondo M. Effect of age on short-wavelength sensitive cone electroretinogram and long- and middle-wavelength sensitive cone electroretinogram. *Jpn J Ophthalmol.* 1998 Sep-Oct;42(5):424-30.

Ueno S, Kondo M, Niwa Y, Terasaki H, Miyake Y. Luminance dependence of neural components that underlies the primate photopic electroretinogram. *Invest Ophthalmol Vis Sci.* 2004 Mar;45(3):1033-40.

Vaegan, Graham SL, Goldberg I, Buckland L, Hollows FC. Flash and pattern electroretinogram changes with optic atrophy and glaucoma. *Exp Eye Res.* 1995 Jun;60(6):697-706.

van der Torren K, Mulder P. Comparison of the second and third oscillatory potentials with oscillatory potential power in early diabetic retinopathy. *Doc Ophthalmol.* 1993;83(2):111-8.

Wachtmeister L. Further studies of the chemical sensitivity of the oscillatory potentials of the electroretinogram (ERG) I. GABA- and glycine antagonists. *Acta Ophthalmol (Copenh).* 1980 Oct;58(5):712-25.

Wachtmeister L. Further studies of the chemical sensitivity of the oscillatory potentials of the electroretinogram (ERG). II. Glutamate-aspartate-and dopamine antagonists. Acta Ophthalmol (Copenh). 1981 Apr;59(2):247-58.

Wachtmeister L. Further studies of the chemical sensitivity of the oscillatory potentials of the electroretinogram (ERG). III. Some omega amino acids and ethanol. Acta Ophthalmol (Copenh). 1981 Aug;59(4):609-19.

Wachtmeister L. Oscillatory potentials in the retina: what do they reveal. *Prog Retin Eye Res.* 1998 Oct;17(4):485-521.

Wali N, Leguire LE. The photopic hill: a new phenomenon of the light adapted electroretinogram. *Doc Ophthalmol.* 1992;80(4):335-45.

Yu M, Liang X, Wen F, Wu DZ, Luo T. Analysis of oscillatory potentials of flash electroretinogram in frequency domain and time domain in retinal vein occlusion. *Yan Ke Xue Bao.* 1998 Sep;14(3):176-81, 144.

Zhou W, Rangaswamy N, Ktonas P, Frishman LJ. Oscillatory potentials of the slow-sequence multifocal ERG in primates extracted using the Matching Pursuit method. *Vision Res.* 2007 Jul;47(15):2021-36.

Chapter 4. EFFECT OF GENOTYPE ON RESPONSE TO ANTI-VEGF TREATMENT[3]

INTRODUCTION

Age-related macular degeneration (AMD) is the leading cause of blindness in developed countries for individuals over 60 years of age. The neovascular (wet) form of AMD, although constituting 10% of overall disease prevalence, accounts for 90% of severe vision loss associated with the condition (Ferris, Fine, & Hyman, 1984). The hallmark of wet AMD is abnormal choroidal blood vessel formation and growth (choroidal neovascularization: CNV). Vascular endothelial growth factor (VEGF) is the major mediator of the CNV process (Spilsbury et al. 2000). Therefore, over the past decade, intravitreal administration of anti-VEGF agents (ranibizumab and bevacizumab) has become the mainstay of treatment for wet AMD. Although treatment response varies based on the criteria used, no single study reports universal response to anti-VEGF therapies. Using measurable data of responsiveness evaluation, Krebs et al. (2013) determined that about 15% of patients treated for at least 3 months with anti-VEGF injections would respond insufficiently. These patients will continue to experience decline in visual acuity and/or increase in retinal thickness and lesion size (Krebs et al. 2013).

Previous investigations have associated poor response to ranibizumab and bevacizumab with single nucleotide polymorphisms (SNPs) in the complement factor H (*CFH*) gene (Nissler et al. 2011; Chen et al. 2012) and the age-related

[3] This chapter contains as-yet unpublished data, presented in a paper-based format.

maculopathy susceptibility 2 (*ARMS2*) gene (Teper et al. 2010; Tian et al. 2012). Variants in these genes have been identified in recent genome-wide association studies (GWAS) as major AMD risk loci for the development of the disease and therefore could, to some degree, be associated with worse treatment outcomes. Two of the largest prospective pharmacogenetic studies so far (CATT, IVAN) failed to associate any of the individual high-risk variants with treatment responsiveness (Hagstrom et al. 2013; Lotery et al. 2013). It is, however, unlikely that in complex diseases, such as AMD, a single SNP will adequately explain treatment outcomes. A combination of single-nucleotide polymorphisms (SNPs) may be more likely associated with a phenotype of poor response even if each SNP has little individual effect. In support of such notion, some groups examined the cumulative effect of risk alleles at different loci to create models involving multiple genes. Kloeckener-Gruissem et al. (2011) found that a heterozygous genotype combination at the examined SNPs in the *CFH* and *FZD4* loci was associated with higher likelihood of better visual outcomes. In a similar study, Smailhodzic et al. (2012) showed a cumulative effect of risk alleles in the *CFH*, *ARMS2* and *VEGF* genes with poorer response rate to anti-VEGF treatment. Protective haplotypes and genotypes should also be taken into consideration when designing predictive models of treatment response. Haplotypes spanning the *CFH* (Spencer et al. 2007) and *SKIVL2/MYRIP* (Kopplin et al. 2010) genes have been identified as protective factors for AMD.

Most pharmacogenetic studies for treatment response of AMD have relied on regression analysis and variation in allele frequency between poor and good

responders to identify candidate predictor SNPs. Statistical approaches based on regression analysis may lose statistical power because of the use of statistics with high degrees-of-freedom and the large number of hypotheses tested during combinatorial search involving multiple SNPs. In this current work, we propose the use of machine learning classification techniques to develop a multi-SNP classifier that would accurately predict anti-VEGF treatment outcomes in AMD. The goal is twofold: first, to confirmthe hypothesis that combined genetic information in a selected set of previously associated SNPs can, with high rate of success, predict the response of AMD patients to treatment; and second, to propose a classifier with its decision rules that accurately predicts treatment response. Such methodology will not only provide a potential prediction tool but may also suggest possible epistatic (gene-to-gene) interactions that may otherwise remain undiscovered with regression methods.

METHODS

This study received ethics approval from the Health Research Ethics Board (Biomedical Panel) of the University of Alberta. All procedures conformed to the Code of Ethics of the World Medical Association (Declaration of Helsinki).

Patients

Eighty-four patients (mean age: 73.6, SD: 8.9) with unilateral and/or bilateral neovascular (wet) macular degeneration (Age-Related Eye Disease Study [AREDS] severity scale: 11b; definite end-stage disease) (Davis et al., 2005) were

recruited from the Alberta Retina Consultants (ARC). All patients were undergoing monthly intravitreal injections of ranibizumab (Lucentis, Novartis, Basel, Switzerland) and/or bevacizumab (Avastin, Genentech, South San Francisco, CA, USA) for a minimum of 12 months. In patients with bilateral disease, a single eye per patient was used in the analysis. Central macular thickness (CMT) was measured at baseline and monthly thereafter with optical coherence tomography (Stratus OCT, Carl Zeiss Meditec Inc., Jena, Germany). Snellen visual acuity (logMAR) was measured monthly after initiation of treatment. Patients with visual acuities reduced to counting fingers (CF) were assigned a logMAR value of 2.0. Data were collected from the day of neovascular AMD onset in the study eye (*retrospectively*) until month 12 after the first anti-VEGF injection (*retrospectively and prospectively*). All AMD-related CNV lesion types were included in this study, except for serous pigment epithelial detachments (sPEDs) without evidence of CNV. Patients with missing data were excluded.

Response classification

Evaluation of response to anti-VEGF treatment was based on change in visual acuity and the presence of sub-retinal/intra-retinal fluid. "Poor responders" were characterized by at least two of the following: a) more than 0.1 logMAR loss in visual acuity at 12 months compared to baseline; b) absence of a decrease in CMT at 3 and 6 months after the first injection; and c) new macular fluid at 3 and 6 months in different areas of the retina. Patients who experienced resolution of

fluid with decreased CMT and an increase in visual acuity more than 0.1 logMAR from baseline were considered “good responders”. Patients with preserved visual acuity (less than 0.1 logMAR change) and decreased CMT at 3 and 6 months follow-ups were considered “typical responders”. To simplify the decision tree model, typical and good responders were grouped under a single group. Representative examples of poor and good responders are given in figures 4.1 and 4.2 respectively.

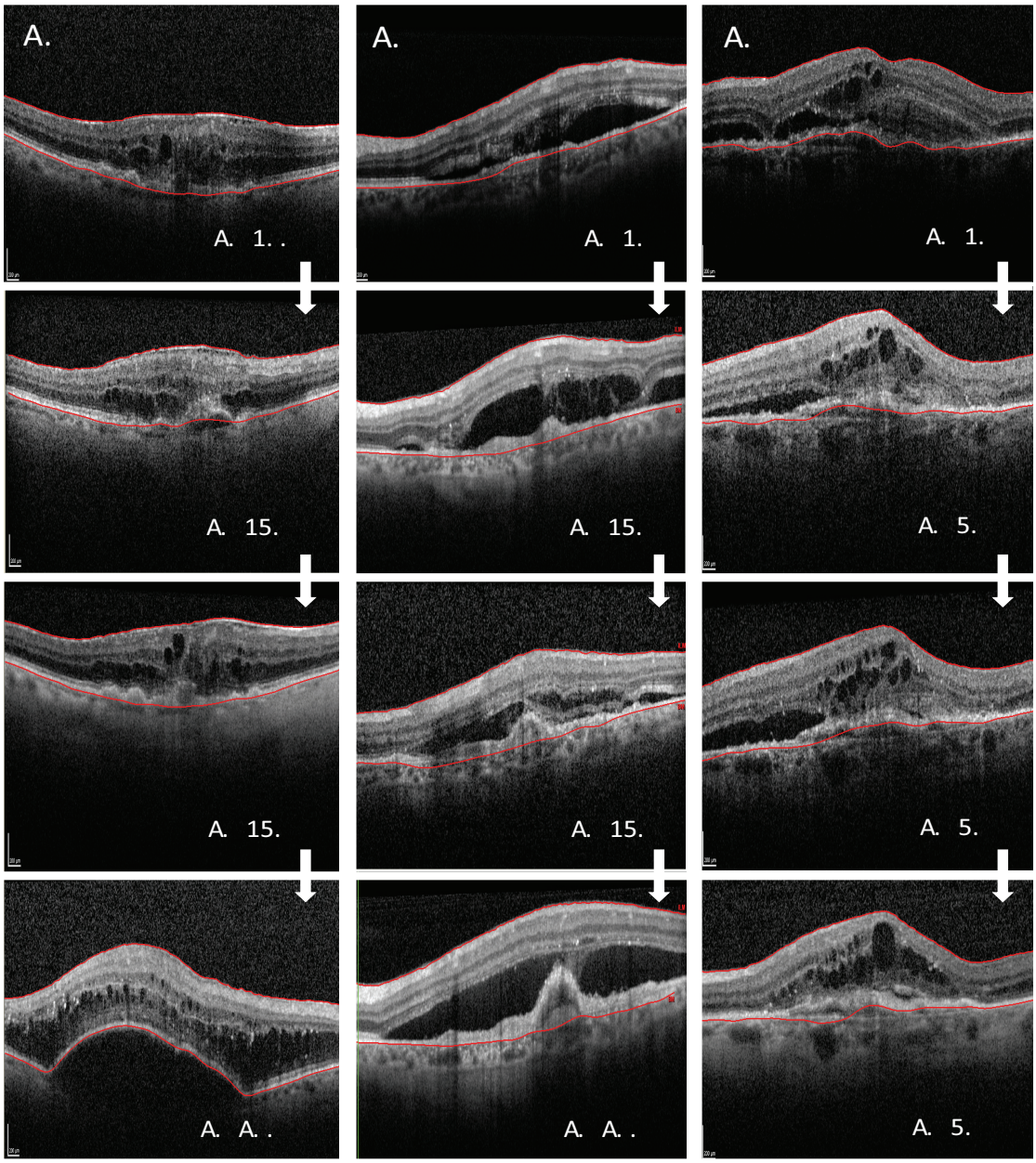

Figure 4.1: Representative cases of poor response to anti-VEGF therapy. OCT scans and visual acuity measurements obtained from three different patients (A-C) at baseline (first row), 3 months (second row), 6 months (third row) and 12 months (fourth row) after initiation of anti-VEGF therapy.

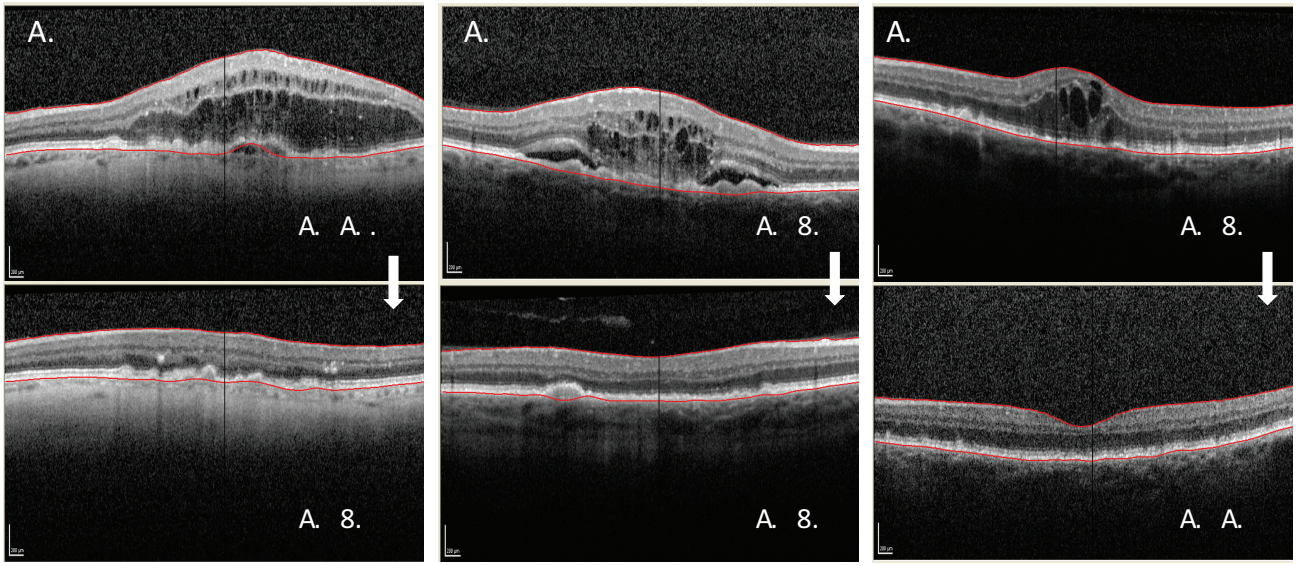

Figure 4.2: Representative cases of good response to anti-VEGF therapy. OCT scans and visual acuity measurements obtained from three different patients (A-C) at baseline (top row) and 3 months (bottom row) after initiation of anti-VEGF therapy.

Genotyping and SNP selection

Peripheral venous blood (10mL) was collected from each study participant in EDTA tubes. Genomic DNA was extracted form whole blood using the Gentra Puregene Blood kit (Gentra Systems, Inc., Minneapolis, Minn.) according manufacturer's instructions. Patients were genotyped for 53 single nucleotide polymorphisms (SNPs) in 30 genes. SNP analysis was performed using high-throughput matrix-assisted laser desorption-ionization time-of-flight mass spectrometry (MALDI-TOF MS) on the Mass ARRAY iPLEX Platform

(Sequenom, San Diego, CA). SNPs were selected based on previous genome wide association reports. Implicated genes could be clustered into four different biological pathways: a) inflammation and complement system regulation; b) lipid metabolism; c) oxidative stress and extracellular matrix remodeling; and d) angiogenesis. Several new loci recently associated with AMD development were also considered. (Fritsche et al. 2013) A summary of the selected SNPs is provided in table 4.1.

Gene	SNP
Inflammation/ Complement system	
CFH	rs10737680(Fritsche et al., 2013), rs1061170, rs1065489, rs800292
C2-CFB	rs429608(Fritsche et al., 2013), rs9332739
C3	rs2230199(Fritsche et al., 2013), rs1047286
CFI	rs4698775(Fritsche et al., 2013), rs10033900
IL-23R	rs10127763 (Wang et al., 2012)
IL-8	rs2227306, rs2227532(Tsai et al., 2008)
CCL2	rs4586(Anand et al., 2012)
CCR2	rs1799865(Anand et al., 2012)
Lipid Metabolism	
APOE	rs4420638(Fritsche et al., 2013)
CETP	rs1864163(Fritsche et al., 2013), rs1799865
LIPC	rs920915(Fritsche et al., 2013), rs10468017
PLA2G12A	rs2285714(Wang et al., 2012)
ABCA1	rs1883025
Oxidative Stress/ Extracellular Matrix Remodeling	
HTRA1	rs11200638(Fritsche et al., 2013)
SYN3/TIMP3	rs5749482(Fritsche et al., 2013), rs9621532
COL8A1-FILIP1L	rs13081855(Fritsche et al., 2013)
COL1OA1	rs3812111(Fritsche et al., 2013)
Angiogenesis	
VEGFA	rs3025039, rs699947, rs833069, rs943080
KDR (VEGFR-2)	rs7671745, rs2071559
FLT-1 (VEGFR-1)	rs622227, rs2387632, rs9319425
PPARGC1A	rs3736265(SanGiovanni et al., 2013)
PEDF	rs1136287(Bhutto et al., 2006)
Other	
SCARB1	rs5888(Zerbib et al., 2009)
TNFRSF10A	rs13278062(Fritsche et al., 2013)
IER3-DDR1	rs3130783(Fritsche et al., 2013)
SLC16A8	rs8135665(Fritsche et al., 2013)
TGFBR1	rs334353(Fritsche et al., 2013)
RAD51B	rs8017304(Fritsche et al., 2013)
ADAMTS9	rs6795735(Fritsche et al., 2013)
B3GALTL	rs9542236(Fritsche et al., 2013)

Table 4.1: Summary of selected SNPs for genotyping AMD patients. Candidate genes are represented in biological pathways.

Classifier

The tool we used to perform our analyses was the WEKA machine learning toolkit (http://www.cs.waikato.ac.nz/~ml/weka/ provided in the public domain by the University of Waikato, Hamilton, NZ). We employed the J48 implementation of C4.5 algorithm, an extension of the basic ID3 algorithm designed by Quinlan (Quinlan, 1993). C4.5 builds decision trees from a set of training data in the same way as ID3, using the concept of information entropy. At each node of the tree, C4.5 chooses the attribute of the data that most effectively splits its set of samples into subsets enriched in one class or the other. The splitting criterion is the normalized information gain (difference in entropy). The attribute with the highest normalized information gain is chosen to make the decision. J48 constructs a decision tree based on the training data and produces rules of how decisions are made. An additional step, referred to as pruning, omits nodes/branches that can be removed without affecting the performance significantly. Pruning reduces the risk of over-fitting to the training data.

Synthetic Minority Over-Sampling Technique (SMOTE)

The classification of imbalanced data is a commonly encountered problem in the context of medical pattern recognition and data mining. A dataset is considered imbalanced if the classification classes are not evenly distributed. Non-responders to anti-VEGF therapy constitute a minority class, as in any cohort of neovascular AMD patients undergoing anti-VEGF treatment, the frequency of

non-responders has been estimated to be close to 15-20% (Krebs et al. 2013). The remaining 75% of patients are expected to be good/typical responders and as such constitute the majority class. A simple default strategy of guessing the majority class would give a predictive accuracy of 75% with a fairly low rate of correct detection of poor responders. To improve prediction of the minority class "oversampling" is required. The synthetic minority over-sampling technique (SMOTE) is a powerful approach to achieve oversampling without replicating minority class instances. With this method, the minority class is over-sampled by introducing "synthetic" examples that lie in close proximity to the *k*-minority class nearest neighbors (Chawla and Nitesh, 2002). The value of a nominal attribute in a generated synthetic instance is determined by the most frequently occurring value in its nearest neighbors. The "synthetic" examples cause the classifier to create more general and less specific decision regions for the minority class and as such decision trees generalize better. In our cohort, the amount of over-sampling needed was 200%. 38 "synthetic" examples were added to the minority class to produce a total number of 122 instances.

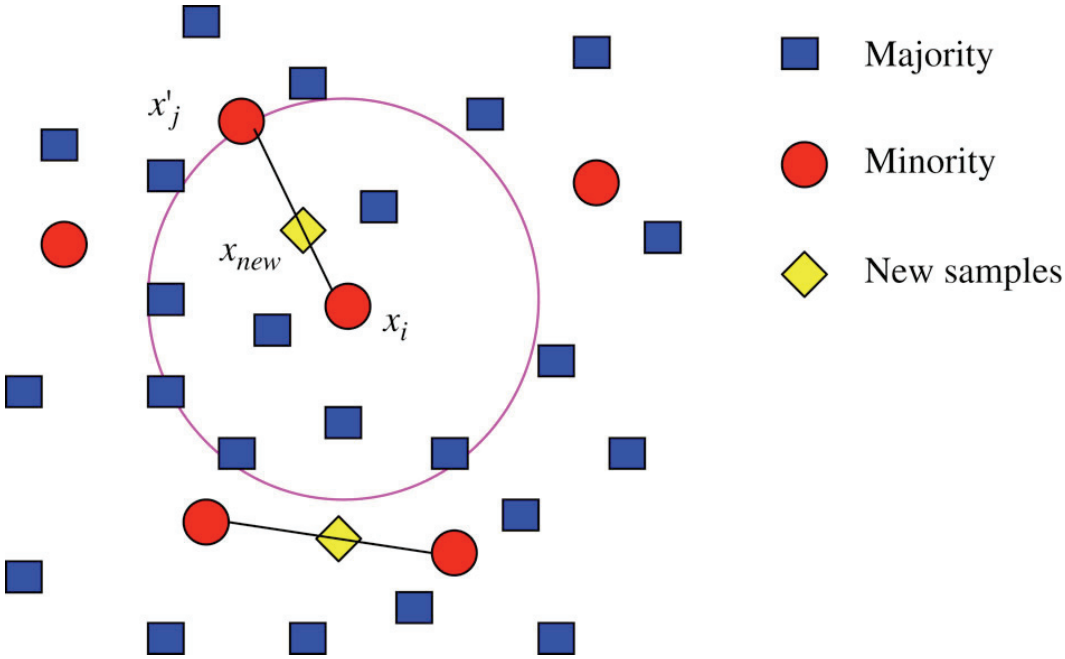

Figure 4.3: SMOTE (Synthetic Minority Over-sampling Technique). The minority class is over-sampled by taking each minority class sample and introducing synthetic examples along the line segments joining any/all of the k minority class nearest neighbors. Image adapted from Sun et al. (2013).

K-fold Cross Validation

In *k*-fold cross-validation, the original sample is randomly divided into *k* equal size subsets. Of the *k* subsets, a single subset is retained as the validation data for testing the model, and the remaining $k - 1$ subsets are used for training. The cross-validation process is then repeated *k* times, with each of the *k* subsets used exactly once as the validation data. The average performance on the *k* test sets is then computed. Typically, *k* values between 5 and 10 are used.

To avoid over-fitting of the training module, a randomized filter can be applied to equally distribute SMOTE-generated synthetic instances within folds.

Analysis Metrics

In a two-way (binary) classification, four classification outcomes are possible, which can be displayed in the following confusion matrix:

	Predicted Class	
Actual Class	Good/Typical Responder	Poor Responder
Good/Typical Responder	True Positive (TP)	False Negative (FN)
Poor Responder	False Positive (FP)	True Negative (TN)

To measure performance of a classification model three measures are commonly used: *precision*, *recall and accuracy*. Precision or positive predictive value (PPV) is the proportion of class members classified correctly (TP) over the total number of instances classified as class members (TP+FP).

$$Precision = PPV = \frac{TP}{TP + FP}$$

Recall is the equivalent of sensitivity and true positive rate (TPR). It is defined by the proportion of class members classified correctly (TP) over the total number of class members (TP+FN).

$$Recall = TPR = \frac{TP}{TP + FN}$$

Another important measure is the fall-out of false positive rate (FPR). It is closely related to specificity (FPR=1-specificity) and represents the proportion of proportion of negatives cases that were incorrectly classified as positive

$$FPR = \frac{FP}{FP + TN}$$

Accuracy of a model is the proportion of true results (both true positives and true negatives) in the population.

$$Accuracy = \frac{TP + TN}{TP + TN + FP + FN}$$

The receiver operating characteristic (ROC) curve is defined by the plot of model's sensitivity on the y-axis against 1-specificity or false positive rate (FPR) on the x-axis. The area under the ROC curve measures the probability that a group of patients will be correctly classified with the evaluated classification model.

RESULTS

Baseline Characteristics

All neovascular AMD patients were of Caucasian origin. Among them 65/84 (78%) patients were classified as either good or typical responders and 19/84 (22%) as poor responders. Median baseline Snellen visual acuity did not vary significantly between the poor responder (0.41 logMAR) and the combined good/typical group (0.47 logMAR) [p=0.10 two-tailed Mann-Whitney U-test]. Equal number of patients presented with visual acuities reduced to counting fingers (CF) in each group (n=5). Median baseline central macular thickness (CMT) was comparable between the two groups (404 μm vs. 436 μm; p=0.41 two-tailed Mann-Whitney U-test). A summary of baseline and follow-up visual acuity and macular thickness measurements is provided is supplementary figure I.

Decision Tree with SMOTE oversampling

Average performance was optimized with *k*=7 test sets. The summary statistics are provided in table 4.2. Cross-validation estimate of accuracy was 78.68%. From a total of 122 real and synthetic cases, 52/65 (TPR=80%) good responders and 44/57 (TPR=77%) poor responders were classified correctly. 13 poor responders were misclassified as good (FPR=22%) and 13 good responders as poor (FPR=20%). ROC area was 0.77 and 0.835 for good and poor responders, respectively. Upon manual validation, the decision tree classified correctly 77/84 (accuracy: 91%) of the non-synthetic ("real") instances. Instances with missing values in the root node SNP (see below) were considered misclassified.

Class	TPR[a]	FPR[b]	Precision	Recall	ROC Area
Good Responders	0.8	0.228	0.8	0.8	0.77
Poor Responders	0.772	0.2	0.772	0.772	0.835

Table 4.2: Cross-validation statistics. Both non-synthetic and SMOTE-generated instances were used in validation of the model by the WEKA machine learning toolkit.

[a]TPR: true positive rate; fraction of true positives out of the total actual positives

[b]FPR: false positive rate; fraction of false positives out of the total actual negatives

The following 13 SNPs were used to create the pruned J48 decision tree: rs4586 (*CCL2*), rs8192678 (*PPARGC1A)*, rs1065489 (*CFH),* rs2285714 (*PLA2G12A)*, rs699947 (*VEGFA),* rs9319425 (*FLT-1),* rs10468017 (*LIPC),* rs10033900 (*CFI),* rs1799865 (*CCR2),* rs8017304 (*RAD51B),* rs5888 (*SCARB1),* rs9542236 (*B3GALTL)* and rs3130783 (*IER3/DDR1*). An illustration of the merged decision tree is presented in figure 4.4. Class distribution per each SNP genotype is given in supplementary figure II. Supplementary figure III reports the actual and predicted class for all 84 patients based on genotype on the 13 SNPs used to create the decision tree.

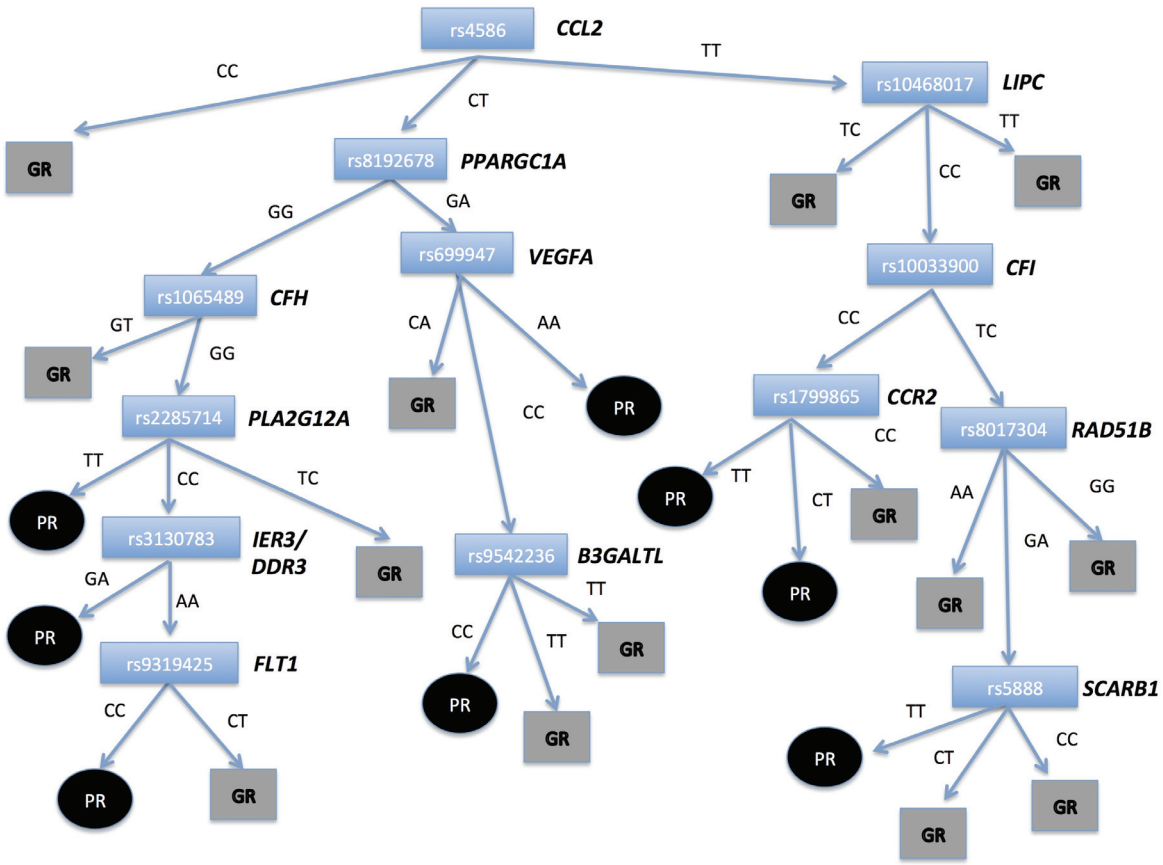

Figure 4.4: Decision tree. Each branch represents genotype on respective SNP locus and each leaf node the class label. PR: poor response; GR: good response.

The rs4586 SNP (*CCL2*) served as the root node of the decision tree, leading to the most homogeneous branches (highest information gain principle). As such, it was considered the most important "split" in the decision tree,

The rs9319425 (*FLT-1)*, rs9542236 (*B3GALTL)*, rs5888 (*SCARB1)* and the rs1799865 (*CCR2)* SNPs served as leaf decision nodes. Genotypic variation on these SNPs determined whether the patient would be classified as a good or poor responder after taking into consideration genotype in multiple other loci.

Two distinct decision paths classified the majority (70%) of poor responders in this cohort: a) the *CCL2->PPARGC1A->CFH->PLA2G12A->FLT-1* (genotype combination: CT, GG, GG, TT, CT) and b) the *CCL2->LIPC->CFI->CCR2* path (genotype combination: TT, CC, CC, TT/CT).

DISCUSSION

The first step in developing a pharmacogenomics classifier is to extract generalized learning algorithms from a dataset of training instances. The classification accuracy depends greatly on the quality of the training data. Especially in the case of a binary or dichotomous classification, the two classes need to be clearly separated based on measurable and reproducible criteria. In neovascular AMD, universal consensus of what defines good and poor response does not exist. Pharmacogenetic results regarding anti-VEGF therapy are thus sometimes inconsistent and not replicative in every study, possibly due to underlying differences in study endpoints used (visual acuity, anatomic response, number of retreatments required, etc.) (Schwartz and Brantley, 2011). Visual acuity by itself can lead to inaccurate classifications regarding anti-VEGF therapy efficacy. Despite marked improvement in retinal thickness and complete resolution of retinal fluid, visual acuity may continue to decline due to progression of atrophy to involve the foveal region. The opposite is also possible: improvement of visual acuity despite evidence of active neovascularization extrafoveally. Therefore, in our study, the combination of functional (visual acuity) and morphologic (decrease in retinal thickness) criteria allowed for more

accurate identification of insufficient responders to establish true pharmacogenetic associations.

A limitation of our study is that differences in underlying CNV lesion type characteristics were not taken into account. In one study (Ying et al. 2012), predominantly and minimally classic lesions were reported to be associated with less gain in vision compared to occult lesions. However, other studies failed to support such associations (Lalwani et al. 2009; Lux et al. 2007). In addition, rare CNV variants such as retinal angiomatous proliferation (RAP) and polypoidal choroidal vasculopathy (PCV) may respond differently than other CNV lesion types to anti-VEGF treatment (Ying et al. 2012). Although none of the patients in our cohort was diagnosed with RAP or PCV, it is possible that other clinical factors or baseline OCT characteristics-apart from age, baseline visual acuity and lesion size- influence treatment outcome. Vitreomacular adhesions (VMAs), for example, have been associated with poor response to anti-VEGF treatment and less gain in visual acuity (Krebs et al. 2013; Lee et al., 2009). VMA's may reduce response to anti-VEGF therapy via maintaining exposure of the macula to vitreous pro-inflammatory cytokines or interfering with its oxygenation and nourishment.

Cross-validation was used as a model validation technique to evaluate performance of the classifier. With all instances included (both real and synthetic, SMOTE-generated), the estimated false positive rate (FPR) for the good responder class was 22%. Based on the assumption that 15% of patients in any neovascular AMD cohort will respond insufficiently to anti-VEGF therapy, the classifier's FPR is higher than that obtained when randomly classifying every

patient as a good responder (null hypothesis). Current practice affords such 15% FPR in anti-VEGF monotherapy. To be proven clinically useful, a prediction model will have to minimize existing FPR for the good responder class. A reason for the relatively high FPR could be sought at the introduction of synthetic values. Although necessary to construct a classifier with improved prediction of the minority class, these synthetic instances may have "invaded" the majority class territory and thus caused considerable confusion. In support of this notion, is the fact that manual validation using the "real" instances led to correct classification of 81/84 patients. Such high accuracy is suspicious of an "over-fitted" decision tree, particularly tied to the current dataset that cannot be easily generalized. Two applied methods in the development of the decision tree minimized significantly the risk of over-fitting: cross-validation and pruning. Nevertheless, validation in an independent cohort is required to evaluate the classifier's exact performance and accuracy.

The root node of the decision tree was a SNP in the *CCL2/MCP-1* gene. Genotypic variation in its receptor gene (*CCR2)* was also found to be a critical determinant of treatment response. The chemokine (C-C motif) ligand 2 (CCL2), also referred to as monocyte chemotactic protein-1 (MCP-1), is a 13kDa cytokine that belongs to the family of CC chemokines. CCL2 acts primarily as a chemoattractant of monocytes, inducing differentiation and polarization of macrophages in peripheral tissues (Luster AD, 1998). Under physiologic conditions, the human retina is devoid of macrophages (microglial cells) in the subretinal space. In AMD, macrophages and microglial cells are pathologically

recruited in the subretinal space, secreting pro-inflammatory cytokines and angiogenic factors (VEGF) that promote photoreceptor degeneration (Combadiere et al. 2007) and choroidal neovascularization (CNV) (Ambati et al. 2003). Macrophage recruitment is thought to be partially mediated through CCL2 and its receptor (CCR2). Mice deficient in CCR2 have a predilection for developing CNV (Tsutsumi et al. 2003). A plausible role of the CCL2/CCR2 signaling pathway in AMD is further supported by the fact that SNPs in the *CCL2* and *CCR2* genes have been associated with an increased risk of developing the disease (Anand et al., 2012). In addition, serum levels of CCL2 have been found to be significantly higher, while expression of CCR2 in peripheral blood mononuclear cells (PBMCs) significantly lower in AMD patients (Anand et al. 2012). Jonas et al. (2010) found a significant association of intraocular levels of CCL2 with neovascular AMD, even in the presence of normal VEGF concentrations. Refractoriness to anti-VEGF treatment may therefore be the result of an elicited inflammatory and angiogenic response in the microenvironment of the retina that is VEGF-independent. In cancers resistant to anti-VEGF treatment, the cytokine IL-17 promotes such VEGF independent pathway through recruitment and functional activation of myeloid derived suppressor cells that express MCP-1 and other pro-inflammatory and angiogenic factors (Chung et al. 2013).

The classifier was unable to unify all unresponsive patients under a single "SNP haplotype" (combinational genotype). This finding highlights once again the genetic complexity underlying AMD and its treatment prediction. Nevertheless, the majority of poor responders could be characterized by two

distinct SNP haplotypes. One of these haplotypes suggests interaction of an AMD-associated variant in the PPAR gamma (PPARG) co-activator 1 alpha gene (*PPARGC1A*) with genes of the complement (*CFH*), lipid metabolism (*PLA2G12A)*, and VEGF signaling systems (*FLT-1*). *PPARGC1A* is a major transcriptional co-activator of the proliferator-activated receptor C (PPARG). PPARs act as regulators of gene transcription and have demonstrated ability to reduce the likelihood and severity of pathologic retinal neovascularization (Del Cano and Gehlbach, 2008). ω3 long chain fatty acids, which can act as endogenous PPAR agonists, exert much of their modulatory effects on retinal neovascularization through PPARG (Stahl et al. 2010; SanGiovanni et al. 2005). In three independent cohorts, variants in *PPARGC1A* were shown to confer protection against neovascular AMD (SanGiovanni et al. 2013). Interaction analysis showed statistical significant interactions with complement (*CFH*, *CFB*, *C3*, *C2*) and VEGF *(VEGFA*, *FLT1*, *KDR*) variants. The rs8192678 SNP, in particular, was found to interact with variants in the VEGFR-1 receptor gene (FLT-1), as in our study. Thus, the PPAR-axis may not only be important in the pathogenesis of neovascular AMD but also potentially interfere with responsiveness to anti-VEGF treatment.

A previous suggestive association between rs2285714 SNP (*PLA2G12A*) and response to anti-VEGF therapy was supported in our cohort. The TT genotype was conditionally associated with poor response in a subset of patients. Wang et al. (2012) reported that carriers of the T allele were 3 times more likely to be poor responders than good responders. *PLA2G12A* codes for group 12A secretory

phospholipase 2. Phospholipase A2 (PLA2) is a family of enzymes that catalyzes the hydrolysis of glycerophospholipids to arachidonic acid and lysophospholipids (Murakami et al. 2011) and can exert proangiogenic effects by inducing VEGF production in vascular endothelial cells (Barnett et al. 2010). Increased PLA2 activity may also lead to overproduction of arachidonic acid and subsequent conversion to prostaglandin E2 (PGE2) that can potentiate pathologic ocular angiogenesis through interaction with its E4 receptor. In rat models of oxygen-induced retinopathy and laser-induced choroidal neovascularization, the E4 receptor has been shown to promote Müller cell VEGF production and enhance endothelial cell proliferation (Yanni et al. 2009).

Overall, the current study provides a novel approach to investigate potential pharamacogenetic interactions in the treatment of neovascular AMD. Although external validation in an independent cohort is required to assess the generalizability of the model, we herein provide preliminary evidence that variation in multiple susceptibility loci might better explain differential response to anti-VEGF therapy. AMD is a genetically complex disease and it seems highly likely that predicting treatment response will be genetically complex as well.

BIBLIOGRAPHY

Ambati J, Anand A, Fernandez S, Sakurai E, Lynn BC, Kuziel WA, Rollins BJ, Ambati BK. An animal model of age-related macular degeneration in senescent Ccl-2- or Ccr-2-deficient mice. Nat Med. 2003 Nov;9(11):1390-7.

Anand A, Sharma NK, Gupta A, Prabhakar S, Sharma SK, Singh R, Gupta PK. Single nucleotide polymorphisms in MCP-1 and its receptor are associated with the risk of age related macular degeneration. PLoS One. 2012;7(11):e49905.

Barnett JM, McCollum GW, Penn JS. Role of cytosolic phospholipase A(2) in retinal neovascularization. Invest Ophthalmol Vis Sci. 2010 Feb;51(2):1136-42.

Chawla, Nitesh V., et al. "SMOTE: synthetic minority over-sampling technique. Journal of Artificial Intelligence Research 16 (2002) 321–357.

Chen H, Yu KD, Xu GZ. Association between variant Y402H in age-related macular degeneration (AMD) susceptibility gene CFH and treatment response of AMD: a meta-analysis. PLoS One. 2012;7(8):e42464.

Chung AS, Wu X, Zhuang G, Ngu H, Kasman I, Zhang J, Vernes JM, Jiang Z, Meng YG, Peale FV, Ouyang W, Ferrara N. An interleukin-17-mediated paracrine network promotes tumor resistance to anti-angiogenic therapy. Nat Med. 2013 Sep;19(9):1114-23.

Combadière C, Feumi C, Raoul W, Keller N, Rodéro M, Pézard A, Lavalette S, Houssier M, Jonet L, Picard E, Debré P, Sirinyan M, Deterre P, Ferroukhi T, Cohen SY, Chauvaud D, Jeanny JC, Chemtob S, Behar-Cohen F,

Sennlaub F. CX3CR1-dependent subretinal microglia cell accumulation is associated with cardinal features of age-related macular degeneration. J Clin Invest. 2007 Oct;117(10):2920-8.

Davis MD, Gangnon RE, Lee LY, Hubbard LD, Klein BE, Klein R, Ferris FL, Bressler SB, Milton RC; Age-Related Eye Disease Study Group. The Age-Related Eye Disease Study severity scale for age-related macular degeneration: AREDS Report No. 17. Arch Ophthalmol. 2005 Nov;123(11):1484-98.

Del V Cano M, Gehlbach PL. PPAR-alpha Ligands as Potential Therapeutic Agents for Wet Age-Related Macular Degeneration. PPAR Res. 2008;2008:821592.

Ferris FL 3rd, Fine SL, Hyman L. Age-related macular degeneration and blindness due to neovascular maculopathy. Arch Ophthalmol. 1984 Nov;102(11):1640-2.

Fritsche LG, Chen W, Schu M, et al. Seven new loci associated with age-related macular degeneration. Nat Gen. 2013; 45: 433–439.

Hagstrom SA, Ying GS, Pauer GJ, Sturgill-Short GM, Huang J, Callanan DG, Kim IK, Klein ML, Maguire MG, Martin DF; Comparison of AMD Treatments Trials Research Group. Pharmacogenetics for genes associated with age-related macular degeneration in the Comparison of AMD Treatments Trials (CATT). Ophthalmology. 2013 Mar;120(3):593-9.

Jonas JB, Tao Y, Neumaier M, Findeisen P. Monocyte chemoattractant protein 1, intercellular adhesion molecule 1, and vascular cell adhesion molecule

1 in exudative age-related macular degeneration. Arch Ophthalmol. 2010 Oct;128(10):1281-6.

Kloeckener-Gruissem B, Barthelmes D, Labs S, Schindler C, Kurz-Levin M, Michels S, Fleischhauer J, Berger W, Sutter F, Menghini M. Genetic association with response to intravitreal ranibizumab in patients with neovascular AMD. Invest Ophthalmol Vis Sci. 2011 Jul 1;52(7):4694-702.

Kopplin LJ, Igo RP Jr, Wang Y, Sivakumaran TA, Hagstrom SA, Peachey NS, Francis PJ, Klein ML, SanGiovanni JP, Chew EY, Pauer GJ, Sturgill GM, Joshi T, Tian L, Xi Q, Henning AK, Lee KE, Klein R, Klein BE, Iyengar SK. Genome-wide association identifies SKIV2L and MYRIP as protective factors for age-related macular degeneration. Genes Immun. 2010 Dec;11(8):609-21.

Krebs I, Glittenberg C, Ansari-Shahrezaei S, Hagen S, Steiner I, Binder S. Non-responders to treatment with antagonists of vascular endothelial growth factor in age-related macular degeneration. Br J Ophthalmol. 2013 Nov;97(11):1443-6.

Lalwani GA, Rosenfeld PJ, Fung AE, Dubovy SR, Michels S, Feuer W, Davis JL, Flynn HW Jr, Esquiabro M. A variable-dosing regimen with intravitreal ranibizumab for neovascular age-related macular degeneration: year 2 of the PrONTO Study. Am J Ophthalmol. 2009 Jul;148(1):43-58.e1.

Lee SJ, Lee CS, Koh HJ. Posterior vitreomacular adhesion and risk of exudative age-related macular degeneration: paired eye study. Am J Ophthalmol. 2009 Apr;147(4):621-626.e1.

Lotery AJ, Gibson J, Cree AJ, Downes SM, Harding SP, Rogers CA, Reeves BC, Ennis S, Chakravarthy U; Alternative Treatments to Inhibit VEGF in Patients with Age-Related Choroidal Neovascularisation (IVAN) Study Group. Pharmacogenetic associations with vascular endothelial growth factor inhibition in participants with neovascular age-related macular degeneration in the IVAN Study. Ophthalmology. 2013 Dec;120(12):2637-43.

Luster AD. Chemokines--chemotactic cytokines that mediate inflammation. N Engl J Med. 1998 Feb 12;338(7):436-45.

Lux A, Llacer H, Heussen FM, Joussen AM. Non-responders to bevacizumab (Avastin) therapy of choroidal neovascular lesions. Br J Ophthalmol. 2007 Oct;91(10):1318-22.

Murakami M, Taketomi Y, Miki Y, Sato H, Hirabayashi T, Yamamoto K. Recent progress in phospholipase A2 research: from cells to animals to humans. Prog Lipid Res. 2011 Apr;50(2):152-92.

Nischler C, Oberkofler H, Ortner C, Paikl D, Riha W, Lang N, Patsch W, Egger SF. Complement factor H Y402H gene polymorphism and response to intravitreal bevacizumab in exudative age-related macular degeneration. Acta Ophthalmol. 2011 Jun;89(4):e344-9.

Quinlan, JR. *C4. 5: Programs for Machine Learning*. *Machine Learning*. Vol. 240, 1993.

SanGiovanni JP, Chen J, Sapieha P, Aderman CM, Stahl A, Clemons TE, Chew EY, Smith LE. DNA sequence variants in PPARGC1A, a gene encoding a

coactivator of the ω-3 LCPUFA sensing PPAR-RXR transcription complex, are associated with NV AMD and AMD-associated loci in genes of complement and VEGF signaling pathways. PLoS One. 2013;8(1):e53155.

SanGiovanni JP, Chew EY. The role of omega-3 long-chain polyunsaturated fatty acids in health and disease of the retina. Prog Retin Eye Res. 2005 Jan;24(1):87-138.

Schwartz SG, Brantley MA Jr. Pharmacogenetics and age-related macular degeneration. J Ophthalmol. 2011;2011:252549.

Smailhodzic D, Muether PS, Chen J, Kwestro A, Zhang AY, Omar A, Van de Ven JP, Keunen JE, Kirchhof B, Hoyng CB, Klevering BJ, Koenekoop RK, Fauser S, den Hollander AI. Cumulative effect of risk alleles in CFH, ARMS2, and VEGFA on the response to ranibizumab treatment in age-related macular degeneration. Ophthalmology. 2012 Nov;119(11):2304-11.

Spencer KL, Hauser MA, Olson LM, Schnetz-Boutaud N, Scott WK, Schmidt S, Gallins P, Agarwal A, Postel EA, Pericak-Vance MA, Haines JL. Haplotypes spanning the complement factor H gene are protective against age-related macular degeneration. Invest Ophthalmol Vis Sci. 2007 Sep;48(9):4277-83.

Spilsbury K, Garrett KL, Shen WY, Constable IJ, Rakoczy PE. Overexpression of vascular endothelial growth factor (VEGF) in the retinal pigment epithelium leads to the development of choroidal neovascularization. Am J Pathol. 2000 Jul;157(1):135-44.

Stahl A, Sapieha P, Connor KM, Sangiovanni JP, Chen J, Aderman CM, Willett KL, Krah NM, Dennison RJ, Seaward MR, Guerin KI, Hua J, Smith LE. Short communication: PPAR gamma mediates a direct antiangiogenic effect of omega 3-PUFAs in proliferative retinopathy. Circ Res. 2010 Aug 20;107(4):495-500.

Teper SJ, Nowinska A, Pilat J, Palucha A, Wylegala E. Involvement of genetic factors in the response to a variable-dosing ranibizumab treatment regimen for age-related macular degeneration. Mol Vis. 2010 Dec 7;16:2598-604.

Tian J, Qin X, Fang K, Chen Q, Hou J, Li J, Yu W, Chen D, Hu Y, Li X. Association of genetic polymorphisms with response to bevacizumab for neovascular age-related macular degeneration in the Chinese population. Pharmacogenomics. 2012 May;13(7):779-87.

Tsutsumi C, Sonoda KH, Egashira K, Qiao H, Hisatomi T, Nakao S, Ishibashi M, Charo IF, Sakamoto T, Murata T, Ishibashi T. The critical role of ocular-infiltrating macrophages in the development of choroidal neovascularization. J Leukoc Biol. 2003 Jul;74(1):25-32.

Wang VM, Rosen RB, Meyerle CB, Kurup SK, Ardeljan D, Agron E, Tai K, Pomykala M, Chew EY, Chan CC, Tuo J. Suggestive association between PLA2G12A single nucleotide polymorphism rs2285714 and response to anti-vascular endothelial growth factor therapy in patients with exudative age-related macular degeneration. Mol Vis. 2012;18:2578-85.

Yanni SE, Barnett JM, Clark ML, Penn JS. The role of PGE2 receptor EP4 in pathologic ocular angiogenesis. Invest Ophthalmol Vis Sci. 2009 Nov;50(11):5479-86.

Ying GS, Huang J, Maguire MG, Jaffe GJ, Grunwald JE, Toth C, Daniel E, Klein M, Pieramici D, Wells J, Martin DF; Comparison of Age-related Macular Degeneration Treatments Trials Research Group. Baseline predictors for one-year visual outcomes with ranibizumab or bevacizumab for neovascular age-related macular degeneration. Ophthalmology. 2013 Jan;120(1):122-9.

Chapter 5. DISCUSSION

The aim of the current thesis was to describe genetic and electrophysiological aspects of age-related macular degeneration (AMD) and investigate their clinical implications in the treatment of the condition.

In the first chapter, evidence of non-macular photoreceptor dysfunction in both early and advanced stages of AMD was provided. Previous efforts to assess photoreceptor dysfunction in AMD (Jackson et al. 2002; Jackson and Owsley 2000; Owsley et al. 2007) have relied merely on psychophysical tests, which are prone to subjective biases (fatigue, inattention to stimulus presentation, varying decision criterion among test takers). Our approach utilized the most objective test to assess retina function, which is independent of patient response: the full-field electroretinogram (ffERG). By designing a novel and standardized protocol, we were able to show that even during early stages of the disease (dry AMD), dark adaptation defects are present in patients with AMD. Unexpectedly, a subset of patients was characterized by panretinal cone abnormalities. This finding- previously reported by Ronan et al. (2006) and Ladewig et al. (2003)- may reflect extensive morphologic changes in advanced stages of AMD or represent a distinct phenotypic manifestation within the heterogeneous context of AMD as a disease. The identification of such phenotype suggests the possibility of a distinct genetic physiologic mechanism contributing to AMD (Ronan et al., 2006). This has research implications for the investigation of the genetics underlying AMD. Isolation of a distinct ERG phenotype can propel delineation of the remaining

genetic contributors to AMD. In addition, existence of an AMD subgroup with generalized cone and rod dysfunction may explain why some patients continue to lose visual function even though their clinical picture remains unchanged. This may hold especially true for neovascular AMD patients that continue to experience reduction in visual acuity even though their retinas appear completely "dried up" on OCT scans.

The second chapter provided electrophysiological evidence of changes in inner retina function that occur during normal aging and in AMD. We relied on analysis of the oscillatory potentials (OPs), a component of the ERG thought to originate from cells in the inner plexiform layer (Wachtmeister L. 1998). OP changes in the healthy, dark-adapted retina were found to begin at earlier ages (40 years) than previously shown (minimum of 60 years) and did not progress further at older ages. These changes should be taken into account when evaluating AMD, a disorder that becomes most prevalent after 65 years of age (Kahn et al. 1977; Klein et al. 1992; Mitchell et al. 1995). To study light-adapted OPs, we adapted for the first time in humans a novel analytical method, previously used to study rat ERG signals (Forte et al. 2008): the Morlet Wavelet Transform (MWT). MWT allowed the characterization of two distinct oscillators in the light-adapted retina: a high-frequency band time-locked to the onset of early OPs and a low frequency band that gave rise to both early and late OPs. Aging affected preferentially the power of the low-frequency band. The high-frequency band was identified as an age-independent marker of inner retina function. As such, it can open new

diagnostic avenues for assessing pathologies and/or retinal drug toxicities at widely different ages.

We undertook additional analyses using MWT in subjects afflicted with neovascular AMD under anti-VEGF therapy in one eye and dry AMD in the fellow eye. While the high-frequency band power remained unaffected by age and in the dry form of AMD, it underwent selective reduction in patients undergoing chronic intravitreal anti-VEGF therapy to thwart choroidal neovascularization. Why we see such changes in OPs of neovascular AMD eyes under anti-VEGF treatment remains to be elucidated. Limited by the retrospective nature of the study, we cannot exclude the possibility of extensive inner retina damage caused by the initial hemorrhagic event. Contradicting this possibility is the fact that in treatment-naïve cases of serous Pigment Epithelial Detachment (sPED) associated with AMD, the high-frequency band remained unaffected. Location of the fluid within the retina may explain this observation. In sPED without intra- or sub-retinal fluid, neovascularization is confined to the sub-RPE space. The origin of the high frequency band may lie in the more distal retina and therefore remain unaffected in cases where a pathological state affects primarily the outer retina.

Another explanation for the observed OP power reduction seen in eyes treated with anti-VEGF agents should be sought at the biological consequences of prolonged VEGF signaling blockade. The issue of possible inner retina toxicity caused by prolonged VEGF blockade has been raised before. Several lines of evidence indicate an important role for endogenous VEGF in the maintenance and function of adult retina neuronal cells, such as the photoreceptors and the Müller

cells (Saint-Geniez et al. 2008), as well as the subretinal vasculature. Chronic inhibition of VEGF-A function in normal adult animals has been shown to lead to a significant loss of retinal ganglion cells (Nishijima et al. 2007). In addition, changes in retinal nerve fiber layer thickness have been reported in treated eyes of patients with unilateral neovascular AMD (Martinez-de-la-Casa et al. 2012). The above findings should raise caution to clinicians who are treating patients with anti-VEGF agents. If validated through a prospective, longitudinal study, MWT analysis of the OP component of the ERG can be used to carefully screen patients for the detrimental long-term effects of VEGF blockade. Alternative anti-angiogenic approaches should be explored that target VEGF-dependent or independent pathways without damaging healthy vessels. Hypoxia inducible factors 1 and 2 (HIF) have been suggested as two candidate target molecules. HIFs are basic-helix-loop helix transcription factors that regulate VEGFA production and reduce experimental CNV without causing vision loss or endothelial damage in mice (Kurihara et al. 2012). Susceptibility factors contributing to anti-VEGF toxicity in the eye should also be investigated in the future (Quaggin SE. 2012).

In the last chapter, we aimed to investigate whether an individual's genetic information can be used to predict response to anti-VEGF therapy. Using a novel tool to investigate potential pharamacogenetic interactions in the treatment of neovascular AMD, we provided preliminary evidence that variation in multiple susceptibility loci might better explain differential response to anti-VEGF therapy compared to single gene SNP analysis. Although external validation in an

independent cohort is required to assess the generalizability of the model, it seems likely that prediction of treatment response in a complex disease such as AMD will be a complex task as well (Kanoff and Miller, 2013). For this study, we relied on SNPs in genes previously associated with development of advanced AMD through genome-wide association studies (Fritsche et al. 2013). AMD associated genes can be clustered into four different biological pathways: a) inflammation and complement system regulation; b) lipid metabolism; c) oxidative stress and extracellular matrix remodeling; and d) angiogenesis. In addition, we included gene variants reported to influence response to anti-VEGF therapy as well haplotypes spanning the *CFH* (Spencer et al. 2007) and *SKIVL2/MYRIP* (Kopplin et al. 2010). These haplotypes have been shown to be protective factors for AMD. It is possible that inclusion of additional putative variants will increase accuracy of the model in the future.

Up to date, pharmacogenetic results regarding anti-VEGF therapy have been inconsistent and not replicative in every study. The reason underlying these inconsistencies should be sought not only in genetic variability, but also in possible differences in CNV lesion features and morphology (Schwartz and Brantley, 2011). Vitreomacular adhesions (VMAs), for example, have been associated with poor response to anti-VEGF treatment and less gain in visual acuity (Krebs et al. 2013; Lee et al. 2009). VMAs possibly exert this effect via maintaining exposure of the macula to vitreous pro-inflammatory cytokines or interfering with its oxygenation and nourishment. Another potential contributing factor associated with responsiveness to anti-VEGF therapy is the level of CNV

maturation. Capillary angiogenesis is a VEGF dependent process until the point of vessel wall maturation. "Mature" vessels in CNV are lined with pericytes, thereby becoming less accessible to antibodies. Regression of mature capillaries seems to be a VEGF-independent process, relying molecularly on factors such as angiopoietin and its receptors (TIE-1 and 2) (Hirschi and D'Amore 1998; Sims DE. 2000; Holash et al. 1999). Therefore, inclusion of clinical predictive factors may improve precision and accuracy of the current genetics-based model.

Our study suggested a potential role of the CCL2/CCR2 signaling axis on modifying response to anti-VEGF monotherapy. Inflammation is one of the key contributors to the pathogenesis of neovascular AMD (Donoso et al. 2006). Apart from strong GWAS associations with complement pathway-associated genes, a number of inflammatory components (complement system proteins, Ig immunoglobulins, C-reactive protein, amyloid β) have been identified as the molecular constituents of drusen, the clinical hallmark of AMD (Anderson et al. 2009). In eyes with neovascular AMD, activated monocytes have been identified on the outer surface of Bruch's membrane (Cousins et al. 2004; Penfold et al. 2001). In addition, abnormal recruitment of macrophages in the subretinal space has been shown to trigger production of vascular endothelial growth factor (VEGF) by the RPE, leading to subsequent angiogenesis (Apte et al. 2006). Supportive of a crucial role of inflammation in neovascular AMD are topical anti-inflammatory therapy trials that have shown to be effective in suppressing development of neovascular AMD when co-administered with or without anti-VEGF drugs (Izumi-Nagai et al. 2008; Gomi et al. 2012; Flaxel et al. 2012). In

patients unresponsive to anti-VEGF monotherapy, a combination “rescue” therapy of anti-VEGF therapy with immunosuppressant drugs (triamcinolone acetonide) has been shown to produce significant anatomic improvements (Veritti et al. 2013).

Understanding the factors underlying suboptimal responsiveness to anti-VEGF monotherapy is important to guide research for future therapies. Until alternative treatments become available, identification of individuals most likely to be unresponsive to anti-VEGF monotherapy is highly demanded, as earlier commencement of combination therapy on these individuals may lead to improved final visual outcomes.

In conclusion, investigation of electrophysiological and genetic aspects of AMD revealed important implications for its treatment. AMD should be considered a heterogeneous group of disorders. In some cases, the whole retina may be involved challenging the widely accepted notion of a disease confined to the macula. Treatment shoud therefore be directed at a systemic level. Prolonged VEGF blockade, as a strategy, may be deemed suboptimal or result in undesired functional impairment in a subset of AMD patients. Pharmacogenetic research holds promise in developing individualized treatment approaches for AMD that optimize final patient outcome while reducing the risk of detrimental adverse effects.

BIBLIOGRAPHY

Anderson DH, Radeke MJ, Gallo NB, Chapin EA, Johnson PT, Curletti CR, Hancox LS, Hu J, Ebright JN, Malek G, Hauser MA, Rickman CB, Bok D, Hageman GS, Johnson LV. The pivotal role of the complement system in aging and age-related macular degeneration: hypothesis re-visited. Prog Retin Eye Res. 2010 Mar;29(2):95-112.

Apte RS, Richter J, Herndon J, Ferguson TA. Macrophages inhibit neovascularization in a murine model of age-related macular degeneration. PLoS Med. 2006 Aug;3(8):e310.

Cousins SW, Espinosa-Heidmann DG, Csaky KG. Monocyte activation in patients with age-related macular degeneration: a biomarker of risk for choroidal neovascularization? Arch Ophthalmol. 2004 Jul;122(7):1013-8.

Donoso LA, Kim D, Frost A, Callahan A, Hageman G. The role of inflammation in the pathogenesis of age-related macular degeneration. Surv Ophthalmol. 2006 Mar-Apr;51(2):137-52.

Flaxel C, Schain MB, Hamon SC, Francis PJ. Prospective randomized controlled trial of combination ranibizumab (Lucentis) and bromfenac (Xibrom) for neovascular age-related macular degeneration: a pilot study. Retina. 2012 Mar;32(3):417-23.

Forte JD, Bui BV, Vingrys AJ. Wavelet analysis reveals dynamics of rat oscillatory potentials. J Neurosci Methods. 2008 Mar 30;169(1):191-200.

Fritsche LG, Chen W, Schu M, et al. Seven new loci associated with age-related macular degeneration. Nat Gen. 2013; 45: 433–439.

Gomi F, Sawa M, Tsujikawa M, Nishida K. Topical bromfenac as an adjunctive treatment with intravitreal ranibizumab for exudative age-related macular degeneration. Retina. 2012 Oct;32(9):1804-10.

Hirschi KK, D'Amore PA. Pericytes in the microvasculature. Cardiovasc Res. 1996 Oct;32(4):687-98.

Holash J, Maisonpierre PC, Compton D, Boland P, Alexander CR, Zagzag D, Yancopoulos GD, Wiegand SJ. Vessel cooption, regression, and growth in tumors mediated by angiopoietins and VEGF. Science. 1999 Jun 18;284(5422):1994-8.

Izumi-Nagai K, Nagai N, Ohgami K, Satofuka S, Ozawa Y, Tsubota K, Ohno S, Oike Y, Ishida S. Inhibition of choroidal neovascularization with an anti-inflammatory carotenoid astaxanthin. Invest Ophthalmol Vis Sci. 2008 Apr;49(4):1679-85.

Jackson GR, Owsley C. Scotopic sensitivity during adulthood. Vis Res. 2000; 40: 2467–2473.

Jackson GR, Owsley C, Curcio CA. Photoreceptor degeneration and dysfunction in aging and age-related maculopathy. Ageing Res Rev. 2002; 1: 381–396.

Kahn HA, Leibowitz HM, Ganley JP, Kini MM, Colton T, Nickerson RS, Dawber TR. The Framingham Eye Study. II. Association of ophthalmic

pathology with single variables previously measured in the Framingham Heart Study. Am J Epidemiol. 1977 Jul;106(1):33-41.

Kanoff J, Miller J. Pharmacogenetics of the treatment response of age-related macular degeneration with ranibizumab and bevacizumab. Semin Ophthalmol. 2013 Sep-Nov;28(5-6):355-60.

Klein R, Klein BE, Linton KL. Prevalence of age-related maculopathy. The Beaver Dam Eye Study. Ophthalmology. 1992 Jun;99(6):933-43.

Kopplin LJ, Igo RP Jr, Wang Y, Sivakumaran TA, Hagstrom SA, Peachey NS, Francis PJ, Klein ML, SanGiovanni JP, Chew EY, Pauer GJ, Sturgill GM, Joshi T, Tian L, Xi Q, Henning AK, Lee KE, Klein R, Klein BE, Iyengar SK. Genome-wide association identifies SKIV2L and MYRIP as protective factors for age-related macular degeneration. Genes Immun. 2010 Dec;11(8):609-21.

Krebs I, Glittenberg C, Ansari-Shahrezaei S, Hagen S, Steiner I, Binder S. Non-responders to treatment with antagonists of vascular endothelial growth factor in age-related macular degeneration. Br J Ophthalmol. 2013 Nov;97(11):1443-6.

Kurihara T, Westenskow PD, Bravo S, Aguilar E, Friedlander M. Targeted deletion of Vegfa in adult mice induces vision loss. J Clin Invest. 2012 Nov 1;122(11):4213-7.

Ladewig M, Kraus H, Foerster MH, Kellner U. Cone dysfunction in patients with late-onset cone dystrophy and age-related macular degeneration. Arch Ophthalmol. 2003; 121: 1557–1561.

Lee SJ, Koh HJ. Effects of vitreomacular adhesion on anti-vascular endothelial growth factor treatment for exudative age-related macular degeneration. Ophthalmology. 2011 Jan;118(1):101-10.

Martinez-de-la-Casa JM, Ruiz-Calvo A, Saenz-Frances F, Reche-Frutos J, Calvo-Gonzalez C, Donate-Lopez J, Garcia-Feijoo J. Retinal nerve fiber layer thickness changes in patients with age-related macular degeneration treated with intravitreal ranibizumab. Invest Ophthalmol Vis Sci. 2012 Sep 14;53(10):6214-8.

Mitchell P, Smith W, Attebo K, Wang JJ. Prevalence of age-related maculopathy in Australia. The Blue Mountains Eye Study. Ophthalmology. 1995 Oct;102(10):1450-60.

Nishijima K, Ng YS, Zhong L, Bradley J, Schubert W, Jo N, Akita J, Samuelsson SJ, Robinson GS, Adamis AP, Shima DT. Vascular endothelial growth factor-A is survival factor for retinal neurons and a critical neuroprotectant during the adaptive response to ischemic injury. Am J Pathol. 2007 Jul;171(1):53-67.

Owsley C, McGwin G, Jackson GR, Kallies K, Cone- Clark M. and rod-mediated dark adaptation impairment in age-related maculopathy. Ophthalmology. 2007; 114: 1728–1735.

Penfold PL, Madigan MC, Gillies MC, Provis JM. Immunological and aetiological aspects of macular degeneration. Prog Retin Eye Res. 2001 May;20(3):385-414.

Quaggin SE. Turning a blind eye to anti-VEGF toxicities. J Clin Invest. 2012 Nov 1;122(11):3849-51.

Ronan S, Nusinowitz S, Swaroop A, Heckenlively JR. Senile panretinal cone dysfunction in age-related macular degeneration (AMD): a report of 52 AMD patients compared to age-matched controls. Trans Am Ophthalmol Soc. 2006; 104: 232–240.

Saint-Geniez M, Maharaj AS, Walshe TE, Tucker BA, Sekiyama E, Kurihara T, Darland DC, Young MJ, D'Amore PA. Endogenous VEGF is required for visual function: evidence for a survival role on müller cells and photoreceptors. PloS One. 2008;3(11):e3554

Schwartz SG, Brantley MA Jr. Pharmacogenetics and age-related macular degeneration. J Ophthalmol. 2011;2011:252549.

Sims DE. Diversity within pericytes. Clin Exp Pharmacol Physiol. 2000 Oct;27(10):842-6.

Spencer KL, Hauser MA, Olson LM, Schnetz-Boutaud N, Scott WK, Schmidt S, Gallins P, Agarwal A, Postel EA, Pericak-Vance MA, Haines JL. Haplotypes spanning the complement factor H gene are protective against age-related macular degeneration. Invest Ophthalmol Vis Sci. 2007 Sep;48(9):4277-83.

Veritti D, Sarao V, Lanzetta P. Bevacizumab and triamcinolone acetonide for choroidal neovascularization due to age-related macular degeneration unresponsive to antivascular endothelial growth factors. J Ocul Pharmacol Ther. 2013 May;29(4):437-41.

Wachtmeister L. Oscillatory potentials in the retina: what do they reveal. Prog Retin Eye Res. 1998 Oct;17(4):485-521.

Supplementary Figures

Figure I: Baseline and follow-up VA and CMT measurements. For response evaluation, visual acuity (VA) was recorded at baseline and at 12 months post-treatment. Central macular thickness (CMT) was recorded at baseline, 3 months and 6 months after the first injection.

Patient ID	BasVA	12moVA	BasCMT	CMT3mo	CMT6mo	Response Outcome
R2930	0.47	0.47	321	274	273	Typical
R2931	0.69	0.39	367	219	239	Good
R2932	0.6	0.09	478	350	313	Good
R2933	0.54	0.3	398	305	254	Good
R2934	1	0.87	379	326	323	Typical
R2935	0.3	0.17	485	443	404	Typical
R2936	1.3	1.3	532	260	265	Typical
R2937	2	0.47	538	351	311	Good
R2938	0.87	0.3	329	268	295	Good
R2939	0.3	0.87	394	415	432	Poor
R2940	0.875	0.17	360	286	268	Good
R2941	0.6	0.69	356	293	277	Poor
R2942	0.17	0.09	460	340	279	Good
R2943	0.87	0.17	455	314	273	Good
R2945	0.47	0.39	447	485	426	Good
R2946	0.87	0.17	333	386	313	Good
R2947	0.54	0.54	475	424	403	Typical
R2949	1.3	1	458	322	255	Good
R2950	2	1	480	540	556	Good
R2953	0.17	0.3	405	285	297	Poor
R2954	2	2	335	372	319	Poor
R2955	0.47	0.87	506	267	443	Poor
R2957	2	2	410	427	434	Poor
R2959	0.39	0.54	451	381	413	Poor
R2960	0.39	0.69	411	358	378	Poor
R2961	0.54	0.47	388	280	348	Good
R2962	0.3	0	338	263	253	Good
R2963	0.09	0.09	469	383	301	Typical
R2965	**0.4**	**0.17**	322	458	364	Good

R2966	0.87	0.39	489	318	362	Good
R2967	0.17	0.09	301	296	304	Good
R2968	2	2	399	403	301	Poor
R2969	0.4	0.3	400	327	273	Typical
R2971	0.87	2	452	462	458	Poor
R2972	2	0.69	530	326	402	Good
R2973	0.47	0.4	228	219	222	Good
R2974	2	2	242	336	321	Poor
R2975	0.17	0.17	359	337	327	Typical
R2976	0.69	0.6	382	275	287	Typical
R2977	1	0.69	530	281	396	Good
R2978	0.47	0.17	360	405	345	Good
R2979	0.87	0.6	482	215	214	Good
R2980	0.39	0.3	413	249	237	Good
R2981	0.39	0.3	353	284	288	Good
R2982	0.3	0.39	337	247	242	Typical
R2983	0.87	0.17	559	303	300	Good
R2984	2	2	501	320	394	Good
R2987	0.6	0.39	435	207	219	Good
R2988	0.3	0.3	522	389	349	Typical
R2991	2	0.17	452	208	266	Good
R2992	0.39	0.3	281	351	239	Typical
R2993	0.39	1	460	517	503	Poor
R2994	0.87	0.69	626	648	451	Good
R2995	0.6	0.17	546	259	269	Good
R2996	0.3	0.3	278	235	280	Good
R2999	2	2	491	375	314	Good
R3000	0.39	0.39	494	296	321	Typical
R3002	0.87	0.47	526	239	285	Good
R3003	0.3	0.3	271	228	244	Typical

R3004	0.69	1	446	457	459	Poor
R3005	0.39	0.3	680	440	686	Good
R3006	0.54	0.54	440	313	319	Typical
R3007	0.47	0.09	334	249	253	Good
R3008	0.39	0.69	349	320	312	Poor
R3009	0.39	0.87	402	826	544	Poor
R3010	0.69	0.39	456	488	545	Good
R3013	0.39	0.3	370	380	330	Typical
R3015	0.3	0.39	354	321	326	Poor
R3016	0.3	0.17	311	293	278	Good
R3017	0.69	0.3	472	381	323	Good
R3018	0.47	0	367	235	268	Good
R3019	2	1.3	683	496	508	Good
R3020	0.39	0.39	484	310	342	Typical
R3021	0.3	0	384	301	327	Good
R3022	1	0.39	390	272	286	Good
R3023	0.87	0.3	745	275	299	Good
R3024	0.69	0.09	562	301	473	Good
R3025	0.47	0	330	229	334	Good
R3028	1	0.39	509	278	253	Good
R3029	0.3	0.39	576	589	525	Poor
R3086	0.47	0.09	528	432	349	Good
R3118	1	1.3	468	448	528	Poor
R3123	0.47	0.87	484	503	515	Poor
R3126	0.3	0.09	356	339	298	Good

Figure II: Class distribution per SNP genotype. Distribution of good and poor responders based on genotype in 13 SNPs used to create the J48 decision tree. Both non-synthetic and SMOTE-generated instances are included. Each bar represents one possible genotype class per SNP: homozygous major, homozygous minor or heterozygous. Within each bar, class distribution is denoted with different color: Blue=good/typical responders; red=poor responders; black=missing values.

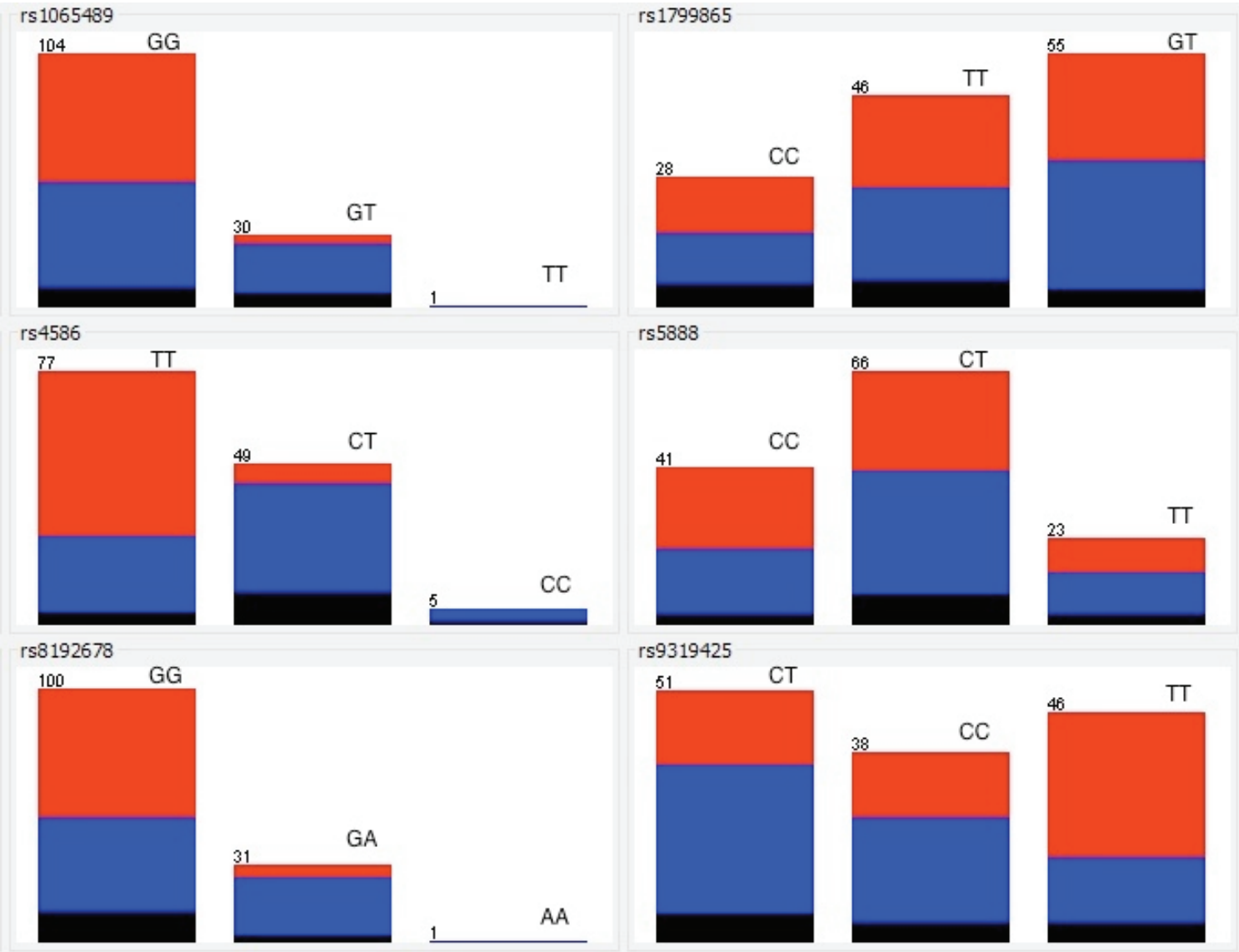

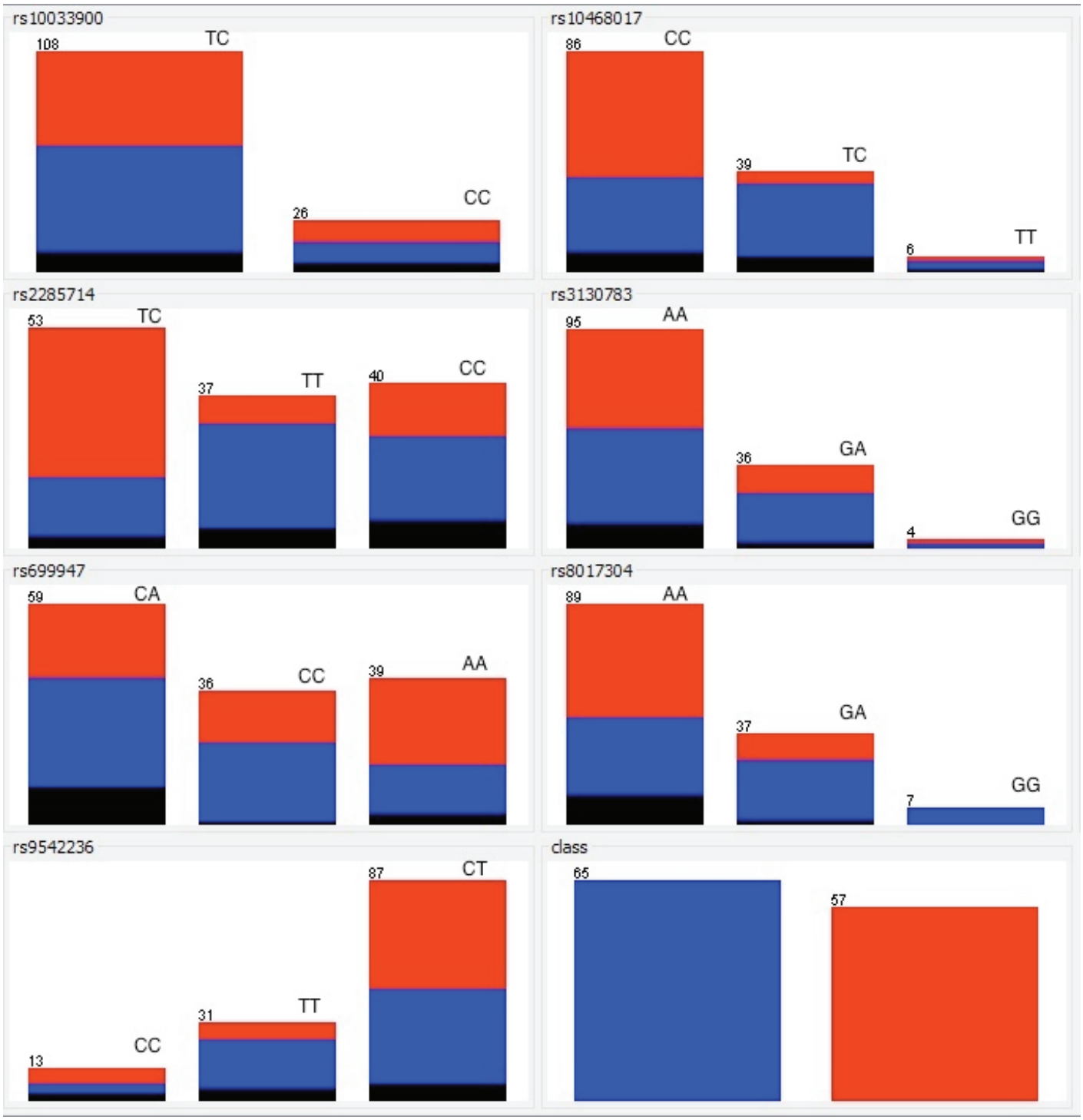
rs10033900
108
TC
26
CC
rs10468017
86
CC
39
TC
6
TT
rs2285714
53
TC
37
TT
40
CC
rs3130783
95
AA
36
GA
4
GG
rs699947
59
CA
36
CC
39
AA
rs8017304
89
AA
37
GA
7
GG
rs9542236
13
CC
31
TT
87
CT
class
65
57

Figure III: Manual model validation. Actual and predicted class for all 84 patients based on genotype in 13 SNPs used to create the decision tree. Highlighted in grey are the misclassified instances. Instances with missing values in the root node SNP (rs4586) could not be manually classified and have been marked with a question mark in the predicted class column.

Patient ID	rs4586	rs8192678	rs699947	rs9542236	rs1065489	rs2285714	rs3130783	rs9319425	rs8017304	rs833069	rs10468017	rs10033900	rs5888	rs1799865	Actual Class	Predicted Class
R2930	CT	GG		CT	GT	TC			GA	AA	CC	TC	CC	CC	1	1
R2931	TT	GG	CA	TT	GG	TC	AA	CC	GG	GA	TC	TC	CT	CT	1	1
R2932	TT	GG	CA	TT	GG	TT	AA	TT	GG	GA	TC	TC	CC	CT	1	1
R2933	TT	GG	CC	CT	GT	TC	GA	CC	AA	GA	TC	TC	CT	TT	1	1
R2934			CC		GG		AA	TT							1 ?	
R2935	CT	GG	AA	TT	GG	TT	AA	TT	AA	AA	TT	TC	CC	TT	0	0
R2936	TT	GG	CA	CT	GG	TC	AA	TT	AA	GA	CC	TC	CT	CC	1	1
R2937	TT	GG	CA	CT	GG	TT	GA	CT	GA	GA	TC	TC	TT	TT	1	1
R2938	TT	GG	CA	CT	GG	CC	AA	CC	GG	GA	TC	CC	CC	TT	1	1
R2939	TT	GG	CA	TT	GT	TT	GA	CT	AA	AA	TC	TC	CC	CT	1	1
R2940	CT	GG	CC	TT	GG	TC	AA	CT	AA	GA	TC	TC	CT	CT	1	1
R2941	TT	GG	AA	TT	GG	CC	GA	CT	GA	AA	TC	CC	CT	CT	1	1
R2942	TT	GG	AA	CC	GT	TC	AA	CT	AA	AA	TC	TC	CT	CT	1	1
R2943	CT	GG	AA	CT	GT	TC	AA	CC	AA	AA	CC	TC	CT	TT	1	1
R2945	TT	GG	AA	CC	GG	TC	AA	CT	GG	AA	TT	TC	CT	CT	1	1
R2946	TT	GG	CA	TT	GT	CC	GA	CC	AA	GA	TC	TC	CT	CT	1	1
R2947	CC	GG	CC	CT	GG	TC	AA	CT	AA	AA	CC	TC	CT	CT	1	1
R2949	CT	GA	CA	CT	GT		GA	CT	GA		TC	TC	CT	CT	1	1
R2950	TT	GG	AA	CC	GG	CC	GG	CT	AA	AA	CC	CC	CT	TT	0	0
R2953	CT	GA	CC	CT	GT	TT	AA	CT	AA	GA	TC	TC	CT	TT	1	1
R2954	TT	GG	AA	CT	GT	CC	AA	CT	GA	AA	TC	TC	TT	CT	1	1
R2955	TT	GG	CA	TT	GG	CC	AA	CT			TC		CC	CC	1	1
R2957	CT	GG	CC	TT	GG	CC	GA	CT	AA	GG	TC	CC	CC	TT	0	0
R2959	CT	GG	CA	CT	GG	TT	GA	TT	AA	AA	CC	TC	CT	TT	0	0
R2960	TT	GG	CA	CT	GG	TC	AA	CC	GA	GA	CC	TC	TT	CT	0	0
R2961		GG	CC		GG		AA	CT	AA	GA		TC			1 ?	
R2962	TT	GA	CC	CT	GG	TT	GA	TT	AA	GA	CC	TC	TT	TT	1	1
R2963	CT	GA	CC	TT	GT	TT	AA	CT	AA	GA	CC	TC	CT	TT	1	1
R2965	CC	GA	CA	TT	GG	CC	AA	CT	GA	AA	CC	CC	CT	TT	1	1
R2966	CT	GG	CA	CT	GG	CC	AA	CT	AA	GA	CC	CC	TT	CT	1	1

R2967	TT	GA	CA	CT	GG	TC	GA	CT	AA	GA	CC	TC	CC	TT	1	1
R2968	TT	GG	AA	CT	GG	TT	AA	TT	AA	AA	CC	TC	TT	TT	1	1
R2969	CT	GG	AA	CT	GG	TT	AA	CC	AA	AA	TT	TC	CT	CT	0	0
R2971	CT	GA	AA	TT	GG	CC	AA	TT	AA	AA	CC	CC	CC	CC	0	0
R2972		GA	CA		GG		AA	CC	GA	GA		TC			1 ?	
R2973	TT	GA	CC	TT	GG	TC	AA	CC	GA	GG	TT	TC	TT	CT	1	1
R2974		GG	CA		GG		AA	CT	GG	GA		TC			1 ?	
R2975	CC	GG	CA	CT	GT	TC	AA	TT	AA	GA	CC	TC	CC	CC	1	1
R2976	CT	GA	CC	TT	GG	TC	AA	TT	GA	AA	CC	TC	CT	CT	1	1
R2977	CC	GG	CA	TT	GT	TC	GA	CT	AA	AA	TC	TC	CT	CT	1	1
R2978	TT	GA	CC	CT	GG	TT	GA	TT	GA	GG	CC	TC	CT	CC	1	1
R2979	TT	GG	CA	CT	GG	CC	GA	CT	GA	GA	TC	CC	CT	CC	1	1
R2980	CT	GG	AA	CT	GG	TC	GA	CT	GA	AA	TC	TC	CT	CT	1	1
R2981	TT	AA	CC	TT	GG	CC	AA	CT	GA	AA	CC	CC	CT	CC	1	1
R2982	TT	GA	CC	TT	GG	TC	AA	CT	GA	GA	CC	TC	CT	CT	1	1
R2983	CT	GA	CA	CT	GT	CC	AA	CC	GA	AA	CC	CC	CT	CT	1	1
R2984	TT	GA	AA	TT	GG	CC	AA	CC	GG	AA	TC	TC	CT	TT	1	1
R2987	CT	GA	CA	CT	GG	CC	GG	CT	AA	AA	CC	TC	CC	CC	1	1
R2988	TT	GA	CA	CT	GT	CC	GA	TT	AA	GA	CC	CC	TT	CT	0	0
R2991	CT	GG	CC	TT	GT	TT	GA	CT	GA	GG	TC	TC	CC	TT	1	1
R2992	CT	GA	AA	CT	GG	TC	AA	TT	AA	AA	CC	TC	TT	CC	0	0
R2993	TT	GG	AA	CT	GT	CC	GA	TT	GA	AA	CC	CC	CT	TT	0	0
R2994	CT	GG	AA	TT	GG	CC	AA	CC	AA	AA	TC	CC	CT	TT	0	0
R2995	TT	GG	CC	CC	GT	CC	AA	CC	GA	GG	CC	TC	CT	CT	1	1
R2996	CT	GG	AA	CC	GT	TC	GA	TT	AA	AA	CC	TC	TT	CT	1	1
R2999	CT	GG	CC	CT	GG	TC	GA	CT	GA	AA	TC	TC	TT	CT	0	1
R3000	TT	GA	CC	CT	GG	CC	GA	CC	GA	GA	TC	CC	CC	TT	1	1
R3002	CT	GA	CC	CT	GG	TC	AA	CC	AA	GA	TC	TC	TT	TT	1	1
R3003	TT	GG	CA	CT	GT	CC	AA	CC	GG	GA	TC	TC	CT	TT	1	1
R3004	TT	GG	CA	CC	GG	TT	AA	CC	GA	GA	CC	TC	TT		0	0

R3005	CT	GA	CA	CT	GT	TC	AA	TT	AA	AA	TC	TC	TT	TT	1	1
R3006	CT	GA	CC	CT	GG	TT	GA	CC	GA	GA	TC	TC	CC	CT	1	1
R3007	CT	GA	CA	CT	TT	TC	AA	CC	AA	GA	CC	TC	CC	CT	1	1
R3008		GG	CC		GG		AA	CC	GA	GG		TC			0 ?	
R3009	CT	GG	CA	TT	GG	TT	AA	TT	AA	GA	TC	TC	CT	CT	0	0
R3010	CT	GA	CC	CC	GT	TC	GG	TT	GA	GA	TC	TC	CC	TT	0	0
R3013	CT	GG	CA	CT	GG	CC	AA	CT	GA	GA	CC	CC	CT	TT	1	1
R3015	CT	GA	CC	CC	GT	TC	AA	CT	AA	GA	CC	TC	CT	TT	0	0
R3016	CT	GG	CA	TT	GG	TC	GA	CC	GA	GA	TC	TC	CT	TT	1	1
R3017	TT	GA	AA	CT	GT	CC	GA	CT	AA	AA	TT	TC	CT	CT	1	1
R3018	TT	GG	CA	CT	GT	TT	AA	TT	AA	GA	TC	TC	CT	TT	1	1
R3019	TT	GA	CA	CT	GG	CC	GA	CC	AA	GA	CC	TC	CC		1	1
R3020	CT	GA	CA	CT	GG	CC	AA	CT	GA	GA	CC	TC	TT	CT	1	1
R3021	TT	GG	AA	CT	GG	TT	AA	CC	AA	AA	CC	TC	CC	CT	1	1
R3022	TT	GA	AA	TT	GT	TT	GA	CC		AA	CC	TC	CC	CT	1	1
R3023	CT	GA	CA	CT	GG	TT	AA	TT	GA	GG	TC	TC	CC	CT	1	1
R3024		GG	CC		GG		AA	CC	AA	GA		TC			1 ?	
R3025	CT	GG	CA	CT	GG	TC	AA	CT	AA	GA	TC	TC	TT	CC	1	1
R3028	TT	GG	AA	CT	GG	TC	GG	CC	GA	AA	CC	CC	CT	CC	1	1
R3029	TT	GG	CC	CT	GG	CC	GA	TT	GA	GG	CC	CC	CC	CT	0	0
R3086	TT	GA	CC	CT	GG	CC	AA	CT	AA	GG	CC	TC	CT	CT	1	1
R3118	CT	GG	CA	TT	GG	TC	GA	CT	AA	GA	CC	TC	CT	CC	1	1
R3123	CT	GG	CA	CT	GG	TT	AA	CT	AA	GA	CC	TC	CT	CT	0	0
R3126	TT	GG	CC	CT	GG	TC	AA	TT	AA	GA	CC	TC	CC	TT	1	1